Development of a vibration absorbing handle for rock drills

by

Johannes Petrus De Wet Strydom

A dissertation submitted in partial fulfilment of the requirements for the degree

Master of Engineering

in the Department of Mechanical and Aeronautical Engineering

of the Faculty of Engineering

of the

University of Pretoria

August 2000

Development of a vibration absorbing handle for rock drills

by

Johannes Petrus De Wet Strydom

Supervisor: Professor P. S. Heyns
Co-supervisor: Professor J. L. van Niekerk
Department: Mechanical and Aeronautical Engineering
Degree: M. Eng

Excessive vibration exerted on the human body can cause many harmful phenomena that can result in permanent bodily damage or permanent disability. Human vibration is classified into two main categories: Hand-arm vibration and whole-body vibration. Hand-arm vibration is vibration transmitted through a percussive tool handle via the hand-arm system to the rest of the body. The main diseases concerning hand-arm vibration are Vibration White Finger (VWF), neurological diseases in the hand and fingers and musculoskeletal diseases like carpal tunnel syndrome.

These diseases, especially VWF and musculoskeletal disorders, are mainly associated with lower frequencies. VWF in particular is more likely to occur when an operator is subjected to vibrations with high magnitudes in the 25-40 Hz region. The operating frequencies of most rock drills vary between 30 and 50 Hz. Although there are many other contributing factors like grip force, hand temperature and subject variability, prevalence of VWF among rock drill operators is relatively high in the world. The situation in South Africa is not yet very clear, and further research must be done to evaluate the current status of VWF in South Africa.

Vibration energy at higher frequencies can be attenuated with rubber grips or gloves, and these types of dampers are already available on the market. The problem concerning the operating frequency of the drill has not yet been successfully addressed, and thus remains a problem in the rock drill industry as it is at the moment.

The main objective of this thesis was the development and testing of a concept that can potentially be implemented on a rock drill to attenuate the operating frequency of a rock drill. The concept must be able to account for minor changes in operating frequency on a specific drill. In addition to that, the drill operating frequency varies from one drill to another. The thesis also aims to lay the mathematical foundation to design an attenuating handle for a specific drill with a specific operating frequency. All the objectives must be obtained without noticeable sacrifices in drill control or performance.

The thesis includes the concept generation, optimisation, design and manufacture of a rock drill vibration absorber. The absorber has been tested, and the results are presented.

Keywords: Vibration, absorber, rock drill, vibration white finger, hand-arm vibration, operating frequency

Ontwikkeling van 'n vibrasie-absorberende handvatsel vir rotsbore

deur

Johannes Petrus De Wet Strydom

Leier: Professor P. S. Heyns
Mede-leier: Professor J. L. van Niekerk
Departement: Meganiese en Lugvaartkundige Ingenieurswese
Graad: M. Ing

Wanneer die liggaam aan oormatige vibrasie blootgestel word kan dit 'n aantal hand- of gewrigskwale, of permanente liggaamlike skade of gebrek tot gevolg hê. Vibrasie blootstelling aan die menslike liggaam word in twee katogorië verdeel naamlik hand-arm vibrasie en heelliggaamsvibrasie. Hand-arm vibrasie kom voor wanneer vibrasie deur 'n gereedskap stuk via die hand en arm na die res van die liggaam oorgedra word. Die hoof kwale wat deur hand-arm vibrasie veroorsaak word is Raynaud se fenomeen (Vibration white finger) en spier-en beenkwale soos karpale tonnel sindroom.

Hierdie kwale, en spesifiek Raynaud se fenomeen, word hoofsaaklik geassosieër met laer frekwensies. Raynaud se fenomeen is veral geneig om in die 25-40 Hz gebied voor te kom. Die oorgrote meerderheid van rotsbore se werksfrekwensie is tussen 30 en 50 Hz. Alhoewel Raynaud se fenomeen redelik algemeen onder rotsboor operateurs in die res van die wêreld voorkom, is die situasie in Suid-Afrika nog nie heeltemal duidelik nie.

Hoë frekwensie vibrasie-energie kan geattenueer word met rubbergrepe of handskoene, en hierdie tipe dempers is ook algemeen op die mark beskikbaar. Die probleem ten opsigte van die werksfrekwensie van die boor kon egter nog nie suksesvol aangespreek word nie.

Die hoofdoelwit van hierdie vehandeling was om 'n konsep te ontwikkel en te vervaardig wat die werksfrekwensie van 'n rotsboor attenueer, en potensieel op 'n rotsboor implementeer kan word. Die attenueerder moet kan kompenseer vir klein variasie in die werksfrekwensie van 'n boor gedurende bedryf. Werksfrekwensies verskil egter ook van boor tot boor, en moet ook geakkomodeer kan word in die ontwerp. Die verhandeling mik ook om die basiese wiskundige grondslae wat nodig is vir die ontwerp van so 'n absorbeerder te lê.

Sleutelwoorde: Vibrasie, absorbeerder, rotsboor, Raynaud se fenomeen, hand-arm vibrasie, werksfrekwensie

Acknowledgements

I wish to thank the following persons and contributors for making this research possible:

- Professor Stephan Heyns, my mentor, for his guidance, support and enthusiasm
- Professor Wikus van Niekerk, my co-mentor, for additional guidance and assistance
- SIMRAC for their financial contribution
- My parents for their love and support throughout my studies
- For Sanette, my wife, for all her love, support and patience.

List of symbols

Symbol	*Meaning*	*SI Units*
A	Area	m^2
a	Port area	m^2
a_i	Acceleration measured at the i^{th} element	m/s^2
b	Base area	m^2
[C]	Damping	Ns/m
C_{eqx}	Equivalent damping coefficient	Ns/m
c_f	Damping due to flow losses	Ns/m
c_i	i^{th} integration constant	
c_i	Damping coefficient of the i^{th} damper	Ns/m
D	Material constant	
D_b	Diameter of base	m
D_h	Diameter of handle	m
D_p	Diameter of port	m
D_1	Housing diameter	m
E	Young's modulus	GPa
E_k	Kinetic energy	J
E_p	Potential energy	J
f_{ex}	Excitation frequency	Hz
F_L	Damping force due to flow losses	N
F_i	Force applied at the i^{th} element	N
f_I	Frequency of minimum T_r	Hz
f_{MT}	Frequency of maximum T_r	Hz
f_n	Natural frequency	Hz
g	Gravitation	m/s^2
h_{fMT}	Fluid flow losses	m
H_{ii}	Transfer function of MDOF system	
I	Moment of inertia	m^4
[K]	Stiffness	N/m
k_i	Stiffness coefficient of i^{th} spring	N/m
k_r	Polyurethane rubber stiffness	N/m
K_{SE}	Loss coefficient due to sudden expansion	
K_{SC}	Loss coefficient due to sudden contraction	
L	Length	m
ℓ	Length	m
[M]	Mass	kg
M_{eqx}	Equivalent mass	kg
m_a	Apparent mass	kg
m_1	Mass to be attenuated	kg
m_2	Absorbing mass	kg
n_p	Number of ports	
P	Phase angle	Degrees
P_L	Pressure loss	Pa
Q_1	Distributed load	N/m
R	Rayleigh's dissipation function	Nm/s
R_{ed}	Reynolds number	Dimensionless
r	Radial length	m

r_a	Radial length	m
r_b	Radial length	m
s	Laplace transformation	
T_r	Transmissibility	Dimensionless
T_{ii}	Transmissibility of MDOF system	
t	Thickness	m
t	Time	s
W	Transverse deflection	m
X_i	Amplitude of $x_i(t)$	m
x, y, z	Cartesian co-ordinates, displacements	m
x_1	Handle displacement	m
x_2	Absorbing mass displacement	m
x_3	Drill displacement	m
$\dot{x}_i$	i^{th} element velocity	m/s
$\ddot{x}_i$	i^{th} element acceleration	m/s^2
β	Structural damping coefficient	
γ	ω_{MT}/ω_I	Dimensionless
γ_t	Natural frequency ratio	Dimensionless
κ	Radius of gyration	m
μ	Mass ratio	Dimensionless
μ_f	Fluid viscosity	Ns/m^2
θ	Angular displacement	Radians
$\dot{\theta}$	Angular velocity	Rad/s
ρ	Density of fluid	kg/m^3
ν	Poisson's ratio	
ω	Frequency	Rad/s
ω_{ex}	Excitation frequency	Rad/s
ω_I	Frequency of minimum T_r	Rad/s
ω_i	i^{th} natural frequency	Rad/s
ω_{MT}	Frequency of maximum T_r	Rad/s
ω_n	Natural frequency	Rad/s
ζ	Damping ratio	Dimensionless
ζ_i	i^{th} damping ratio	Dimensionless

Table of contents

1. Literature review

Man-machine interaction has become an important factor in engineering design. Much emphasis is placed on human safety, and employers are under increasing pressure to create a healthy and safe environment to ensure not only maximum production, but also the minimum injuries. In the mining industry, this becomes more difficult. Working conditions are very hostile, and it is not easy to implement safety procedures and international standards.

Human vibration is an aspect that receives considerable attention in the research world at the moment. Although vibration can be used to treat certain medical pathologies, it is actually detrimental to the human body. Human vibration is evident in most dynamic machines where human control is important for proper functioning of the machine.

Rock drills are high-powered impact machines that induce large amplitude vibration. Till recent times, no concept in terms of an attenuating handle has been generated that is currently in production and functioning in South African mines. The main problem is that an attenuating handle should be just as robust as an ordinary rock drill handle, and no sacrifice should be made in terms of drilling control.

For the purpose of this study it is important to quantify the problem in terms of vibration frequency and amplitude, based on previous work and measurements done in this field. Once the vibration energy is quantified in terms of vibration amplitude and frequency, a proper concept development and evaluation must be executed. A mathematical model will then be generated to be able to simulate the functioning of the chosen concept when subjected to vibration. All the critical parameters required to design an experimental prototype, can be identified with such a model. The mathematical model will also be used to optimise the relevant variables for a given set of constraints. The design should then be evaluated in terms of practical aspects for a manufacturing process. A thorough experimental procedure of vibration measurements should then be executed, so that the concept can be evaluated, and compared to the theoretical model.

The main objective of this study is to ensure that the concept chosen in the concept evaluation can potentially be implemented on a rock drill, that the vibration energy at the predefined critical frequency is adequately reduced, and to identify the critical design parameters in terms of dynamic response.

1.1 Human vibration

The human body is a very complex, dynamic and intelligent structure, and thus it is not easy to analyse the effect of vibration on a human being. Vibration can be a source of pleasure or pain; it can heal or impair health. One of the factors that make human vibration so difficult to analyse and quantify, is the fact that the response of the human body varies from person to person. Some people experience symptoms of vibration diseases sooner than other. Griffin (1990:635) reports that one must consider many of the physical and medical factors of an individual's present and past before attempting to report occupational hand transmitted vibration. Researchers distinguish between two

forms of human vibration, Whole Body Vibration (WBV), and Hand-Arm Vibration (HAV). Griffin (1990: 27) defines WBV as: "Whole-body vibration occurs when the body is supported on a surface which is vibrating." This can happen in any man-machine interface situation where there is no particular local point of contact. HAV occurs when the point of contact between the person and the vibrating machine is the hand-arm system.

1.1.1 Hand-arm vibration

The main aspects that should be taken into consideration when analysing HAV are vibration axes, vibration magnitude, vibration frequency and vibration duration (Griffin, 1990: 540). There are other factors like grip force, contact area and posture, but these are more difficult to quantify, as they would probably vary with time and from one individual to another. International standards make it relatively easy to study the influence of vibration axes, vibration magnitude and vibration frequency, but vibration duration, or dose response, is not so easy to quantify. The effects of vibration duration have been studied in the past, but more research is required in the field (Brammer, 1986; Bovenzi, 1994).

Another aspect that has received attention in the past is attempts to build a dynamic model of the human hand. To present a successful solution to the problem of HAV, an appropriate mathematical model has to be created. The effect of the hand-arm system has to be compensated for in some mathematical way. Griffin (1982) proposes the apparent mass model, which basically implies that the mass of the human arm varies with frequency, arm angle, push and pull forces and grip force. Thomas *et al.* (1996) have simulated the hand as a multi-degree of freedom system with mass and stiffness constants. Lundström *et al.* (1988) have measured the mechanical impedance of the human upper extremity and verified Griffin's finding that grip force plays an important role.

1.1.2 Hand-arm vibration syndrome

Probably the most important pathology associated with HAV is the vascular disorder hand-arm vibration syndrome, also known as Raynaud's phenomenon or Vibration White Finger (VWF). VWF is a vascular disorder that was first recognised around 1890 – 1900 on men using pneumatic hand-held drills. At that time it was reported that five factors caused the condition: long, continued vibration exposure, tight hand grip, continued muscular contraction of the fingers, using a worn air hammer and cold in the work place (Taylor, 1987). There is a dispute in the literature as to whether a cold work place is a necessary condition for the occurrence of VWF. Taylor (1987) reported that blanching is more frequent and prolonged in cold winters, but with higher vibration input the attacks would also occur at summer temperatures.

Griffin (1990: 584) postulates a hypothetical model of vascular disorders of the hand where thermal stimuli constitute but one of the amplifying factors of VWF. Another problem that relates to this thesis is the fact that pneumatic equipment tends to cool during the adiabatic expansion of air (Griffin, 1990: 587).

Griffin (1990, 571) also discusses the classification of the severity of VWF, which is known as staging. Table 1.1 explains the different stages of VWF and the severity in terms of work and social interference.

Table 1.1: Stages of VWF (Griffin, 1990:572)

Stage	Condition of digits	Work and social interference
0	No blanching of digits	No complaints
0_T	Intermittent tingling	No interference with activities
0_N	Intermittent numbness	No interference with activities
1	Blanching of one or more fingertips with or without tingling and numbness	No interference with activities
2	Blanching of one or more complete fingers with numbness usually confined to the winter	Slight interference with home and social activities. No interference at work.
3	Extensive blanching usually all fingers bilateral. Frequent episodes summer as well as winter	Definite interference at work, at home and with social activities. Restriction of hobbies
4	Extensive blanching. All fingers; frequent episodes summer and winter	Occupation changed to avoid further vibration exposure because of severity of signs and symptoms

An important factor studied in the literature is the vibration frequencies that are likely to cause VWF. Griffin (1990: 613) states that tools with operational frequencies above 250 Hz and below 25 Hz are not likely to cause VWF. He also states that prevalence of VWF is much higher at frequencies around 25 – 40 Hz. This statement is confirmed in another article where it is stated that many common causes of injury have their dominant components of vibration below 250 Hz (Griffin, 1997).

1.1.3 Other pathologies

A few other pathologies have been mentioned in the literature, and although they are not as severe or as likely to occur as VWF, they are still worth mentioning.

Bone and joint disorders are mainly found in workers using pneumatic hammers such as rock drills where high magnitude shocks around 30 Hz are present. Since 1929 about 10000 workers have been compensated, and vibration induced bone and joint damage is also a compensated occupational disease in Italy (Griffin, 1990: 597 – 599).

There are other pathologies like muscular (Griffin, 1990: 604), neurological disorders (Brammer *et al.*, 1987) and carpal tunnel syndrome (Griffin, 1990: 604), which will not be discussed in detail.

1.2 Hand-arm vibration case studies

Various case studies have been performed in the literature, and it is important to study these in terms of workplace environment, tool type, tool usage, exposure period, disease prevalence, and especially the relevant frequency.

Brubaker *et al.* (1986) conducted a study of VWF among underground rock drill operators in British Columbia. The study showed that 45% of 58 operators suffered periodic attacks of VWF. 9% of the cases were classified as severe. Symptoms were present in 25% of operators exposed for less than five years, and in 80% of operators exposed more than sixteen years. Weighted acceleration levels measured on the handles of the drills ranged from 15 - 32 m/s^2. The article emphasises the fact that these acceleration levels are excessive according to the international standard ISO 5349.2, and recommends that the drills should be modified to reduce the acceleration amplitudes to acceptable levels. Until this is achieved more reliance should be placed on worker education, and mechanised drilling where the operator's hands are not exposed to excessive vibration.

Taylor *et al.* (1984) studied the effect of air hammers on the hands of stonecutters working in the quarries of Bedford, Indiana. The study indicated that 63% of a test group of 30 showed prevalence of VWF. Two types of hammers were used, a 3 - 4 pound and a 30-pound hammer. A retired group of 8 stone cutters with a mean age of 73 and a mean vibration exposure time of 45 years were also surveyed. In this group of 8 subjects, 5 stage 2 and two stage 3 VWF cases were found.

Bovenzi *et al.* (1988) studied the prevalence of VWF and assessment of vibration exposure among travertine workers in Italy. Among the 76 stone drill operators, 27 subjects were affected with VWF. The measured vibration on the drills after frequency weighting was between 19,7 and 36,4 m/s^2. Typical rock drill spectra presented in this article is shown in Fig. 1.1. The fundamental frequency of the rock drill is situated at 35 Hz, where excessive vibration energy is present.

Narini *et al.* (1993) studied occupational exposure to hand vibration in Northern Ontario gold miners. Nineteen underground rock drill operators were evaluated against sixteen control subjects. In total 16 of the nineteen drill operators reported symptoms of VWF. Only one of the control group reported numbness and pain.

Peters (1993) did a case study on hand-arm vibration in railway maintenance. Of the 240 subjects, 40% experienced one or more white fingers, 87% had feelings of numbness, tingling or cramps in their hands, and 82% had musculo-skeletal complaints. Measured exposure levels varied from 4 to 60 m/s^2 (not weighted), depending on the tool type used.

Moon *et al.* (1982) investigated the status of vibration hazards among rock drill operators in the antracite mines. The article reported that 12.5% of 208 rock drill operators suffered from white fingers. The prevalence of white finger increased as the vibration exposure time increased. The average temperature of the working environment was 18.5 °C.

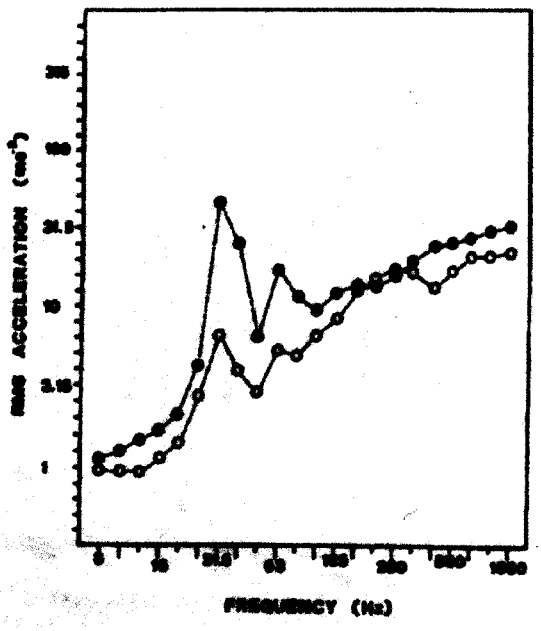

Figure 1.1: Rock drill spectra (Bovenzi, 1988)
• - Z – Axis (Operating axis)
o - Y – Axis

Gemne *et al.* (1987) conducted a literature survey with regard to the radiological documentation of bone and joint pathology in the hands and arms of workers using vibrating tools. About 250 pertinent works were initially examined of which about 180 were used for further observation. The reviewed works were of various nationalities. The article states that most of the vibration with frequencies up to 40 Hz is transmitted to the bones and elbow joints in work with normal grip and press forces, thus constituting a potential risk for bone and joint injury. The article also states that there is an association between work with hand-held vibrating tools with percussive frequencies up to 40 Hz and the prevalence of elbow and wrist osteoarthrosis.

These case studies clearly indicate that VWF is currently a serious problem in the industry.

1.3 Isolation approaches

Most of the isolation approaches presented thus far in the literature implement damping elements. The force transmissibility of these elements can be modelled as a single degree of freedom system (Rao, 1995:593), and is plotted in Fig. 1.2 as a function of the frequency ratio r.

From Fig. 1.2 it is clear that the isolation region is situated above $r = \sqrt{2}$. This means that the natural frequency of the system has to be lowered to less than the excitation frequency. With $\omega_n = \sqrt{\frac{k}{m}}$ the resulting stiffness will be relatively low and the handle mass relatively high. This has serious implications in terms of the controllability of the system. Fig. 1.1 also indicates that the transmissibility can be reduced by reducing the

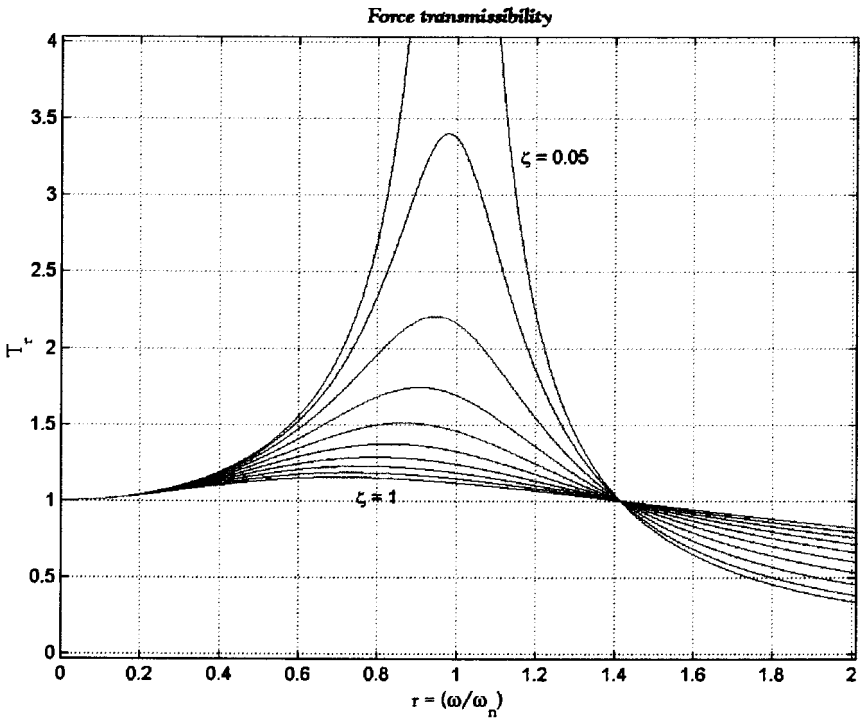

Figure 1.2: Force transmissibility of damping elements

damping ratio (ζ), but a too low damping ratio will result in excessive vibration at the natural frequency of the system.

Damping elements

- Miwa presents a vibration isolation system for hand-held vibrating tools that consists of a compound Nighthart isolator that is mounted on a jack-leg drill and a pneumatic grinder (Brammer; Taylor, 1982: 302). The isolator works on a lever concept and reduces the vibration levels with about 10 dB. Miwa states that vibration levels on a rock drill can be reduced from 137 dB to 120dB in the Z-axis (frequency weighted). The stiffness of the isolator is not mentioned in the article.
- Andersson (1990) presents a design of a vibration attenuating handle that attempts to confront the problem of still having firm, stiff control of the tool, while at the same time reducing the vibration. According to the results, a 68% reduction is achieved with the handle operating on a hammer drill. The handle consists of a grip and a rubber element acting like a universal joint. The article concludes that more research is necessary to assess the real value of the design.
- Prajapati *et al.* (1999) designed a damping handle for a rock drill, which basically aims to attenuate vibration energy with frequencies above 100 Hz. The damper does not attenuate vibration energy in the region of the operating frequency of the drill which is 36 Hz.

Cushioned handles

- De Souza *et al.* (1993) evaluate the performance of a cushioned handle relative to that of the ordinary steel handle. The handle is made of a material known as HD damped elastomer, and has a diameter of 41 mm. The design is such that the air

pressure supplied to the drill is controlled by twisting the handle. The article concludes that the proposed design reduces vibration significantly at frequencies between 500 and 800 Hz.

- Suggs *et al.* study the attenuation effect of resilient handgrips like foam rubber and foam plastics (Brammer; Taylor, 1982: 332). The thickness of the material was varied between 1 and 3.5 cm, and the compression stiffness between 1 and 10 N/cm. It has been found that the resilient handgrips reduce the vibration of a chainsaw by 50%, but most of the attenuation occurs between 300 and 500 Hz.

Gloves

- Rodgers *et al.* study the effect of gloves as protection against vibration (Brammer; Taylor, 1982: 321). Subjects are tested with anti-vibration gloves over a frequency range between 20 and 1000 Hz. It has been found that the gloves do not provide any protection at frequencies lower than 100 Hz, and protection gradually increases from 200 Hz upwards.

Some of the design proposals that have been found in the literature are presented above. The main problem in terms of frequency is between 25 and 250 Hz (Griffin, 1990: 613), and to achieve attenuation in that frequency range without compromising stiffness and tool control can be troublesome. It is quite clear from the above mentioned proposals that an ordinary damping element like rubber or other elastomers are not a solution to the problem. Damping elements like these are only effective at the higher frequencies, and cannot attenuate vibrations in the 25-250 Hz region. Cushioned handles and rubber gloves generally have the same problem.

The design by Andersson is maybe the closest to a solution to the problem, and although the design implements an elastomer, the damping effect is achieved through a lever effect and through the elongation and compression difference of the elastomer. To implement the Andersson design on a rock drill may however be cumbersome.

1.4 Absorbers

The previous section concluded that damping elements have not yet proved to be a viable solution to the hand-arm vibration that a rock drill produces at its operating frequency. Although both absorbers and dampers have been studied, absorbers can be tuned to attenuate a specific frequency, which immediately makes it a very attractive option. A conventional vibration absorber can be modelled and tuned as Bursal (1995) and Tsai (1995) describe in their papers on vibration absorbers. Bursal (1995) also proposes a dual absorber strategy, that is very convenient when multiple anti-resonant frequencies are required.

The problem with conventional absorbers is, as Flannelly (1963) describes in his article on the dynamic anti-resonant absorber, that it requires very large static deflections, and thus very soft springs. The result is less control over the isolated system, and this is generally undesirable. Flannelly (1963) introduces the so-called DAVI (Dynamic Anti-resonant Vibration Isolator). This is an absorber that functions on the lever principle. The definition given in the article describes it as a vibration isolation device, which provides a very high degree of isolation at a predetermined frequency with very low static deflection. The low ARF (Anti-Resonant Frequency) of the DAVI is obtained by

rotary coupling between the input and the output. The article explains the parameter deviations that determine the ARF placement and illustrates difficulties that may occur when an ARF is required to be in front of the resonant frequency in the frequency spectrum. The DAVI has been used in helicopter applications (Gabel *et al.* 1981), and Heyns and Benadé (1996) investigated the possibility of using the DAVI concept on aircraft cannons.

A variation on the above-mentioned concept was developed by NASA, and is known as the Liquid Inertia Vibration Eliminator (LIVE). The LIVE system incorporates a hydraulic fluid with an area advantage to achieve the desired lever effect. The result is a very compact, less complex, bearingless design (Halwes, 1981). The article concludes that, although a bit impractical for helicopter applications, the LIVE system is effective with area ratios up to 20:1. The main problem associated with this concept according to this report is structural and viscous damping which, according to the author, can be reduced to less than 2%.

Halwes *et al.* (1981) conduct an analytical study on a total main rotor isolation system, which also involves the implementation of the LIVE concept. The most important issue that this article reveals is the fact that although the LIVE system can isolate well over 95%, it cannot overcome poor natural frequency placement.

Although many articles concerning dampers have been studied, it is important to realise that damping elements can generally not be tuned to attenuate at a certain frequency like inertia absorbers. As stated earlier, the focus of this thesis is to minimise the force transfer to the operator's hand at the operating frequency of the tool. Nevertheless, damping elements have definitely not been ruled out, and a literature survey on these elements and other elements called impact dampers has been carried out.

1.5 Smart materials

An alternative way of damping vibration energy is by the use of smart materials. One advantage of these materials is that the forcing frequency can easily be actively controlled by electrical input. There are various types of smart materials as described in a document about solid state smart materials (http://www.mide.com). According to this document shape memory alloys have the largest elongation, which is between 2 and 8%. The rest of the solid state smart materials are only capable of less than 0.2% elongation. This proves to be quite cumbersome if seen in the light of rock drill displacements, which in general, are quite large.

Another problem associated with smart materials is the fact that they require, in general, powerful, expensive amplifiers. This would not be very practical in a mining environment. However, Inman (1998) presents a potential solution to this problem with the so-called passive shunt circuit. The conventional shunt circuit consists of three electrical components: a capacitor, an inductor and a resistor. The capacitor in this circuit is replaced by a piezo ceramic element. The mechanical energy is converted into electrical energy by the piezo element, and then dissipated in the resistor. The inductor is used to tune the circuit to a certain resonant frequency.

1.6 Scope of this research

Human vibration is definitely not very easy to quantify, simulate or measure. Researchers distinguish between two types of human vibration, whole-body vibration and hand-arm vibration. The most important pathology associated with HAV is vibration white finger. This pathology is most likely to occur in the 25–250 Hz region. Bone and joint disorders are also likely to occur in the 30 Hz region. Various case studies confirm vibration white finger as an extensive problem in the industry at the moment. No design proposal found in the literature was notably satisfactory in the sense that frequencies between 25 and 250 Hz (especially the operating frequency of the tool) could be attenuated.

Although the dynamic anti-resonant absorber gives a theoretical solution to the problem, it would not be practical to implement this concept on a rock drill. A more acceptable concept is the liquid inertia type absorber, which has no bearings and less mechanical complexity. Damping elements would not be the optimum solution to attenuate one target frequency. Although smart materials could easily be controlled, factors like cost, small displacements and large power requirements make it a less feasible option.

This thesis will attempt to quantify the above-stated problem in mathematical and practical terms. Typical rock drill measurements will be evaluated and weighted with the relevant weighting functions. This will identify the hazardous vibration frequencies in terms of the relevant medical pathologies. The practical operational environment of a typical rock drill will be evaluated in order to identify possible problems regarding the practical implementation of a solution.

A theoretical solution to the problem will be stipulated by the mathematical modelling and simulation of different hypothetical solutions. This will be done by evaluating the performance of current attenuation devices, and identifying the problems of these devices. A concept development process will follow where the pros and cons of existing and newly developed concepts are compared. A feasible solution will then be selected for optimisation and detail design.

The proposed concept will then be optimised by means of a proper sensitivity study and a graphical optimisation process. A mathematical simulation will be executed to ensure that the concept does respond as postulated. A detail design process will follow to prepare the concept for manufacturing.

The manufactured design will be subjected to a proper experimental verification. Most of the critical parameters will be varied during the experimental procedure to ensure that the design can be characterised not only theoretically, but also experimentally. The results of the experimental verification will be compared with that of the theoretical simulations, and possible deviations will be explained.

2 Rock drill vibration

In defining the problem, certain aspects should first be emphasised. The first factor that has been noticed in the light of certain facts mentioned in the literature is that the operating frequency of a rock drill is situated in the 25-250 Hz range, which are the frequencies most likely to cause VWF. Secondly, it has to be taken into consideration that this operating frequency will vary from drill to drill and the same drill's operating frequency will vary from one stope to another.

The problem statement can now be defined as the attenuation of the vibration energy at the operating frequency of a rock drill with the ability to compensate for operating frequency variations.

2.1 Operating procedures

In discussing the operating procedures, the environment of operation will also be reviewed. In South Africa the conditions under which these drills operate are generally very hot and humid. The mining environment is confined and uncomfortable, and while working in these uncomfortable circumstances, operators cannot necessarily concentrate on handling the drill according to procedures set by the manufacturers. The drills must thus be able to withstand the mining environment, and the treatment it receives from operators working in these conditions.

The procedure that is being followed when a hole has to be drilled is relatively simple. The drill bit is placed on the specified location on the rock, and the first part of the hole is drilled slowly so that the drill bit can locate itself and does not move around too much (hole collaring). It is important to notice that for most part of this stage of the hole, the drill is operating below its normal operating frequency. Although manufacturers recommend that thrust force should be reduced, operator control is important at this stage. After the hole has been collared, the rest of the hole is drilled within a few minutes. The handgrip force that is necessary to perform this part of the operation varies from person to person, because of the fact that the hydraulic thrust cylinder does much of the actual drill thrusting. Some operators use only one hand to drill, some operators use both hands to drill, while others will use other parts of the body to assist in the thrusting process.

2.2 Co-ordinate systems

Rock drill vibration is associated with quite severe accelerations over a relatively large frequency band. Vibration magnitude also varies with direction. The magnitude of vibration in the working axis of the drill is more severe than vibration in a direction normal to that axis. Although the measurement procedure will be described later in the document, the co-ordinate system will be described briefly to clarify the directions of vibration. The two types of co-ordinate systems are shown in Fig. 2.1.

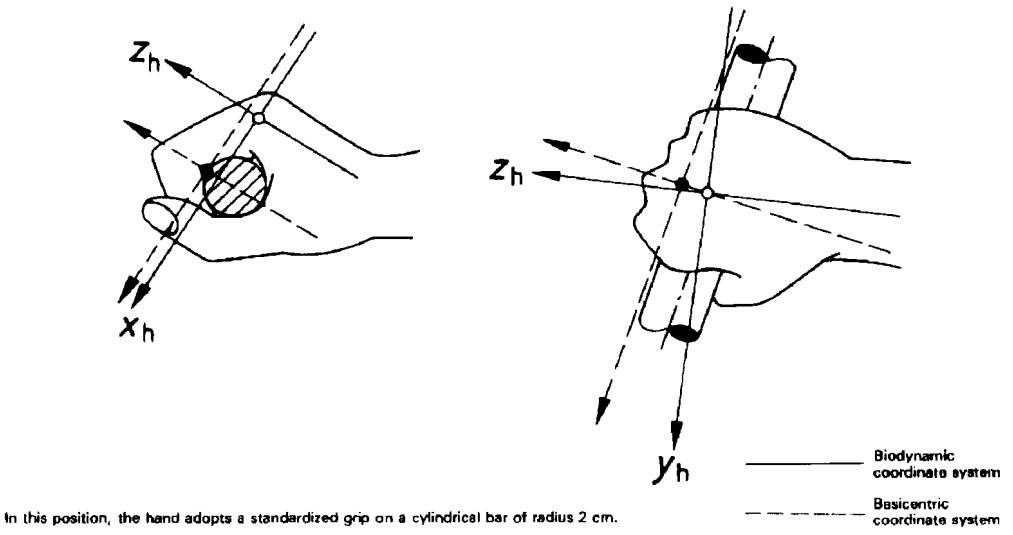

Figure 2.1: Co-ordinate systems

The x-axis of the basicentric co-ordinate system is defined with respect to the tool features but may be broadly parallel to the biodynamic co-ordinate x-axis. The y-axis of the basicentric co-ordinate system may be along the axis of the handle and the z-axis may be perpendicular to the above two axes (Griffin 1990:532).

Measurements are usually obtained with respect to the basicentric co-ordinate system, since it is sometimes difficult to orthogonally and noninvasively mount low triaxial accelerometers to the third metacarpal bone; and the measured acceleration levels represent the highest hazard level available to the operator when he grasps the tool maximally resulting in optimum vibration coupling (Wasserman *et al.* 1991).

2.3 Typical measurements

Typical sets of time domain measurements for the three directions in the basicentric co-ordinate system are shown in Fig. 2.2 and Fig. 2.3 (Van Niekerk *et al.*, 1998), and the frequency domain results are shown in Fig. 2.4 and fig 2.5.

These are typical time and frequency domain data for rock drills. From the frequency domain data, it is important to notice that there is much more energy associated with the higher frequencies than with lower frequencies.

The low frequencies, however, as shown in the next section, are more important in terms of human sensitivity.

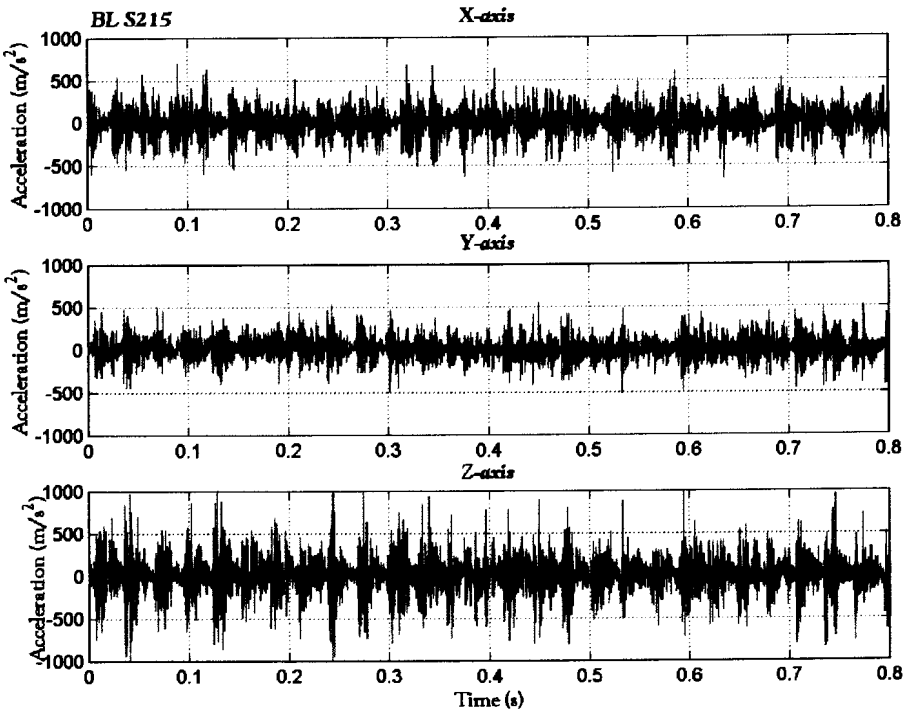

Figure 2.2: Boart Longyear type S215

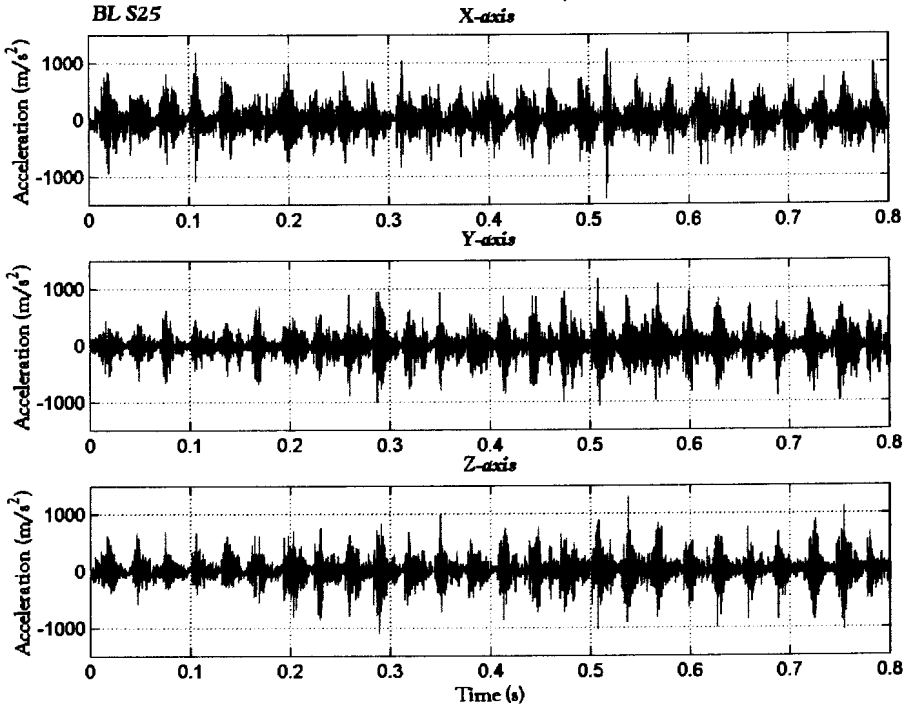

Figure 2.3: Boart Longyear type S25

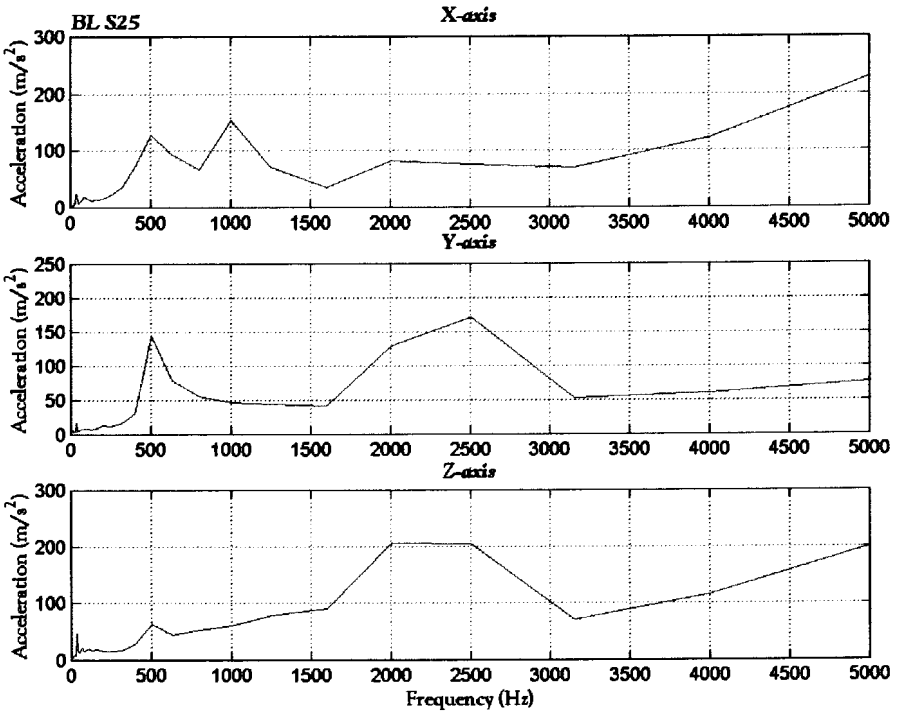

Figure 2.4: Boart Longyear type S25

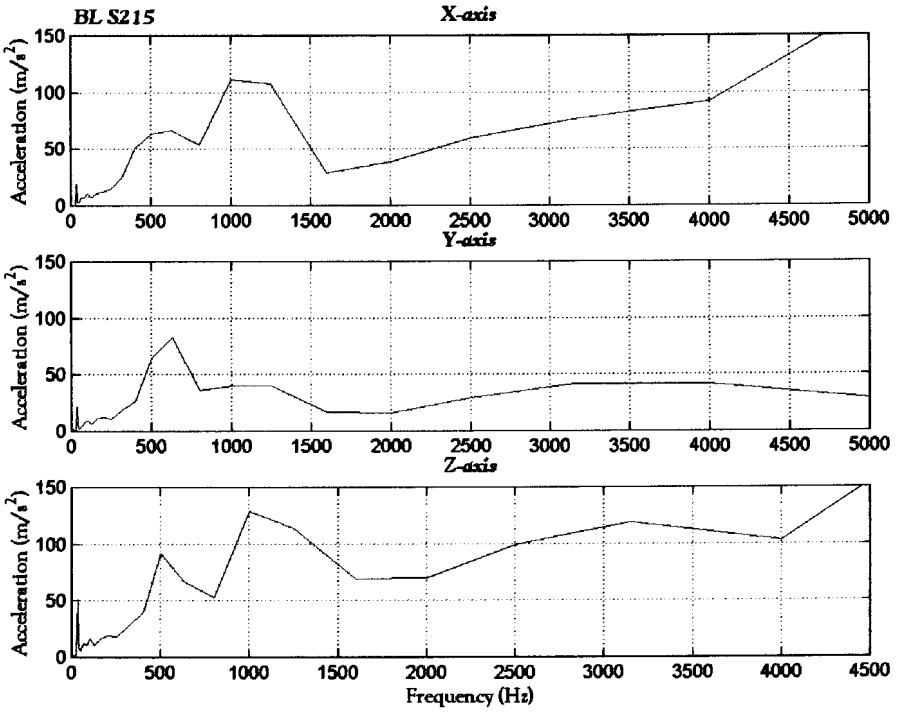

Figure 2.5: Boart Longyear S215

The graphs shown in Fig. 2.6 and Fig. 2.7 are the same as in Fig. 2.4 and Fig. 2.5, but the frequency range for the graphs is between 0 and 100 Hz. The operating frequency of the drill is clearly visible with a maximum acceleration of about 50 m/s^2 in the Z-direction.

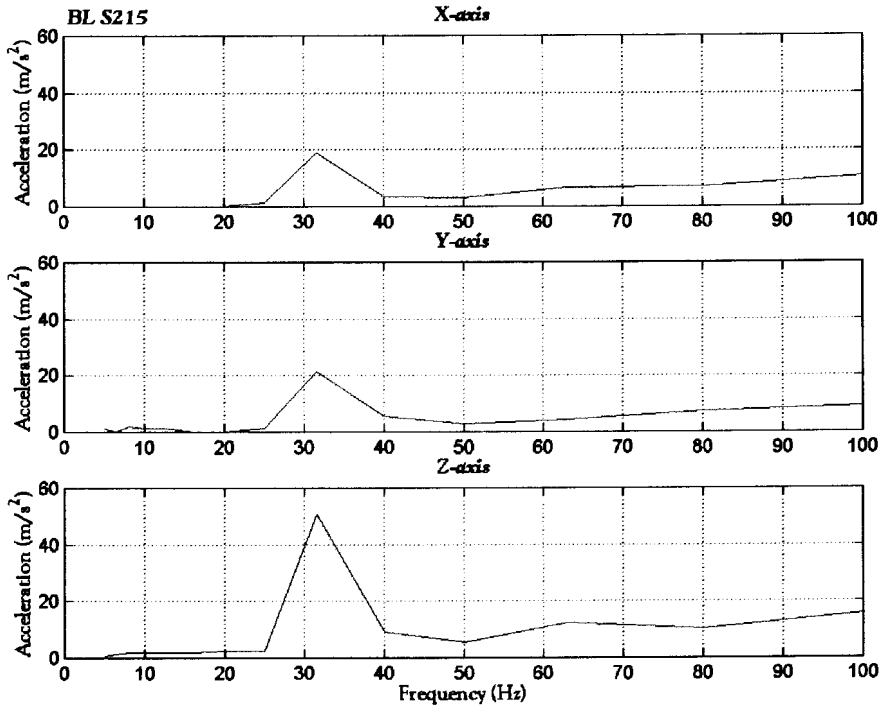

Figure 2.6: Boart Longyear type S215

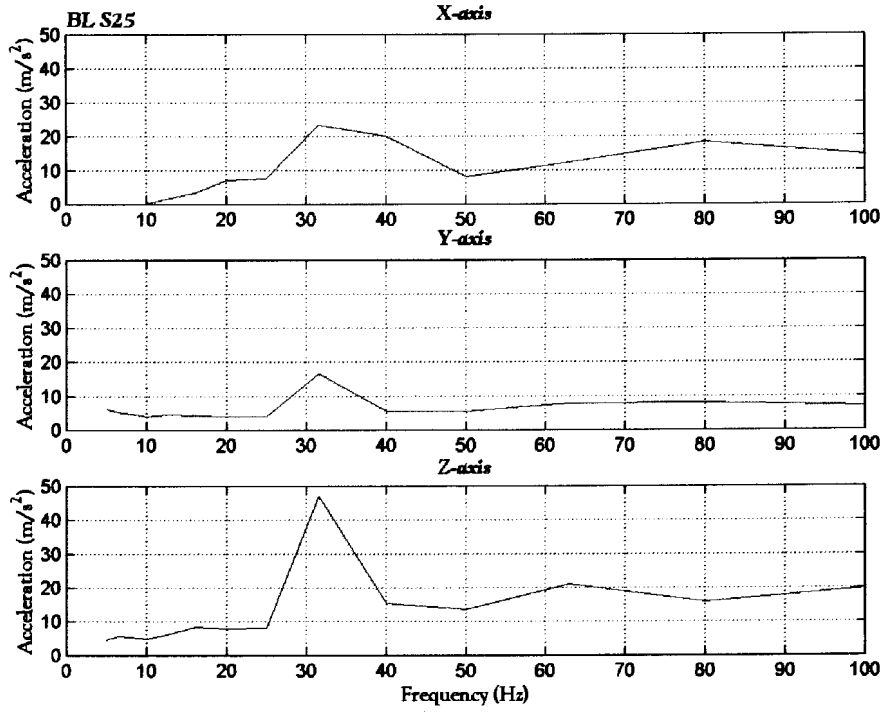

Figure 2.7: Boart Longyear type S25

Both types of rock drills shown in Fig. 2.2-2.6 have operating frequencies at about 33 Hz, and traces of a second harmonic at two times the operating frequency are also visible.

The peaks in Fig. 2.6 and Fig. 2.7 do not seem very sharp, and might create the illusion of a heavily damped structure, but this is due to the low resolution of the measurements.

2.4 Weighting of rock drill vibration

Weighting of measured accelerations is performed in order to emphasise certain frequencies that may tend to be more harmful to the hand-arm system. Although there is still speculation in the literature about the accuracy of the weighting curves (Pelmear *et al.*, 1989), it should be used till further research suggests a change in standards and weighting curves.

The 4 hour equivalent weighting curve for hand-arm vibration according to ISO 5349 is depicted in Fig. 2.8. From Fig. 2.8 it is evident that higher acceleration levels are acceptable at high frequencies. The vibration measurements taken in a typical field experiment would be multiplied with the weighting curve in order to emphasise the critical frequencies.

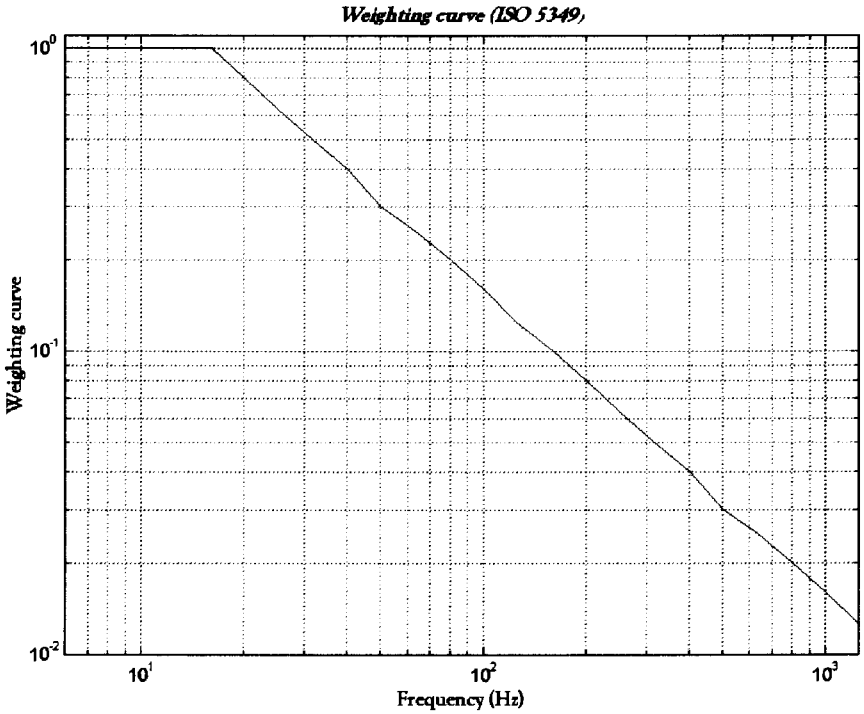

Figure 2.8: Frequency weighting (ISO 5349)

The frequency weighting is done according to ISO 5349 (Fig. 2.8) and the result for the measurements plotted in Fig. 2.4 are shown in Fig. 2.9. The operating frequency is much more dominant after weighting than the vibration energy at the higher frequencies. This implies that the operating frequency of a typical rock drill is

definitely harmful to human hand-arm system, and emphasises the fact that this frequency is indeed an actual problem in modern working environments.

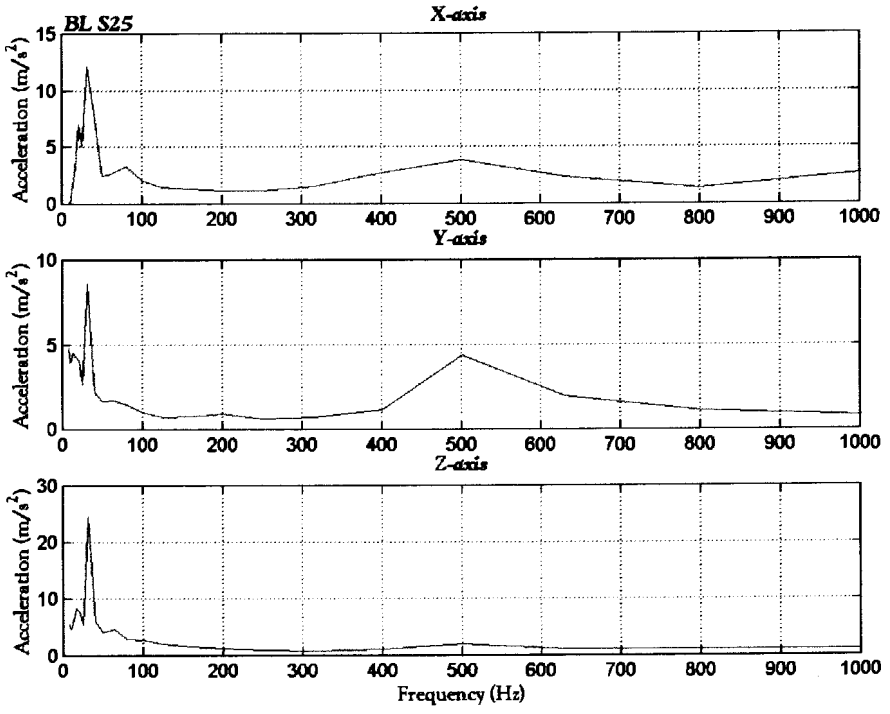

Figure 2.9: Frequency weighting on the Boart Longyear S25 rock drill

2.5 Discussion

The problem has been defined as the attenuation of the vibration energy at the operating frequency of a rock drill with the ability to compensate for operating frequency variations. The drill frequency has been identified, and it has been emphasised that the vibration levels at that particular frequency, although lower in magnitude than higher frequency levels, are dangerous. This statement has been verified by presenting typical hand-arm vibration standards. The concept of frequency weighting has been discussed to illustrate that the vibration energy at higher frequencies will be lower than the vibration levels at low frequencies after frequency weighting. The general conditions of the operating surroundings and typical operating procedures have also been discussed.

The low frequencies, however, as shown in the next section, are more important in terms of human sensitivity.

3 Modelling of vibration absorbers

3.1 Background

In some vibration problems, excessive vibration may occur at one or more specific frequencies. In most of these cases a vibration absorber can be used to change the natural frequencies of the system in such a way that they are shifted away from the problematic frequencies.

A vibration absorber is simply another spring mass system that is mounted on the system, and uses inertia forces to attenuate vibration at a certain frequency. This frequency is known as the isolation or anti-resonant frequency. The isolation frequency can be tuned to attenuate the excitation frequency, and the natural frequencies of the resulting system are away from the excitation frequency.

3.2 Basic absorber theory

A single degree of freedom system is considered in fig 3.1.

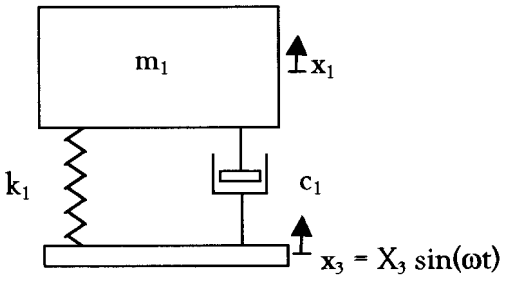

Figure 3.1: Model of SDOF system

The system is excited by base excitation $x_3 = X_3 \sin(\omega t)$. The transmissibility function for a typical system is (refer to appendix B.1 for derivation)

$$T_r = \frac{X_1}{X_3} = \frac{1+i(2\zeta r)}{1-r^2+i(2\zeta r)} \qquad (3.1)$$

The transmissibility of the system is the ratio of the amplitude of the system response, x_1, to that of the base motion, x_3. From fig 3.2 it is clear that vibration would become excessive if the base excitation frequency approaches the natural frequency of the system. If the excitation frequency cannot be shifted or modified, it would be necessary to make structural modifications to the system in order to either damp or absorb the excessive vibration.

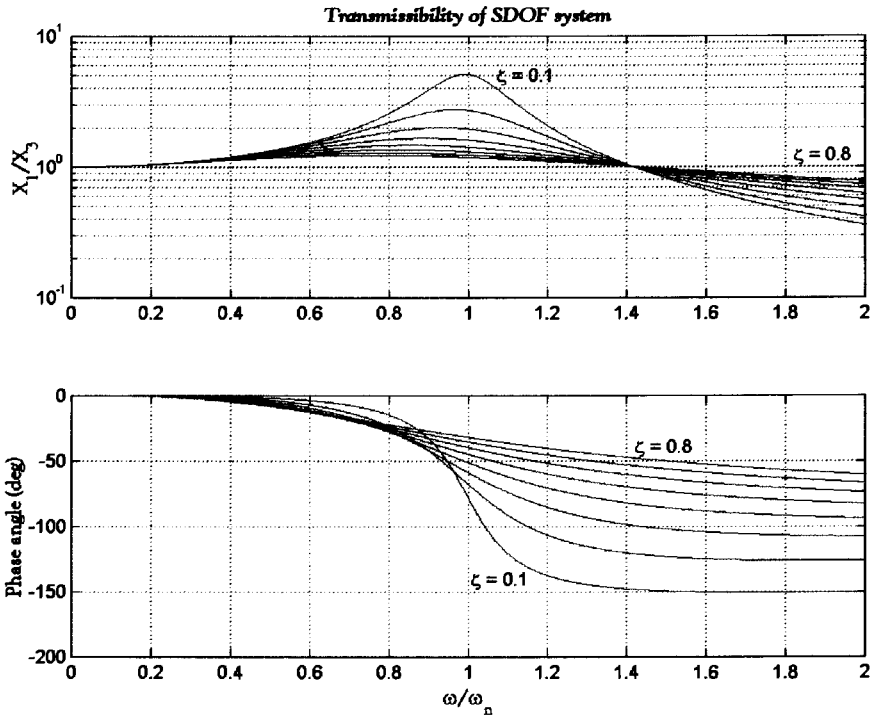

Figure 3.2: Transmissibility of SDOF system

The system can be modified as shown in Fig. 3.3.

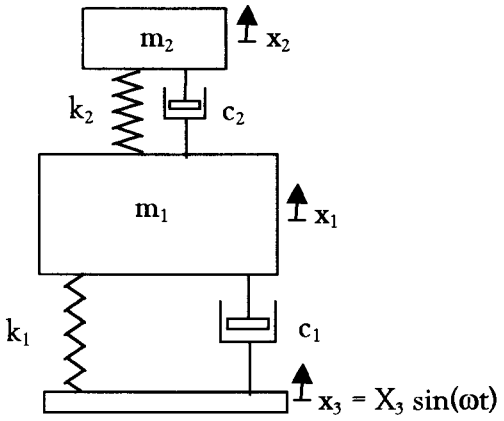

Figure 3.3: *MDOF absorber system*

The mass m_2 acts as the absorbing mass, and m_1 is the mass to be attenuated. The mathematical derivation of the transmissibility function for Fig. 3.3 can be seen in appendix B.2. The transmissibility in dimensionless form is

$$T_{13} = \frac{(1+i(2\zeta_1 r))(1-\gamma_t^2 r^2+i(2\gamma_t\zeta_2 r))}{\left[1+\left(\frac{1}{\gamma_t^2}\right)\mu-r^2+i(2\zeta_1 r)+i\left(\frac{2\mu\zeta_2 r}{\gamma_t}\right)\right]\left[1+i(2\gamma_t\zeta_2 r)-\gamma_t^2 r^2\right]-\left[1+i(2\gamma_t\zeta_2 r)\right]\left[\left(\frac{1}{\gamma_t^2}\right)\mu+i\left(\frac{2\mu\zeta_2 r}{\gamma_t}\right)\right]} \tag{3.2}$$

with

$$\gamma_t = \frac{\omega_1}{\omega_2},\ \omega_1 = \sqrt{\frac{k_1}{m_1}},\ \omega_2 = \sqrt{\frac{k_2}{m_2}} \text{ and } \mu = \frac{m_2}{m_1}.$$

The effect of the absorber can be seen in the graph in Fig. 3.4 at the r = 1 region. This absorber has been tuned to attenuate at the original SDOF system's resonant frequency. To achieve this, the zeros of the system must be found, in other words, the numerator of the transmissibility function (eq. 3.2) must equal to zero. The blue line in Fig. 3.4 represents the tuned absorber, while the red line represents an ordinary SDOF system. As the figure shows, the transmissibility function at the target frequency has been minimised to almost zero.

The natural frequencies and corresponding mode shapes of the system can be evaluated as described in appendix B.2.

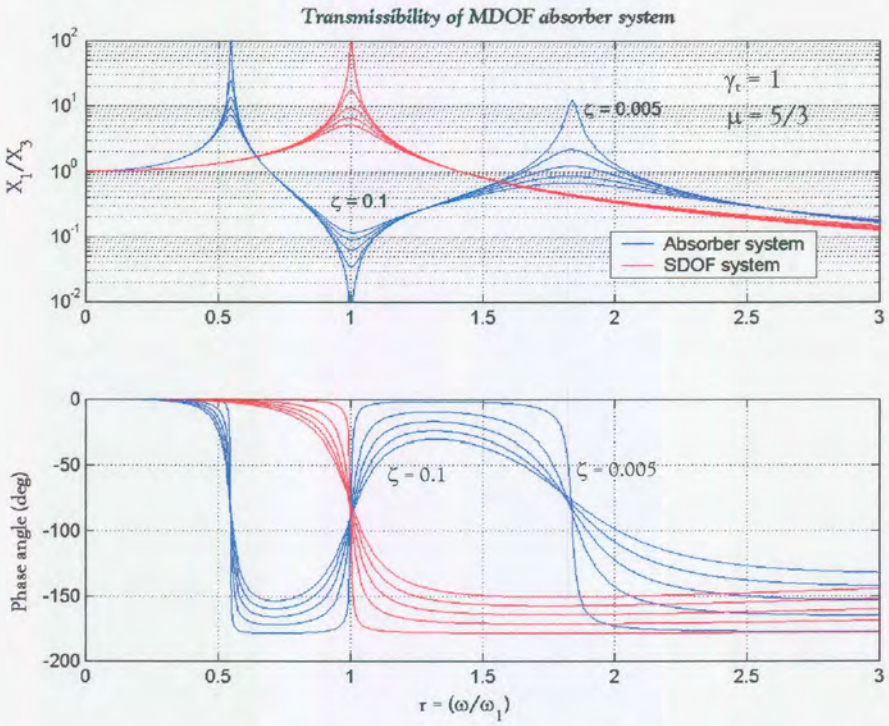

Figure 3.4: Transmissibility of MDOF absorber system

Fig. 3.5b clearly illustrates the isolation frequency concept (The red dashed figures are the static positions and the black figures represent the dynamical status of the elements). All the energy at $\omega/\omega_1 = 1$ is absorbed by m_2, while m_1 is basically not moving. A node point is thus introduced into the system. The two modes at the natural frequencies of the system are shown in Fig. 3.5a and c

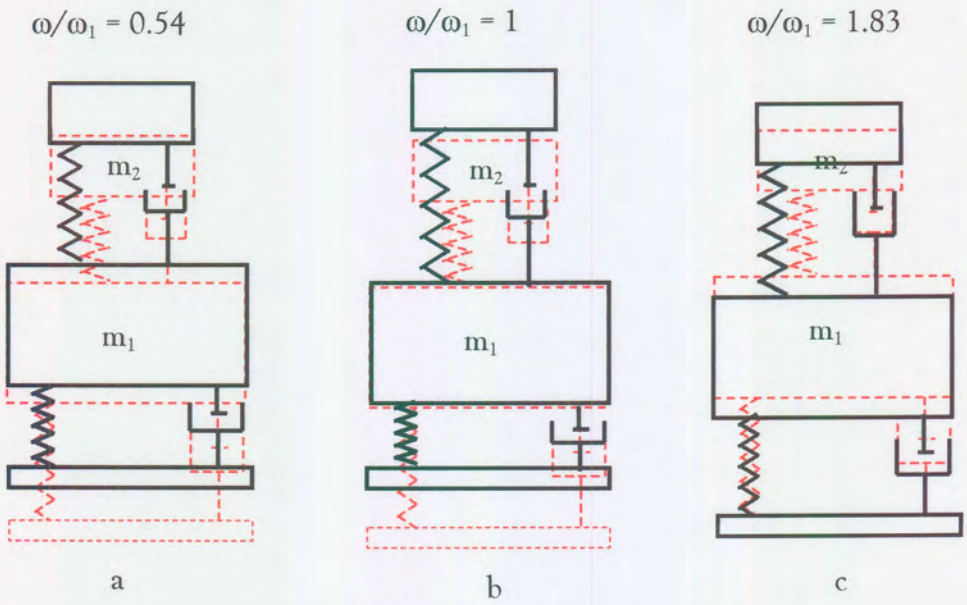

Figure 3.5: Illustration of the mode shapes

The relative movement between m_1 and m_2 is shown in Fig. 3.6.

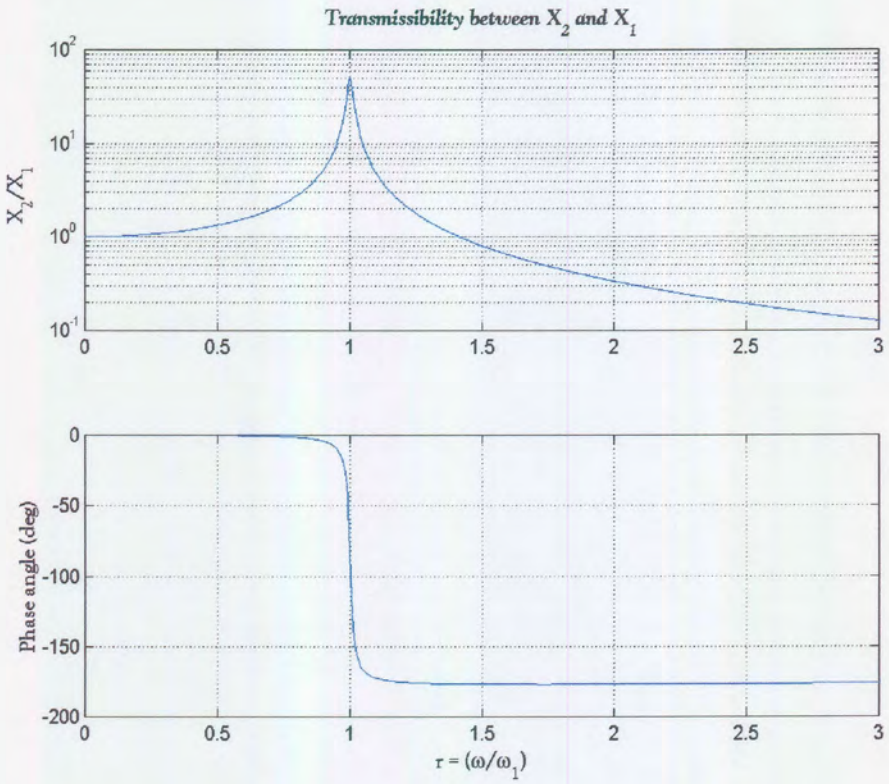

Figure 3.6: Relative movement between m_1 and m_2

The transmissibility

$$T_{12} = \frac{X_2}{X_1} = \frac{1 + i(2\gamma_t \zeta_2 r)}{1 - \gamma_t^2 r^2 + i(2\gamma_t \zeta_2 r)} \tag{3.3}$$

Fig. 3.6 illustrates the phase jump that occurs in the isolation frequency region (ω/ω_1 = 1). The increase in energy absorption at r = 1 is also clearly visible.

From the above-mentioned theory, the motivation for using a vibration absorber to attenuate a certain target frequency is fairly obvious. The conventional absorber has an isolation frequency, which can be exactly tuned to any desired frequency. If a system is subjected to a force with an excessive amount of vibration energy at a specific frequency, an absorber can be tuned to eliminate the vibration at that frequency. An absorber can also be used to change the system's natural frequencies. This would be necessary when the excitation frequency is close to one of the system's natural frequencies.

Although the theoretical absorber has quite a few problems associated with it which will be discussed later in chapter 3.4, the theoretical advantages of the implementation of such an absorber is clear.

3.3 Theoretical lever absorber (DAVI)

The theoretical lever absorber, also known as the Dynamic Anti-resonant Vibration Isolator (DAVI), is a vibration absorber that implements a lever principle which enables it to isolate a stiff system at relatively low frequencies. The system is shown in Fig. 3.7.

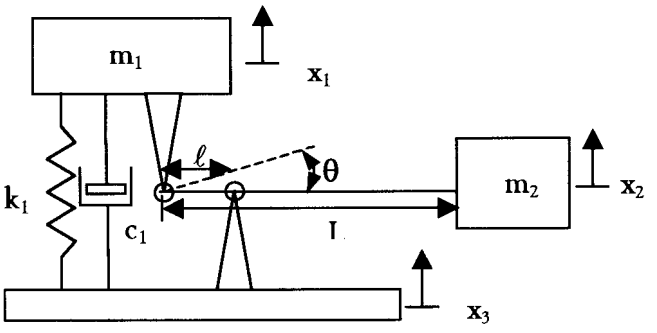

Figure 3.7: Model of DAVI

The system is excited through means of base excitation x_3. The mass m_2 acts as the absorbing mass and operates via the lever ratio ℓ/L. Because of the fact that all the equations are derived for transmissibility and not frequency response functions, the isolation frequency in terms of transmissibility, is not necessarily the same frequency as the anti-resonant frequency. The same applies for the frequency of maximum transmissibility and the natural frequency. For this reason, the terms isolation frequency, and MT frequency (maximum transmissibility) will be indicated with the symbols ω_I and ω_{MT} respectively. The transmissibility of the DAVI system is derived in appendix C and shown in figure 3.8.

$$T_r = \frac{1+i(2\zeta r)-\gamma^2 r^2}{1+i(2\zeta r)-r^2} \qquad (3.4)$$

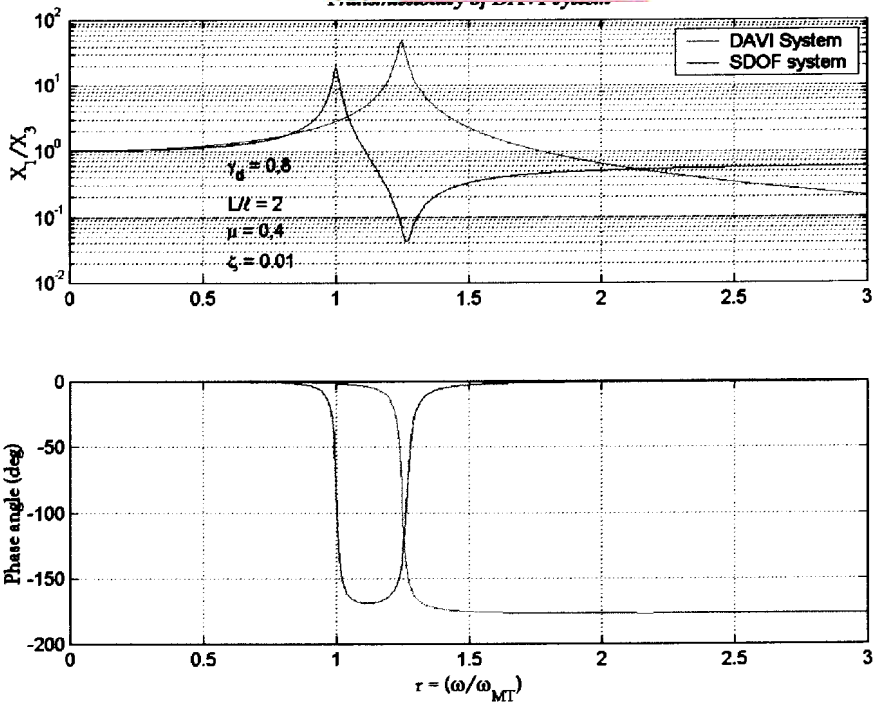

Figure 3.8: Transmissibility of DAVI system

where $\zeta = \dfrac{c_1}{2M_{eq1}\omega_{MT}}$, $r = \dfrac{\omega}{\omega_{MT}}$, $\gamma = \dfrac{\omega_{MT}}{\omega_1}$ and $M_{eq1} = m_1 + \left(\dfrac{L}{\ell} - 1\right)^2 m_2 + \dfrac{I}{\ell^2}$.

The graph in Fig. 3.8 compares the DAVI system to the SDOF system. It is important to notice that with a lever ratio of only two, and a mass ratio, μ, that much lower than the conventional absorber, the DAVI still manages the same isolation frequency. This is what makes the lever type absorber so attractive.

Flannelly (1963), reported some interesting parameter variations:

1. ω_{MT} will be lower than ω_1 when:
   a) $L = 0$
   b) $L < 0$
   c) $L > 0$ and $1 + \dfrac{m_1}{m_2} > \dfrac{L}{\ell}$
   d) $L > 0$ and $L = \ell$
2. There will not be an isolation frequency when either:
   a) $I = 0$ and $L < \ell$ and $L > 0$
   b) $I \neq 0$ and $L > 0$ and $L < \ell$ and $\kappa^2 = L \cdot (\ell - L)$

where κ is the radius of gyration and I is the moment of inertia of the bar about its own centre of gravity.

3. ω_{MT} will be higher than ω_1 when:
   a) $L > 0$ and $\dfrac{L}{\ell} > 1 + \dfrac{m_1}{m_2}$
4. The transmissibility will be unity at all frequencies when:
   a) $L > 0$ and $\dfrac{L}{\ell} = 1 + \dfrac{m_1}{m_2}$

This report also states that for ω_{MT} to be higher than ω_I, a DAVI that is somewhat heavy would be the outcome, because the absorber mass, m_2, must be high for a high lever ratio.

Fig. 3.9 shows the relative movement between m_1 and m_2. Looking at the motion at ω_I, it is clearly visible that m_2 absorbs all the energy, and m_1 is virtually not moving.

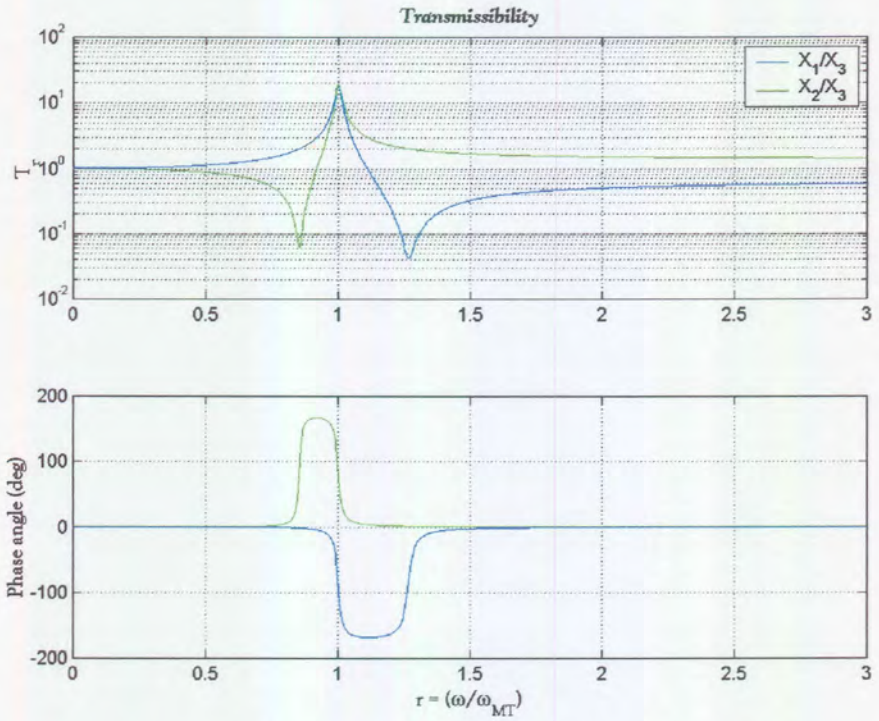

Figure 3.9: Transmissibility comparison – X_1/X_3 and X_2/X_3

A graphical representation in Fig. 3.10 of the response at ω_{MT} and ω_I explains a little more. Only the base and the absorbing mass are moving at the isolation frequency, while m_1 is also moving at the MT frequency.

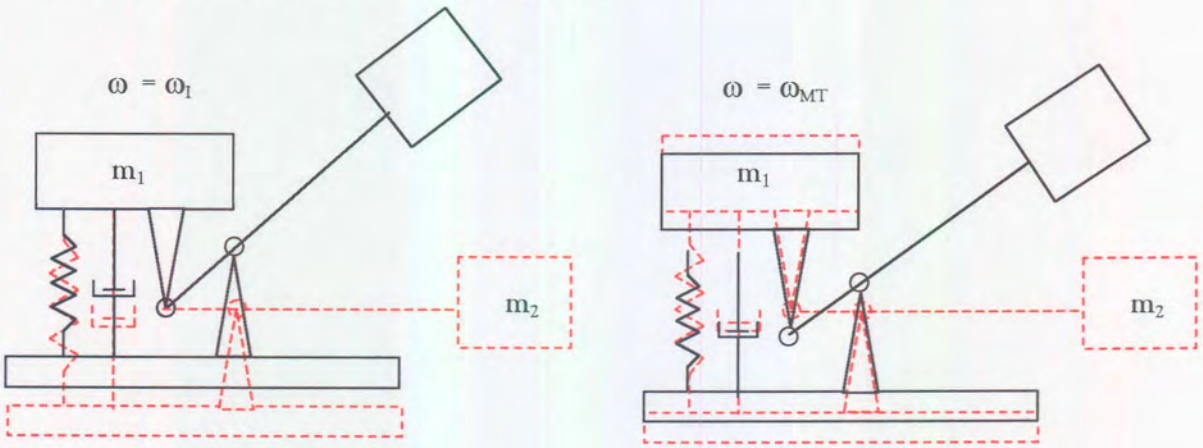

Figure 3.10: Movement of DAVI system

3.4 Concept generation

a) Prerequisites for concepts

A few concepts have been generated to implement on rock drills to reduce the vibration transferred to the handle. One particular problem is the fundamental frequency of the drill, which ranges approximately between 25 and 60 Hz, depending on the type of drill used. This operating frequency fluctuates, and is a function of the hardness of the material that is drilled, and fluctuations in the pneumatic line pressure. The absorber must thus be actively, semi-actively or passively controllable, and must be able to compensate for operating frequency changes of about 10%. Some of the concepts are feasible, and others are not so feasible. The design characteristics that have been used to evaluate the concepts are:

- The isolation frequency for a system with a spring rate of 100 kN/m should be in the 30-60 Hz region.
- Can the concept be practically implemented into a drill?
- Should it prove to be necessary, can the concept be actively, semi-actively or passively controlled?
- The amount by which the drill as it is at the moment has to be changed to implement the concept.
- The cost of the concept, should it be implemented.
- The durability and robustness of the handle.

The system must be very stiff, and the amount of mass that can be implemented is limited. The drill must still function just as well with the absorber, and drill efficiency cannot be sacrificed. To change the design of the drill too much would not be cost effective. The cost of the absorber itself must be minimised. The operating conditions of such a drill are very unfavourable, and the absorber must be just as robust as the drill itself. Although durability is not necessarily a primary concern in this thesis, it will always be a factor to keep in mind in the selection of the concept, the design of the prototype and the material selection. Maintenance procedures should not become more complex as a result of the addition of the absorber handle. The handle should also comply with the latest legislation governing mine equipment.

b) Concepts

Conventional absorber

The schematic representation of the conventional absorber can be seen in Fig. 3.3. Although the conventional absorber has already been discussed earlier in this document, it would be worthwhile to calculate transmissibility with typical system design parameters to be able to compare its performances with the rest of the concepts.

The design parameters m_1, k_1 and c_1 are going to be calculated later in the document (chapter 4), but approximations can be made to evaluate and compare the performances of the concepts. The target isolation frequency should be between 25 and 35 Hz. The corresponding values of the absorbing masses will then be compared to evaluate absorber performance. The value of these parameters will be taken as the following throughout the concept evaluation:

$m_1 = 3$ kg (Mass of handle plus apparent hand mass)

k_1 = 100 kN/m (Design stiffness)
c_1 = 100 Ns/m

The transmissibility plot of the conventional absorber with values m_2 = 4 kg, k_2 = 100 kN/m and c_2 = 50 Ns/m , can be seen in Fig. 3.11.

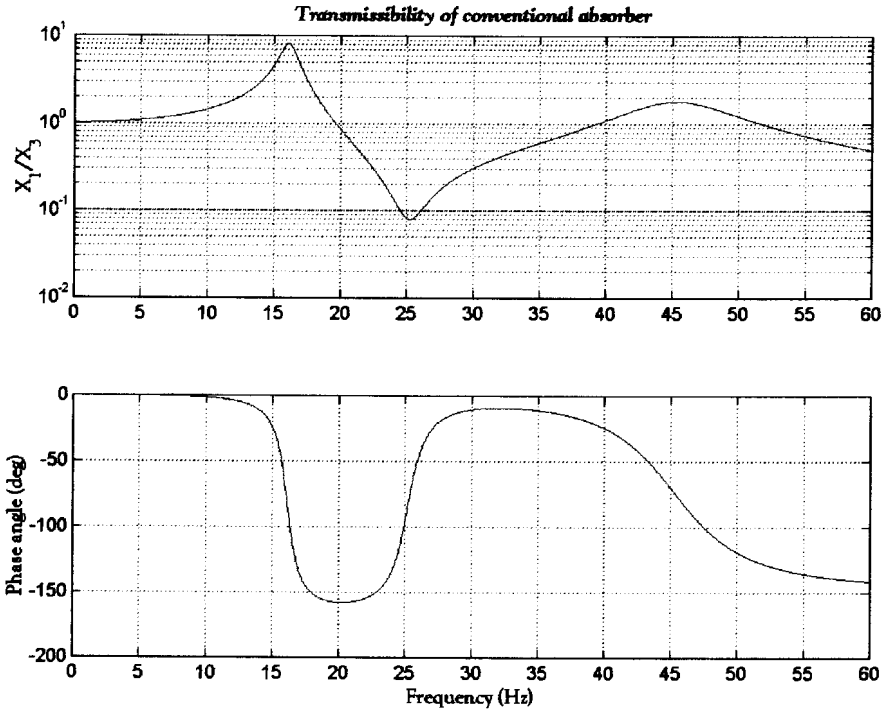

Figure 3.11: Transmissibility of conventional absorber with design parameters

The isolation frequency of the system is situated at the 25 Hz region, and the natural frequencies are situated at 16 and 45 Hz. Although both the spring rates are reasonable values, the mass of the absorber, m_2 is too high. The system would be too heavy, and that would prove to be unacceptable on a portable hand tool. Another problem is that two resonance frequencies would have to be dealt with in the control phase, which would definitely not be ideal. Control on this concept should not be too difficult, if both spring rates can be controlled without much trouble. The practical implementation of this concept on a rock drill might also prove to be cumbersome. The concept does not have any expensive components, although the implementation might be more expensive if it is taken into account that the absorbing mass would have to be guided in the direction of the axes of attenuation. The concept would probably be very robust and durable due to the simplicity of its design.

Theoretical lever absorber (DAVI)

A schematic diagram of the DAVI can be seen in Fig. 3.7. As previously mentioned this absorber works through a lever principle to establish a low isolation frequency with relative high spring rates. A transmissibility plot of the system with design parameters as discussed in the previous evaluation is shown in Fig. 3.12. The absorber mass, m_2, is 0.5 kg, and the lever ratio is 3.23. f_{MT} of the configuration is 20.7 Hz, and the f_1 is 25 Hz.

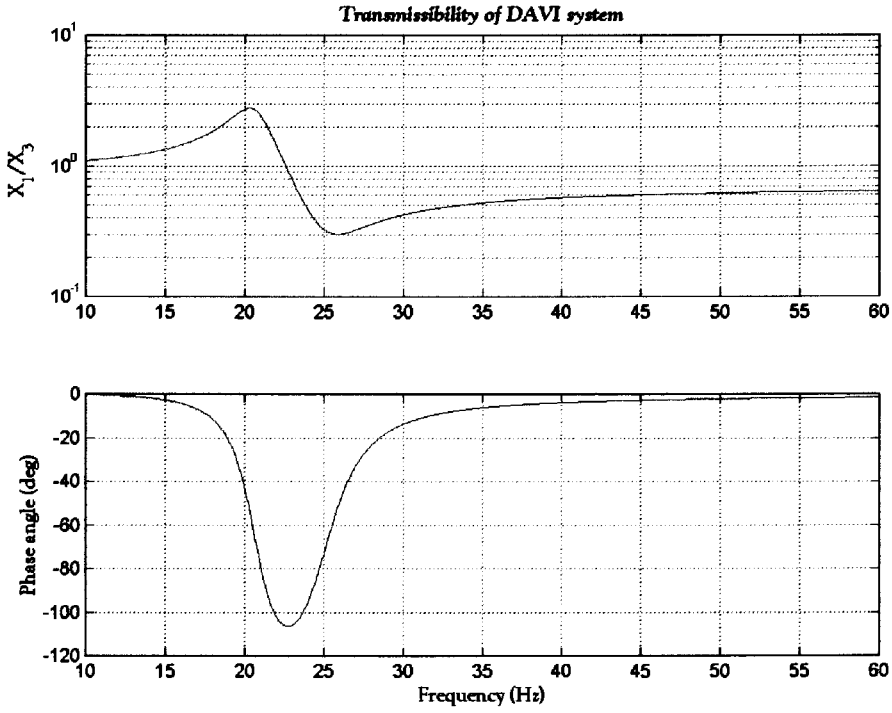

Figure 3.12: Transmissibility of DAVI system with design parameters

This configuration has a high stiffness and a low absorber mass, which makes it very attractive. The transmissibility is also below unity from ω_1 upwards on the frequency spectrum. The damping in the system is the cause for the relative wide band of attenuation in the isolation frequency region. This is a positive occurrence with regard to the control issue, because ω_1 in this instance does not have to be actively controlled. Normally damping is not favourable to the functioning of absorbers, but as far as the control system is concerned, it assures that only compensation for the natural frequency is necessary.

The DAVI can be designed in such a way that ω_1 is lower than ω_{MT}, but as previously mentioned, this type of DAVI would be a bit heavy. In this case, the transmissibility function would be more than unity after the isolation frequency on the frequency spectrum, and this frequency would probably have to be actively controlled to compensate for changes in operating frequency.
(See fig 3.21.)

The DAVI would be quite easily controllable by just adjusting the lever ratio. The practical implementation of the DAVI on a rock drill would be difficult, if not completely impractical. Probably the biggest setback of the DAVI is the number of mechanical bearings it has. This would make maintenance on such an absorber very frustrating on a very robust and relative maintenance insensitive rock drill. The DAVI would probably be not much more expensive than the conventional absorber to manufacture.

Nodal beams

A nodal beam is a beam that is supported on one or more places on the beam, and the system to be isolated is mounted on the beam in such a way that the displacement of the mounting point is zero. The nodal beam configuration is shown in Fig. 3.13.

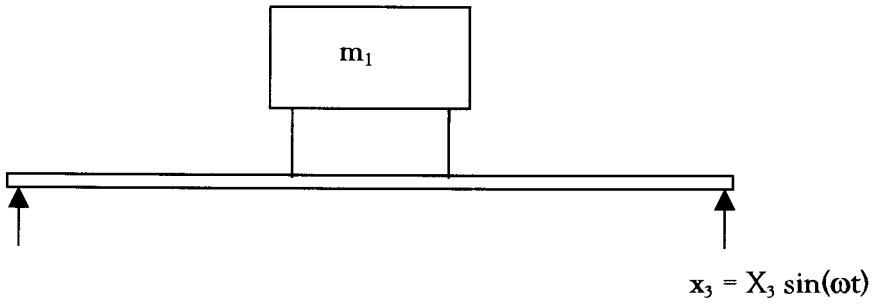

Figure 3.13: Nodal beam configuration

The mass to be isolated, m_1, is mounted on the beam on two node points. The beam is excited on its end points as shown in the figure. The location of the two node points can be determined by looking at the mode shapes of the beam in Fig. 3.14. The derivation of the mode shapes can be seen in appendix D.

The graph represents a nodal beam with a length of 0.3 m and a spring rate of 101 kN/m. A feasible option would be to use the nodal beam in a configuration equivalent to the first graph in fig 3.14. The mass to be isolated then has to be connected to the beam at the co-ordinates [0.05,0.5] and [0.25,0.5].

The frequencies corresponding to the various mode shapes are shown in Fig. 3.14. The frequency of the first mode is 183 Hz. This is clearly too high, and although it would not be impossible to bring the frequency slightly down by applying an axial force to the beam, it would definitely not be easy to get the frequency to 30 Hz. For this reason nodal beams have not been considered as an option for the purposes of this study. The simplicity of the nodal beam configuration ensures that it would not be very expensive, but it is debatable how practical the implementation would be.

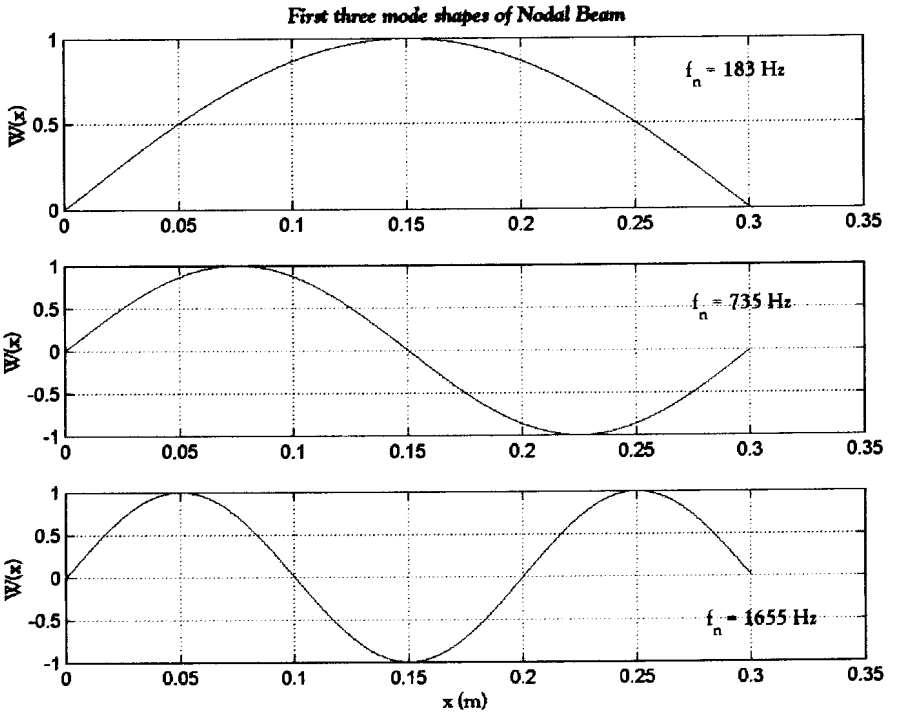

Figure 3.14: First three mode shapes of a nodal beam

LIVE System

The LIVE (Liquid inertia vibration isolator) system is the hydraulic equivalent of the theoretical lever absorber (DAVI). The system uses area ratios to accelerate the liquid, which acts as an inertia mass to establish an isolation frequency. The schematic representation of the system is shown in Fig. 3.15, and the transmissibility of the system is shown in Fig. 3.16.

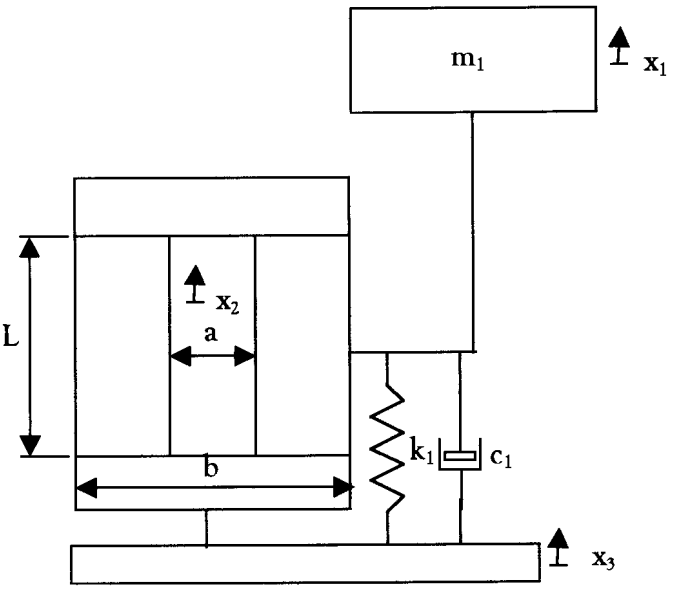

Figure 3.15: The LIVE system

The isolated mass m_1 is connected to the port, and the moving base is connected to the housing. The area ratio, a/b, is a very important variable when the isolation frequency

placement is considered. The port length, L, has a less noticeable effect on the isolation frequency placement. The derivation of the transmissibility function can be seen in appendix B.5.

$$T_r = \frac{X_1}{X_3} = \frac{k_1 + ic_1\omega - M_{eq3}\omega^2}{k_1 + ic_1\omega - M_{eq1}\omega^2} \tag{3.5}$$

where

$$M_{eq1} = m_1 + \left(\frac{b-a}{a}\right)^2 m_2$$
$$M_{eq3} = \left(\frac{b(b-a)}{a^2}\right) m_2 \tag{3.6}$$

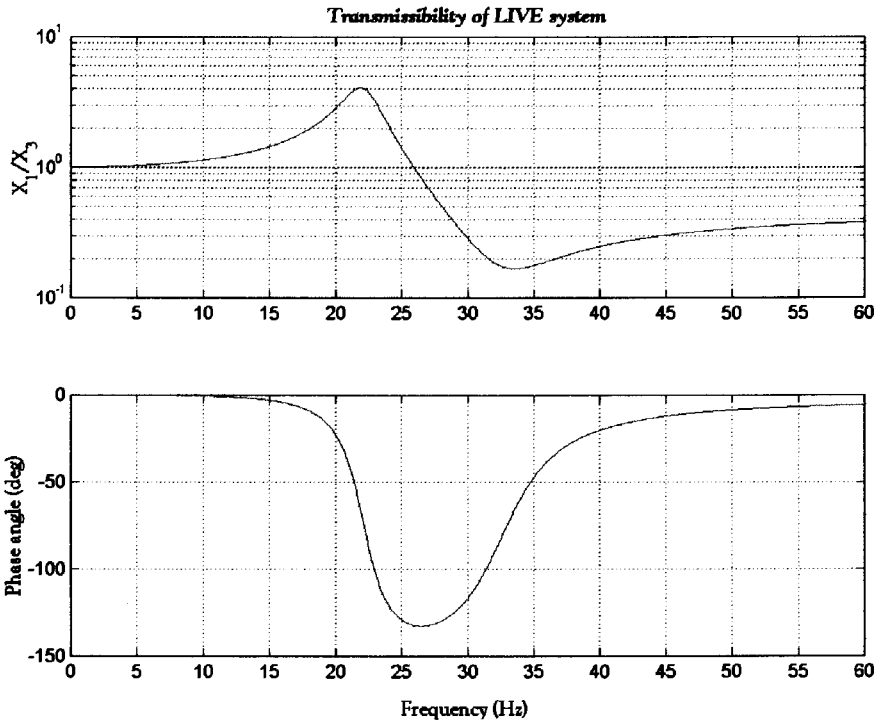

Figure 3.16: Transmissibility of LIVE system

The design parameters for the system are the same as defined for the first concept with an area ratio b/a of 11 and an absorber mass of 0.0212 kg.

The LIVE system does not have any bearings or any other moving parts that need to be lubricated. The system is compact, and does not have any external moving masses. Control of the system would probably be a little difficult, but definitely not impossible. The MT frequency placement of this configuration is also rather troublesome.

Implementation of this concept on a rock drill would not be too difficult, while maintenance would be very favourable, should the rubber, which acts as a seal and a spring, prove to be durable.

Alternative liquid absorber

This concept also functions on the fluid inertia principle, but the flow constriction occurs on the outside. A schematic representation of the concept can be seen in Fig. 3.17. The transmissibility function of the system is derived in appendix F, and can be seen in fig 3.18.

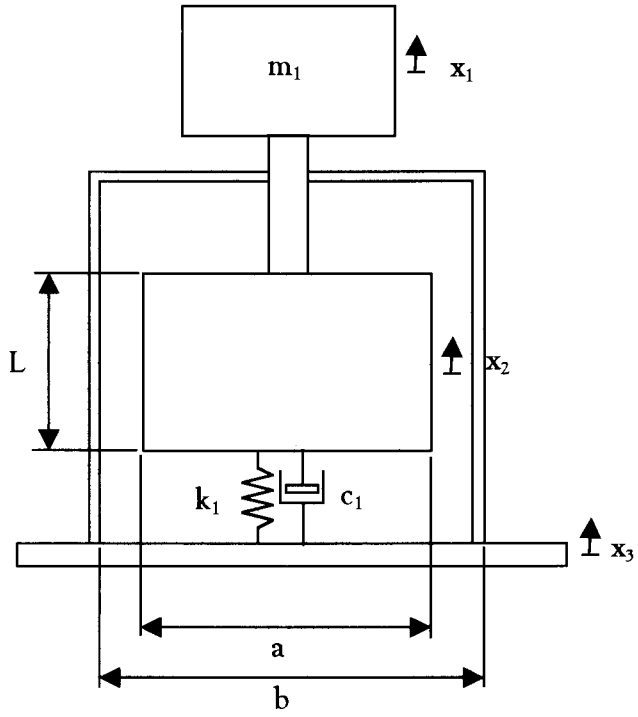

Figure 3.17: The alternative liquid absorber concept

The only difference between this concept and the previous one is a few geometrical factors. MT frequency placement is also unfavourable, and control of the isolation frequency may be difficult. The concept is not very practical in terms of mounting on a rock drill, and guiding bushes may shorten maintenance procedures. The absence of rubber as the elastic element will reduce damping.

The area ratio for the plotted transmissibility function is 12, and the absorber mass is 0.0185 kg.

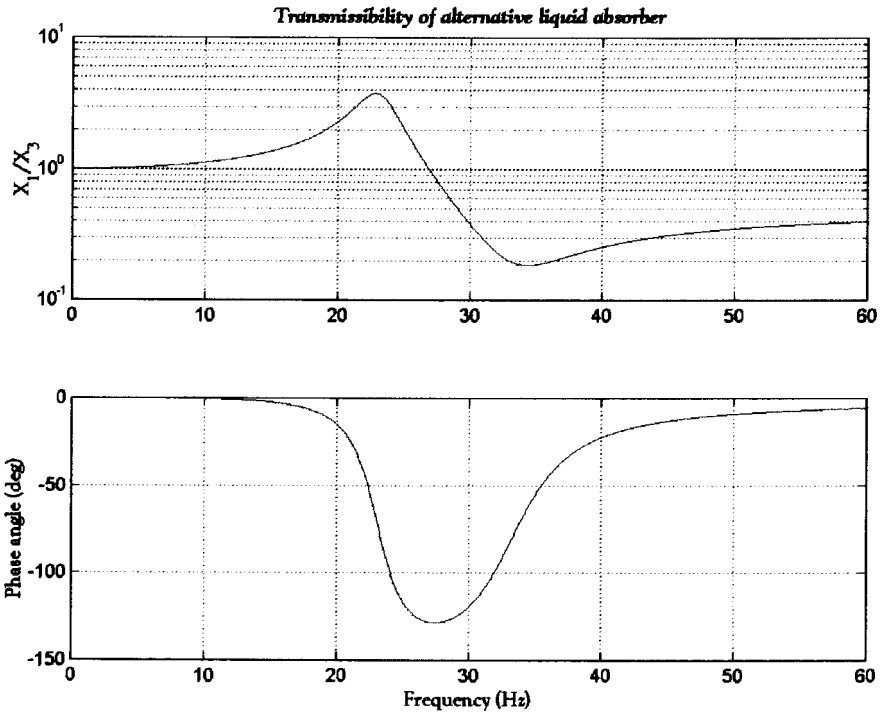

Figure 3.18: Transmissibility of alternative liquid concept

Hand arm vibration absorber

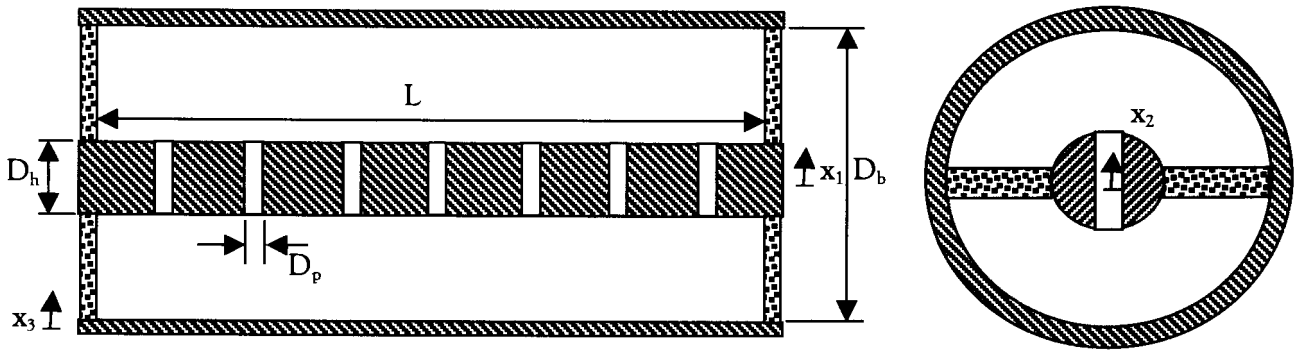

Figure 3.19: Hand-arm-vibration-absorber

The hand arm vibration absorber (Fig. 3.19) operates in the same way as the LIVE system, except that the axial configuration of the LIVE system has been converted into a radial configuration. Du Toit (1998) developed a similar design. Note that the handle is mounted on the shaft with the ports in, and the drill is mounted on the housing. The shaft and the cylinder are connected with rubber ends and rectangle shape rubbers to form the two fluid chambers. The transmissibility of the system looks the same as that of the LIVE system (see appendix G).

Although the radial configuration might seem more favourable for a handle, the configuration is complex, and will be difficult and expensive to manufacture. Control of ω_I might be difficult, but not impossible, while it would probably be easy to

implement this concept onto a rock drill. The most important advantage of this concept is its potential for two-dimensional attenuation, although placing of the rubber elements in such a configuration might be a bit troublesome.

Diaphragm type absorber

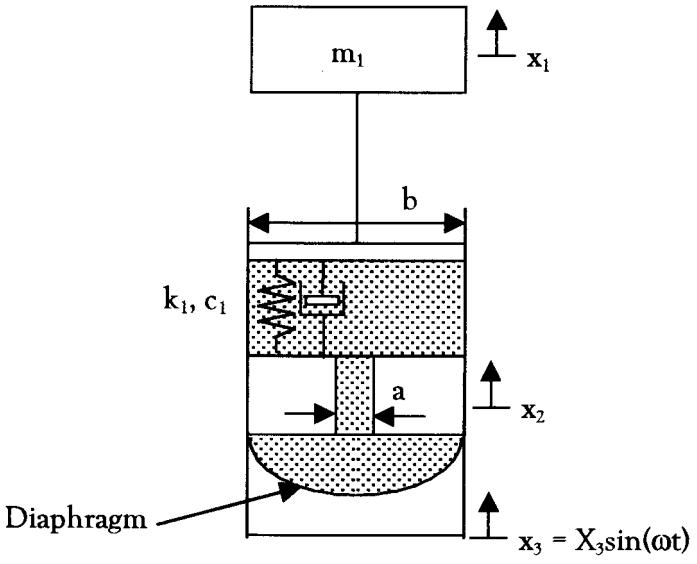

Figure 3.20: Diaphragm type absorber

This absorber also uses the fluid inertia principle with area ratios as lever advantages. The transmissibility function of the system looks the same as that of the LIVE system (see appendix H). The main difference between the LIVE system and the diaphragm type absorber is the fact that the LIVE system has two fluid chambers, while the diaphragm constitutes the second chamber of the diaphragm type absorber. Of all the fluid inertia type absorbers, this system will probably be the easiest to control. The stiffness of the system can be varied by using different type of diaphragms or by rising the air pressure behind the diaphragm, and the port area can easily be reached from the outside.

The system is relatively simple, and would thus be easy and cheap to manufacture. It would be the smallest in size and in mass of all the absorbers, and the mounting of the system onto a rock drill would not be too cumbersome. Durability of the diaphragm will always be a problem, and should easily be replaceable to make maintenance of the concept acceptable.

c) Isolation frequency placement

A very important aspect is that of the isolation frequency placement relative to the MT frequency. At first it would appear to be very advantageous to have ω_I before ω_{MT} on the frequency spectrum (Fig. 3.21). The reason being that when the operator starts the drill, the fundamental frequency of the drill changes from zero to the value under normal operating conditions in a few seconds. This means that if ω_{MT} is before ω_I, the

drill will have to go through ω_{MT} when it is started. The operator may find the drill difficult to control, especially when the first part of the hole is being drilled.

A problem with this configuration, as shown in Fig. 3.21, is that the transmissibility function is more than unity over the rest of the frequency band. This means that vibration at all the frequencies above ω_I is amplified.

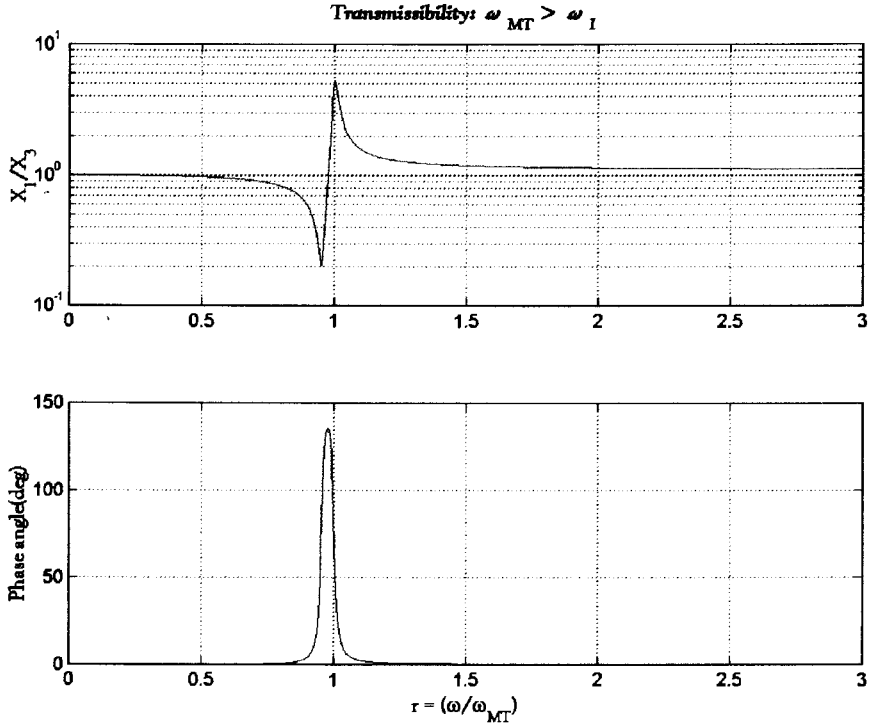

Figure 3.21: MT frequency > Isolation frequency

The second scenario is shown in most of the transmissibility functions plotted thus far; ω_I is after ω_{MT} on the frequency spectrum. The first problem mentioned above would have to be compensated for in some way by the use of a control system. The second problem mentioned above is not associated with this scenario, as seen in Fig. 3.18. The transmissibility function is less than unity after ω_I. This means that some attenuation is still achieved for frequencies higher than ω_I.

To evaluate the possibilities of where the ω_I can be placed, one has to take another look at the theoretical lever absorber (DAVI). Flanelly states in his article that ω_{MT} will be lower than ω_I when:

a) $L = 0$
b) $L < 0$
c) $L > 0$ and $1 + \frac{m_1}{m_2} > \frac{L}{\ell}$
d) $L > 0$ and $L = \ell$

where L/ℓ is the lever ratio.

He also states that ω_{MT} will be higher than ω_1 when:

$$L > 0 \text{ and } \frac{L}{\ell} > 1 + \frac{m_1}{m_2}$$

The mathematics for the fluid absorbers is basically the same as that of the DAVI, and these statements will also be applicable to the fluid absorbers.

From the second statement it is clear that the lever ratio and the value of the mass m_2 must be large in order to satisfy the given equation. In the case of the fluid absorbers, the mass m_2, which is the mass of the fluid in the port, is directly proportional to the port area. In order to satisfy the equation, the value of L (b in the case of fluid absorbers) must be extremely large, and the port must also be very long. Another problem is that even when this is achieved, the ratio ω_1/ω_{MT} is just below unity, which in turn lowers the absorption level to unacceptable values. This is due to the fact that the pole and the zero influence each other.

It is thus evident that such a configuration would not be practical at all, and the better option would be to accept the fact that ω_1 will be after ω_{MT} on the frequency spectrum and that compensation for ω_{MT} will be necessary.

e) **Discussion**

The concepts presented have been critically evaluated by using elements such as cost, complexity, robustness, control complexity, etc. as criteria. The mathematics of most of the fluid inertia absorbers are basically the same, and the advantages of one over the other cannot be evaluated in mathematical terms. The one concept that deserves a lot of attention in the future is the hand arm vibration absorber. The concept probably has a lot of potential to attenuate in two dimensions, and the configuration itself is favourable for implementation on a rock drill. The complexity of this concept, especially the shape of the rubber fluid chambers, and the fact that the idea of an absorber as a rock drill has yet to be proven, ensures that this concept is not yet feasible enough.

The purpose of this thesis is to prove that the idea is feasible, and therefore it has been decided that only the axes of operation of the drill will be considered. The concept will thus be one-dimensional. In the light of that, it is clear that the last concept in the concept evaluation, the diaphragm absorber, is the most cost effective, practical, and compact.

It will be crucial to be able to verify the system's characteristics both analytically and experimentally. The concept will thus be designed in such a way that elements like the diaphragm, rubber and port will be interchangeable with other parts with different geometries and material properties. The diaphragm absorber will simplify this process, because the rubber does not have to be glued onto the port. A single rubber element can be secured to the port assembly by using the proper fastening mechanisms. The rubber element and the port can thus be very easily replaced. Table 3.1 summarises the concept evaluation.

Table 3.1: Summary of concept evaluation

	Low ω_1	Controllability	Drill interface	Cost	Robustness
Conventional	Poor	Medium	Poor	Good	Good
DAVI	Good	Good	Poor	Medium	Medium
LIVE	Good	Poor	Medium	Medium	Medium
Alt. Liquid	Good	Poor	Poor	Medium	Medium
HAVA	Good	Medium	Good	Poor	Medium
Diaphragm	Good	Medium	Medium	Good	Medium

4. Design

This chapter will deal with the accurate modeling, design of dynamical variables m, k and c, and the detail design of the diaphragm absorber. There are two basic configurations for the diaphragm absorber. These two configurations are shown in Fig. 4.1

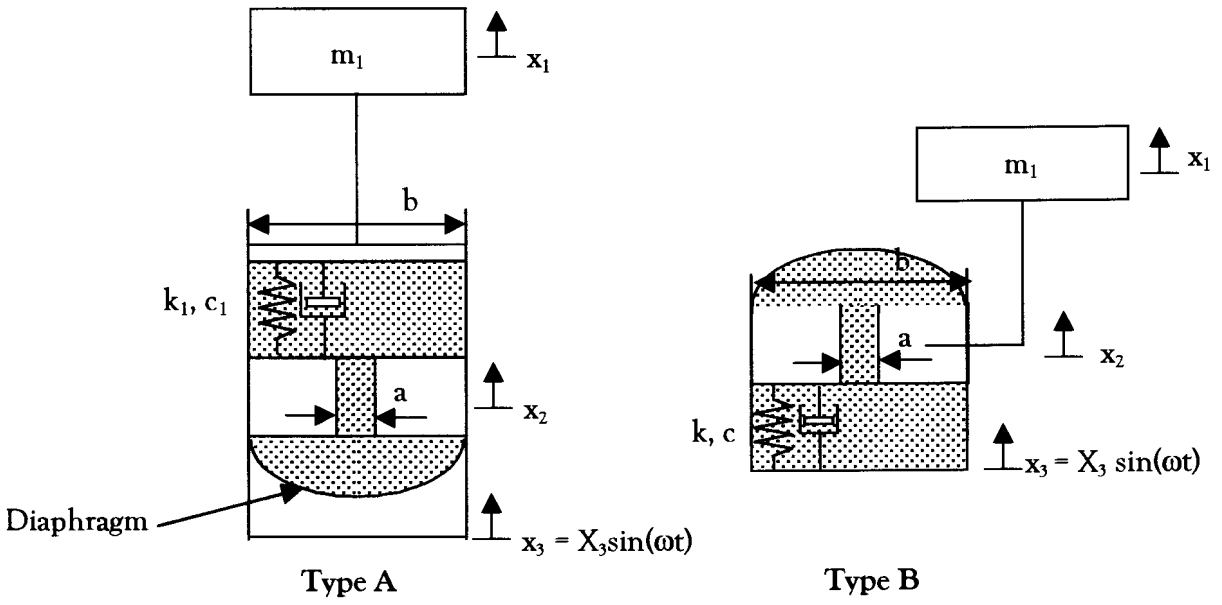

Figure 4.1: Two configurations for diaphragm absorber

The difference between the two types is that type A has the port and the diaphragm mounted on the base of the absorber, while type B has the port and the diaphragm mounted on the handle. The link between the base and the handle will be a polyurethane rubber component, which will act as both a spring and a seal.

The mathematical difference between the two configurations is very small, but notable. The continuity equation for type A as classified in Fig. 4.1 is

$$x_2 = \frac{b-a}{a}x_3 - \frac{b}{a}x_1 \qquad (4.1)$$

For type B, the same equation looks like this:

$$x_2 = \frac{b}{a}x_3 - \frac{b-a}{a}x_1 \qquad (4.2)$$

This difference only affects the MT frequency placement. The isolation frequency is the same for the configurations. ω_{MT} for the type A configuration is slightly lower than ω_{MT} of a similar type B configuration. If the increase in handle mass because of the port and the diaphragm in the case of the type B configuration is accounted for, the

transmissibility plots for the two configurations look basically the same. Fig. 4.2 depicts a comparison between the transmissibility functions of type A and B.

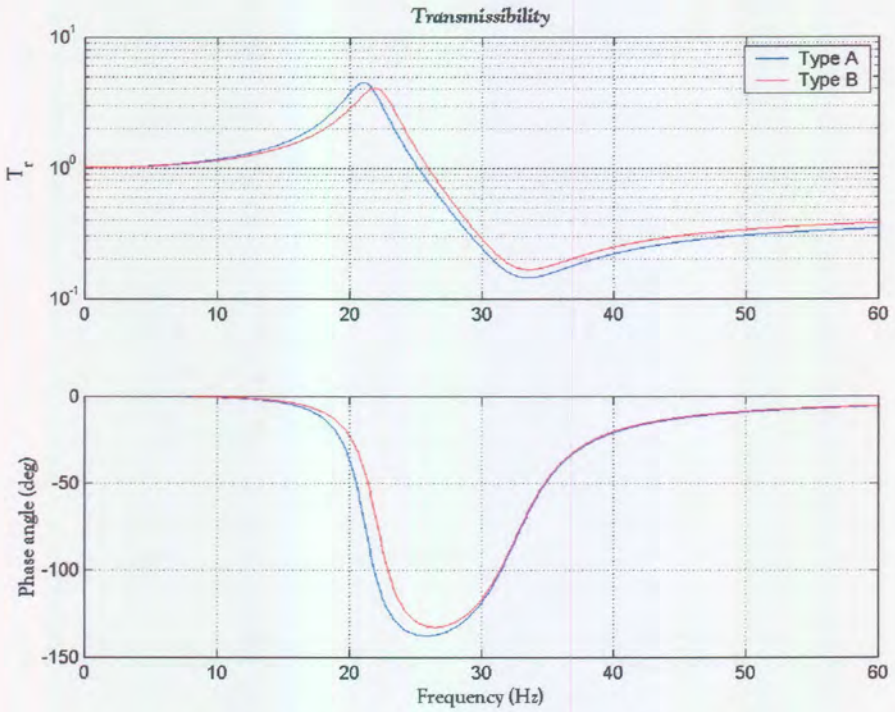

Figure 4.2: Comparison between type A and type B

The type B absorber has been chosen, because it has been much easier to create a suitable, practical and compact design with this concept. The handle-port assembly can compactly fitted onto a base with only one fluid chamber, and secured with a fewer number of bolts than the type A concept.

The absorber as shown in Fig. 4.1 now has to be translated into a physical concept that would be practical in terms of experimental evaluation and parameter characterisation. There are a few important factors that have to be mentioned before the physical concept is generated.

This physical concept must satisfy the mathematical conditions associated with the absorber diagram as shown in Fig. 4.1. The concept must be designed in such a way that the most important parameters of the design can be varied, and that a control system can be implemented after the correct functioning of the system has been verified.

At this stage it is also important to consider certain practical aspects such as the bleeding of the system to ensure that all the air is removed from the system. The system should not leak absorbing fluid at the connection surfaces.

The proposed physical concept is shown in Fig. 4.3 with the chambers containing fluid hatched with dots. It can be depicted from Fig. 4.3 that the port and the diaphragm are removable.

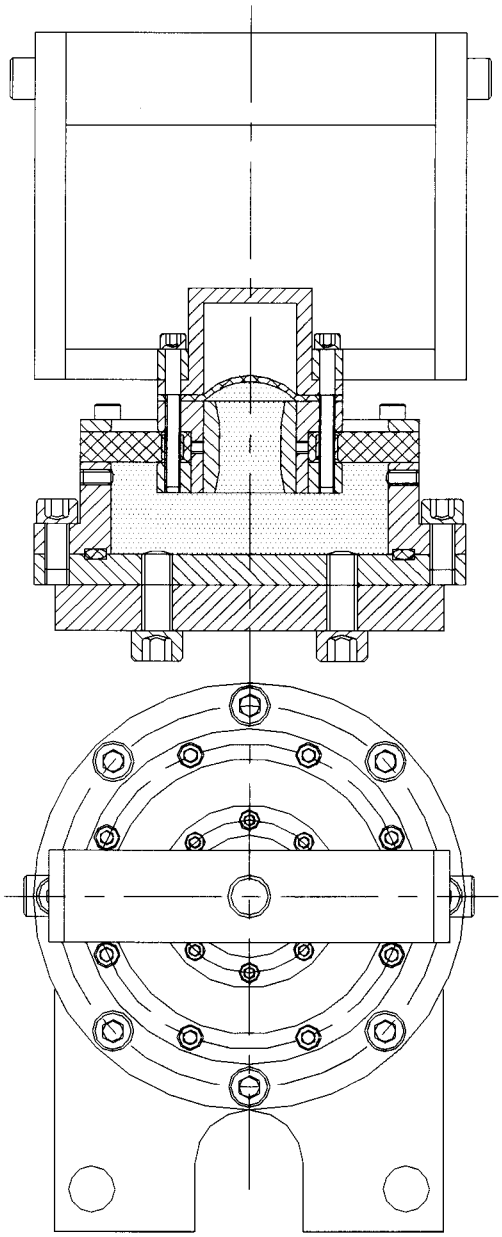

Figure 4.3: Physical concept

4.1 Calculation of stiffness of the rubber

This calculation of stiffness includes only the stiffness of the polyurethane rubber, which acts as both a spring and a seal. The geometry of the rubber is shown in Fig. 4.4.

The rubber element is an annular ring with an outside radius of r_a, and an inner radius of r_b. The thickness of the rubber is t. Q_1 is a shear force per unit length, uniformly distributed over the inner edge, resulting in a total load of $F_t=2\pi r_b Q_1$. The equation for the stiffness is (Derived in appendix I):

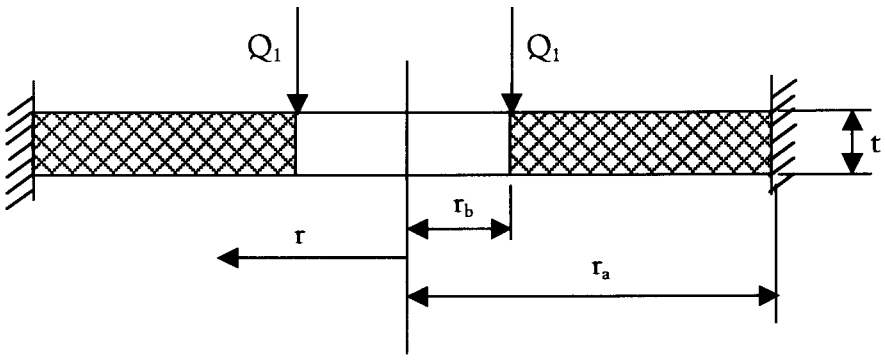

Figure 4.4: Geometry of the rubber

$$k_r = \frac{2\pi r_b}{\frac{r_b^3}{4D}(\ln(r_b)-1)+\frac{c_1 r_b^2}{4}+c_2\ln(r_b)+c_3} \tag{4.3}$$

where c_1, c_2 and c_3 are the integration constants to be solved using the boundary conditions, and D is a material constant defined as $D = \frac{Et^3}{12(1-\nu^2)}$.

The stiffness of the rubber can now be calculated for any given r_a, r_b and t. The Young's modulus for the 55 shore polyurethane is 1.4 MPa, and the Poisson ratio is 0,48. In section 4.5 of this chapter, the optimum values of the critical parameters will be determined from a structural dynamic point of view. The thickness of the rubber will then be determined for a design value of k_r.

4.2 Calculation of Damping

The damping calculation basically includes two mechanisms of damping. The structural damping of the polyurethane rubber and the damping caused by the pressure losses due to fluid flow.

The method used to implement damping is to write the equation of motion in the following way:

$$M_{eq1}\ddot{x}_1 + C_{eq1}\dot{x}_1 + kx_1 = M_{eq3}\ddot{x}_3 + C_{eq3}\dot{x}_3 + kx_3 \tag{4.4}$$

The two C_{eq} variables in eq (4.4) are equivalent damping constants that include both fluid and structural damping:

$$C_{eq} = c_{structural} + c_{fluid} \tag{4.5}$$

The structural damping is a function of frequency, stiffness and a structural damping coefficient β. The equivalent viscous damping term for structural damping is (Rao, 1995: 224)

$$c_{structural} = \frac{\beta k}{\omega} \tag{4.6}$$

where k is the stiffness of the system.

The fluid damping is more complex, and is non-linear because of the fact that the damping constant is a function of the velocity of the fluid in the port, $\dot{x}_2$. It is important to realise that the calculation of the damping coefficient is only an approximation to be able to see the effects of different fluids as a working fluid on the damping coefficient. The calculation of the fluid damping coefficient will not be used for the fine-tuning of geometrical parameters, but only as a general guide. The derivation of the fluid damping is shown in appendix J.

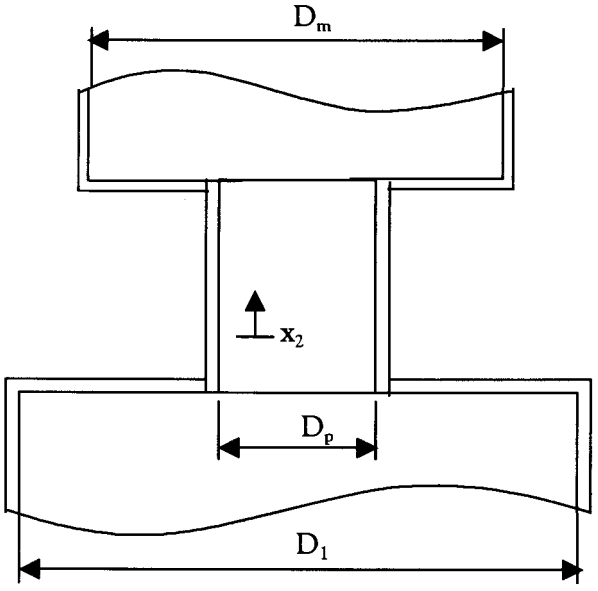

Fig. 4.5: Approximated model for the damping calculation

The fluid damping is calculated by approximating the system as a fluid moving through an orifice, as shown in Fig. 4.5.

The fluid damping that has been taken into account is the wall shear damping and the entrance and exit pressure drops due to sudden contraction and expansion. An equivalent damping coefficient has been calculated by using an energy method presented by Rao (1995, 227).

The resulting equations are complex, and can only be solved by numerical iteration. The two unknowns in the system are the port displacement and velocity, for which initial values are guessed. The next step is to solve the dynamical system numerically, and average values of x_2 and $\dot{x}_2$ are substituted back into the original governing fluid equations. The iteration is completed when the system has converged to a certain specified error.

4.3 Calculation and discussion of hand impedance

There are various methods to mathematically account for the effect of the human hand on the system (see Lundström *et al.*, 1988; Thomas *et al.* 1996). These methods involve the calculation of equivalent mass, stiffness or damping coefficients. The human hand-arm system is very complex, and although it would be possible to measure all the relevant parameters of one particular person, results of such measurements will differ from person to person. One will probably find that the results for one particular person vary from day to day. To analyse and accurately predict hand impedance would be a study of its own, and the facts mentioned above imply that there is no general accurate solution to the hand impedance problem.

Griffin (1990:542) suggests the apparent mass theory, which basically predicts the equivalent mass of the hand at certain frequencies. The graph given by Griffin is shown in Fig. 4.6. (Please note that the axes definition of Fig. 4.6 differs from the definition in chapter 3)

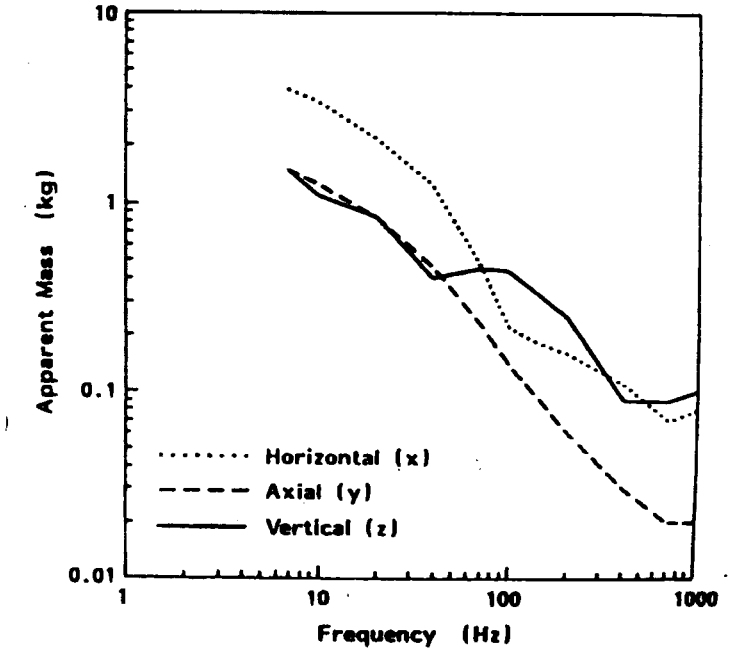

Figure 4.6: Apparent mass for hand-arm system (Griffin: 1990, 542)

This model will be accepted for the purpose of thesis. The hand-arm apparent mass, which will only affect the MT frequency of the system, will be assumed to be the axial value on the graph in fig 4.6 that corresponds to 30 Hz. Factors that will influence the value of the apparent mass are grip force, arm angle, push and pull forces and vibration level. The vibration level affects the apparent mass value to a much lesser extent than the other factors.

It is important to realise that the desired quantity is the vibration level entering the hand, and not the vibration level that is transmitted through the hand-arm system to the rest of the body. This is the reason why the apparent mass theory is sufficient for

the purposes of this study. The goal is to reduce Hand-Arm-Vibration, and Whole-Body-Vibration effects will thus not be considered.

4.4 Sensitivity study of variables on minimum displacement transfer

It is very important to optimise the system to ensure that minimum transfer between the rock drill and the operator hand is accomplished. The displacement transfer function is derived in appendix E, and looks like this:

$$T_r = \frac{k_1 + ic_1\omega - M_{eq3}\omega^2}{k_1 + ic_1\omega - M_{eq1}\omega^2} \tag{4.7}$$

where

$$M_{eq1} = m_1 + \left(\frac{b-a}{a}\right)^2 m_2$$
$$M_{eq3} = \left(\frac{b(b-a)}{a^2}\right) m_2 \tag{4.8}$$

For a sensitivity study, it is often convenient to rewrite eq. (4.7) in non-dimensional form. The result looks like this:

$$T_r = \frac{1 + i(2\zeta r) - \gamma_d{}^2 r^2}{1 + i(2\zeta r) - r^2} \tag{4.9}$$

where

$$\zeta = \frac{c_1}{2M_{eq1}\omega_{MT}},\ r = \frac{\omega}{\omega_{MT}} \text{ and } \gamma = \frac{\omega_{MT}}{\omega_1}. \tag{4.10}$$

The first, and probably most important factor, is the damping coefficient. A system with a high damping coefficient will have very low absorption, and vice versa. Fig. 4.7 illustrates this phenomenon by plotting eq. (4.9) for different damping values.

The figure shows that the minimum transmissibility is a definite function of the damping ratio, ζ.

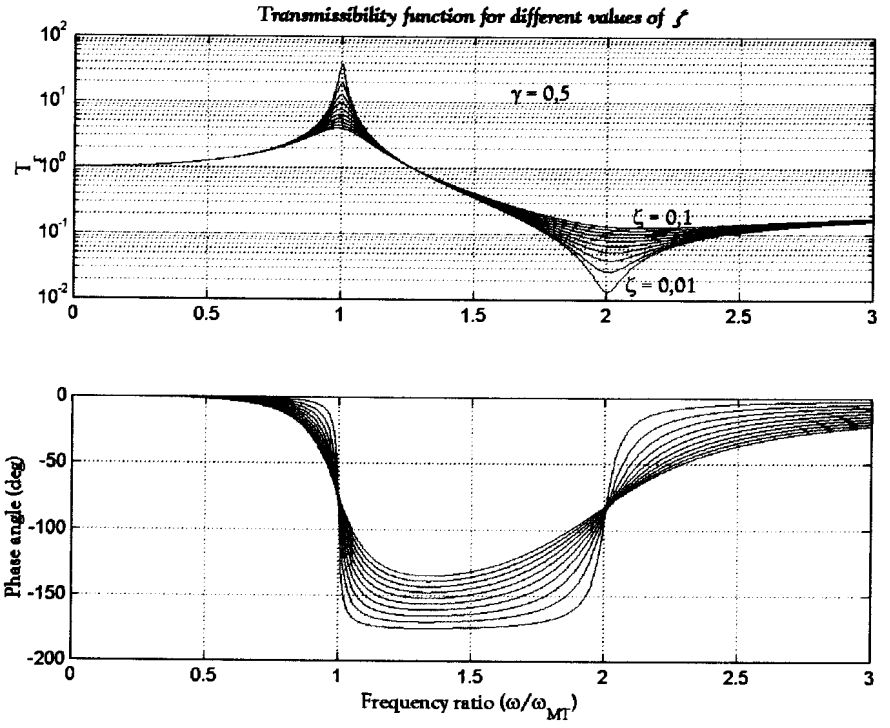

Figure 4.7: Transmissibility function for different values of ζ

Another variable for which the minimum transmissibility is sensitive, is the frequency ratio, γ (ω_{MT}/ω_I). Fig. 4.8 shows that if ω_I is far away from ω_{MT}, the minimum transmissibility is very low, and if the isolation frequency is close to ω_{MT}, the transmissibility is close to unity over most of the frequency spectrum.

As the figure shows, the minimum transmissibility decreases as γ decreases. When $\gamma = 1$, ω_{MT} and ω_I cancel each other out, and when $\gamma = 0$, the system represents an ordinary SDOF system.

t would thus be a good idea to analyse the sensitivity of the variable γ, and investigate the variables that affect the value of γ. Mathematically, γ can be written as

$$\gamma = \frac{\omega_{MT}}{\omega_I} = \sqrt{\frac{M_{eq3}}{M_{eq1}}} \tag{4.11}$$

As seen in section 3.4 (c), the isolation frequency cannot be placed before the MT frequency on the frequency spectrum. It is thus important to get ω_{MT} as low as possible in order to minimise the frequency ratio, γ. Eq. 4.8 shows the mathematical relations for M_{eq1} and M_{eq3}. A simple method to minimise γ would be to make m_1 as heavy as possible. This would lower ω_{MT} , but ω_I would stay the same, thus lowering the frequency ratio, γ. This method has obvious limitations, and will not be used to minimise the transmissibility.

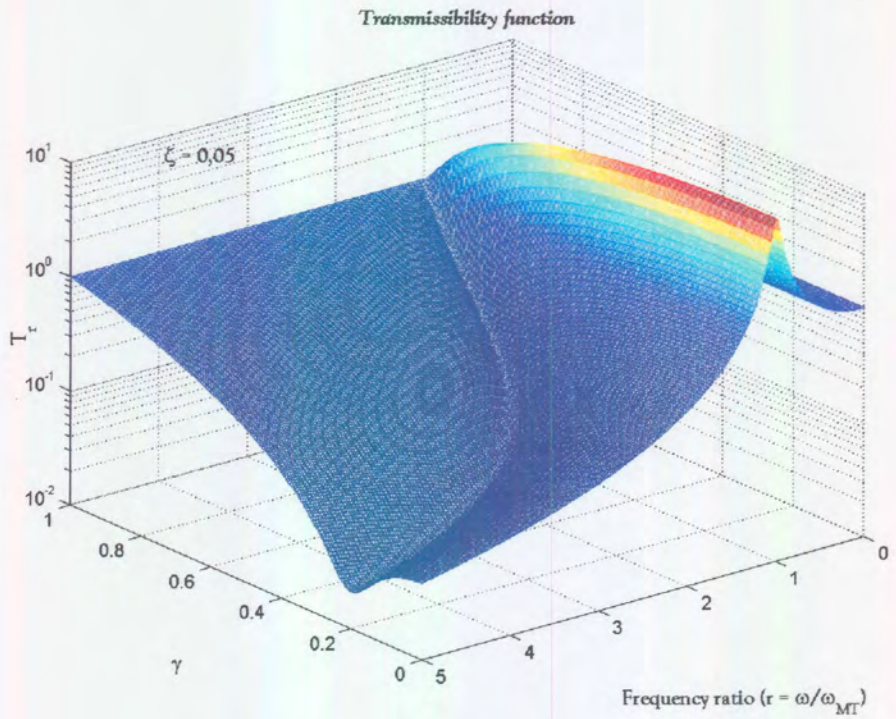

Figure 4.8 Transmissibility as a function of γ

Fig. 4.9 shows a plot of the frequency ratio, γ, vs. the density and the port diameter. It shows that a high-density fluid will increase the frequency ratio, and thus increase the transmissibility. It might then seem to be a better option to use a fluid with a very low density, but it has to be kept in mind that the higher density will result in a lower

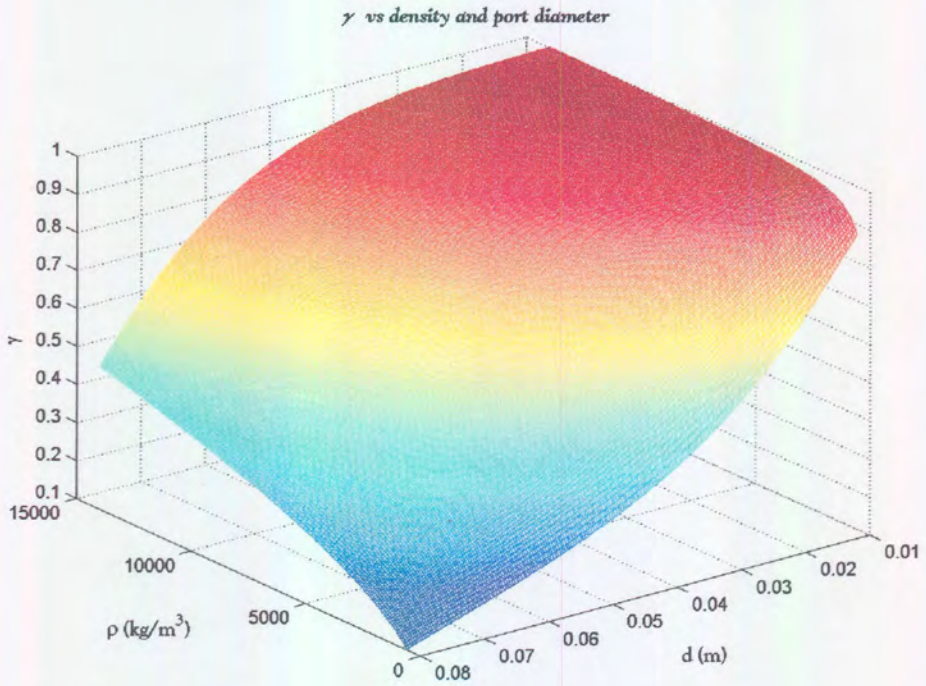

Figure 4.9: Frequency ratio plotted against port diameter (d) and density (ρ)

required area ratio. The figure shows that for higher values of port diameter the frequency ratio also decreases. As a result, this cannot be held as sole reason to use a low-density fluid.

The port length also has an effect on the frequency ratio, as Fig. 4.10 illustrates. A long port means a high frequency ratio, which in turn implies higher transmissibility.

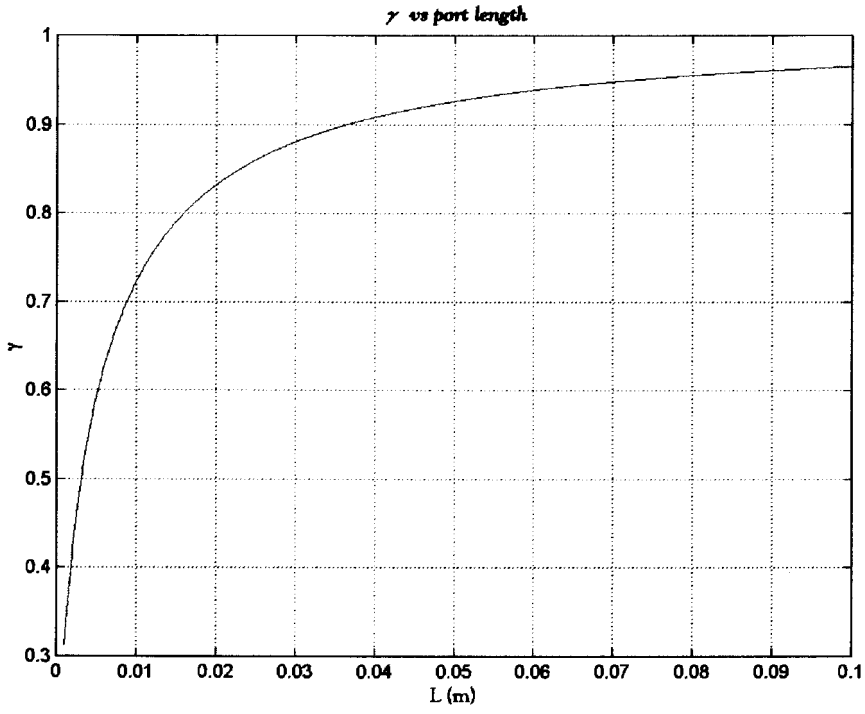

Figure 4.10: Frequency ratio as a function of port length

Fig. 4.11 shows the relation between the frequency ratio and the housing and port diameter. The frequency ratio is very low when the area ratio is low, in other words the housing and port diameters are nearly the same. It is also worthwhile noticing that it is more efficient to use a smaller absorber than a larger one, because of the fact that the same frequency ratio is achieved for a higher area ratio with a smaller absorber as with a larger one. However, fluid damping would become excessive if the size of the absorber is too small.

It has already been mentioned that this type of absorber will be convenient to use in situations where the spring constant has to be relatively low for a low attenuation frequency. This phenomenon is achieved through the hydraulic lever created by the area ratio. The sensitivity study shows that there is a definite upper limit to the amount that the spring constant can be increased for a specific attenuation frequency. The minimum transmissibility decreases when the ratio k/ω_1 is increased.

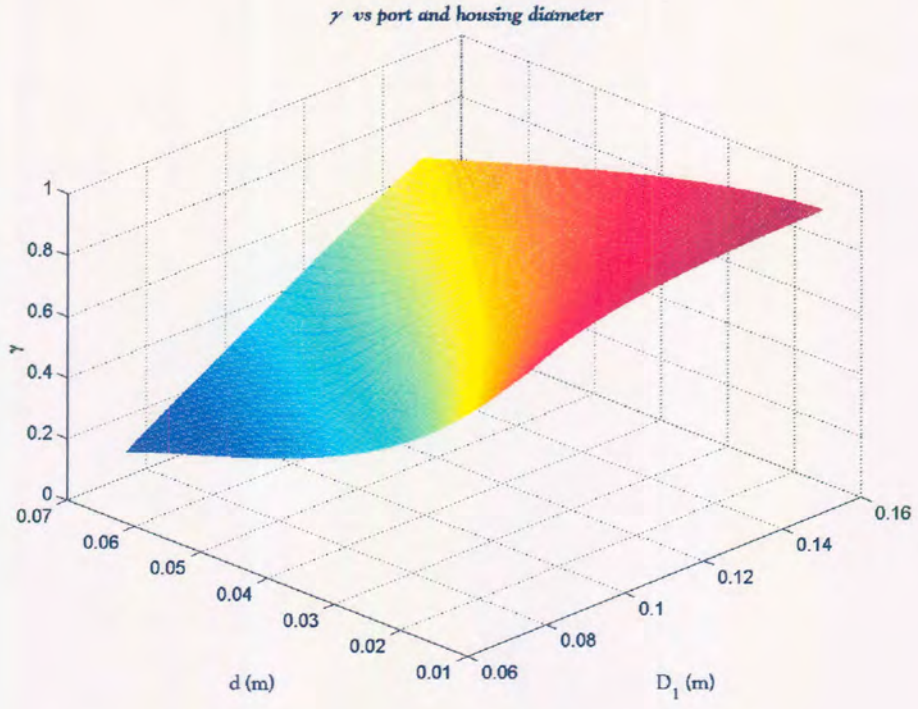

Figure 4.11: Frequency ratio vs. port & housing diameter

4.5 Calculation of concept variables

The optimisation of concept variables will include all the basic geometrical variables that would have a significant impact on the dynamical performance of the absorber. It is important to realise that a change in one of these variables can have several consequences on the dynamical response of the system. An increase in density for example can lower the attenuation frequency, but increases the transmissibility because of an increase in damping and frequency ratio. This chapter must thus not be interpreted without referring back to the sensitivity analysis in the previous section.

The concept variables have been calculated according to the principles stated in the previous sections of this chapter, and where needed, chosen according to certain practical considerations.

Fluid density

The choice of absorbing fluid is dependent on several factors. The two most important factors are density and viscosity. The density determines the absorbing mass inside the port for a given port diameter, while the viscosity determines the amount of wall shear or fluid damping present. A first thought would be to select a fluid with a high density and a low viscosity. This would imply a large absorbing mass, but would also mean an increase in fluid damping. Fig. 4.12 shows the effect of increased density on the fluid-damping coefficient.

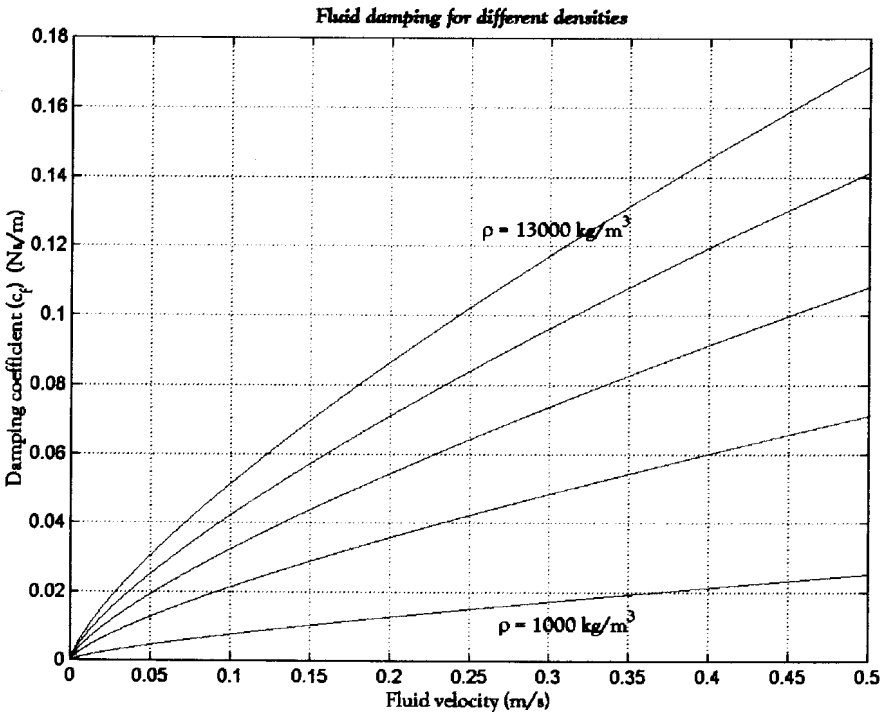

Figure 4.12: Fluid-damping coefficient for different densities

As fig 4.12 shows, the damping increases with an increase in density. This can also be mathematically explained by looking at eq. 10.61.

$F_L = 0{,}158 \cdot R_{ed}^{-\frac{1}{4}} \cdot \pi L^2 \rho \dot{x}_2^{\,2}$, where F_L is the damping force, R_{ed} is the Reynolds number, ρ is the density and L is the port length.

The damping is a function of the density of the absorbing fluid. However, although this has now been mathematically proved and shown by means of a c_f vs. fluid velocity graph, it is a little bit deceiving, and not entirely true. As soon as the density of the fluid is increased, the area ratio can be reduced to achieve the same isolation frequency for the same spring constant. A reduction in area ratio implies an increase in port diameter, which means less fluid damping for the same configuration. The main contributor to this phenomenon is the fluid damping due to entrance effects, which are very sensitive to port diameter change. Furthermore, a density increase will increase the frequency ratio, γ, which, as Fig. 4.8 shows, will increase the transmissibility.

As a result, the problem is a bit more complex, and further analysis is necessary. Fig. 4.13 complements the entrance effects discussion.

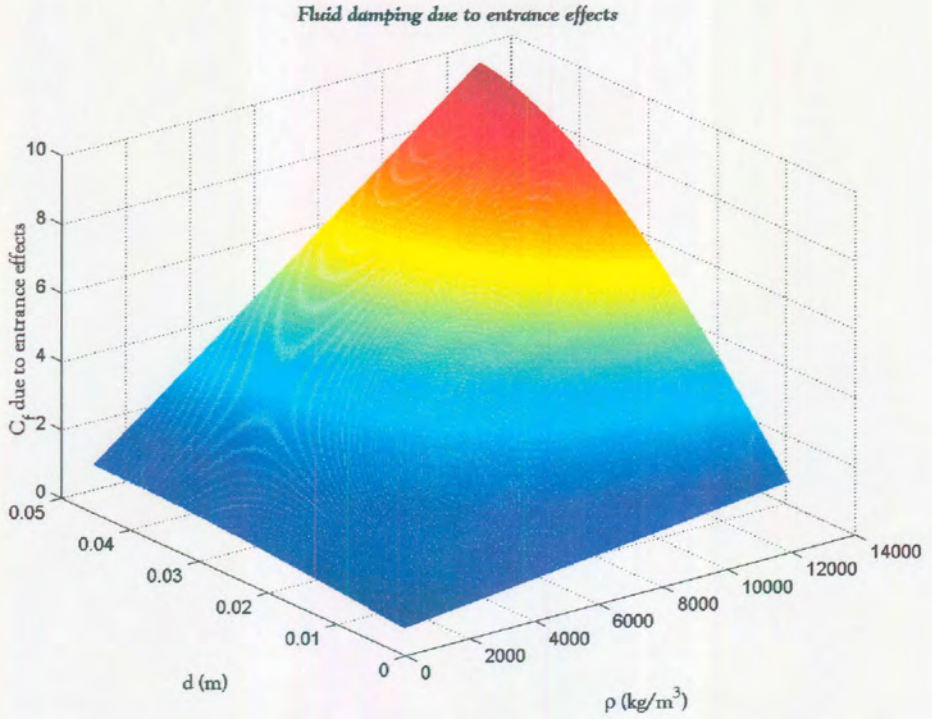

Figure 4.13: Fluid damping due to entrance effects vs. density and port diameter

The flow loss coefficients due to entrance effects are:

$$K_{SE} = \frac{2h_m g}{\dot{x}_2^{\,2}} = \left(1 - \frac{D_p^{\,2}}{D_1^{\,2}}\right)^2 \quad \text{for sudden expansion and} \quad K_{SE} = \frac{2h_m g}{\dot{x}_2^{\,2}} = 0.42\left(1 - \frac{D_p^{\,2}}{D_1^{\,2}}\right)$$

for sudden contraction (White, 1994), with D_1 and D_P the base and port diameters respectively.

To solve and optimise this problem analytically include flow damping and dynamical response calculation. The transmissibility of an absorber of a certain configuration is shown in Fig. 4.14. The simulation has been done for four different working fluids.

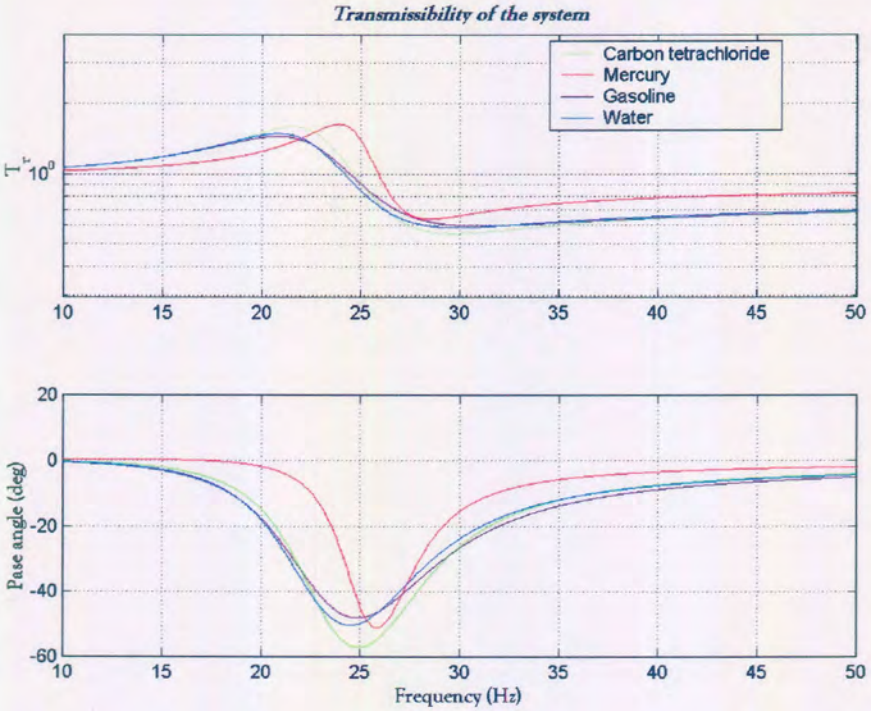

Figure 4.14: Transmissibility with different working fluids

From the figure it becomes evident that although the fluid damping of mercury is much less than that of gasoline, the transmissibility is more than the gasoline configuration, because of the frequency ratio effect. The undamped isolation frequency and stiffness constant is the same for all four the configurations, and the area ratios and frequency ratios are shown in table 4.1:

Table 4.1: Properties of the four different fluid configurations

Fluid	a/b	γ
CCl_4	31,64	0,86
Water	51,84	0,85
Gasoline	73,47	0,85
Mercury	4,6	0,93

A secondary consideration is the practicality of the fluid. This would include factors such as:

- Is the fluid poisonous?
- Does the fluid react with metal or rubber?
- Is the fluid readily available?

In the light of these questions, there really is only one alternative, which is water. Although water will cause the steel to rust, this can easily be overcome by mixing it with another fluid like cutting oil or something similar.

Port and housing diameters, and port length

These are the variables that basically determine the isolation frequency for a given stiffness. The design value isolation frequency has been taken as 30 – 35 Hz, for that is the operating frequency range of the rock drills for which there are available measurements (Van Niekerk *et al.*, 1998).

The design stiffness has been taken as k = 100 – 150 kN/m. This is a value that would still give the drill operator sufficient control of the drill, but would not be unreasonably stiff for the design of such an absorber.

The port length design is shown in Fig. 4.15. The figure shows a plot of the frequency ratio, γ, vs. the port diameter for different values of L. The values for L range from 0,01 to 0,06 m. The asterisks represent an isolation frequency line of 30 Hz, in other words, the port diameter and frequency ratio value that corresponds to an isolation frequency of 30 Hz can be evaluated.

From the graph in Fig. 4.15 it can be seen that the frequency ratio basically remains constant regardless of the port length in order to achieve an isolation frequency of 30 Hz. The port length has thus been chosen as 0,03 m, which is a comfortable design length with relatively low damping.

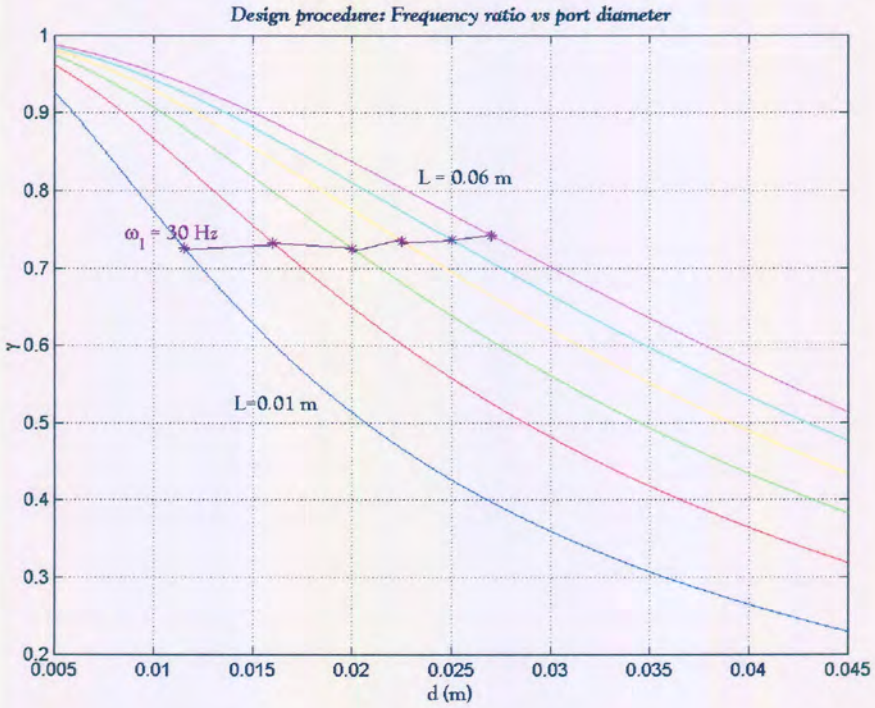

Figure 4.15: Port length design

In designing the port and housing diameters, basically the same method was used as the port length design. Fig. 4.16 shows the plot of the frequency ratio, γ, vs. the port and housing diameters again, but from a different angle. From previous discussions it is

clear that the ideal values for the two diameters will be at the point where γ is a minimum. Considering only Fig. 4.16, that point will be at d = 0,05 and D = 0,06 m.

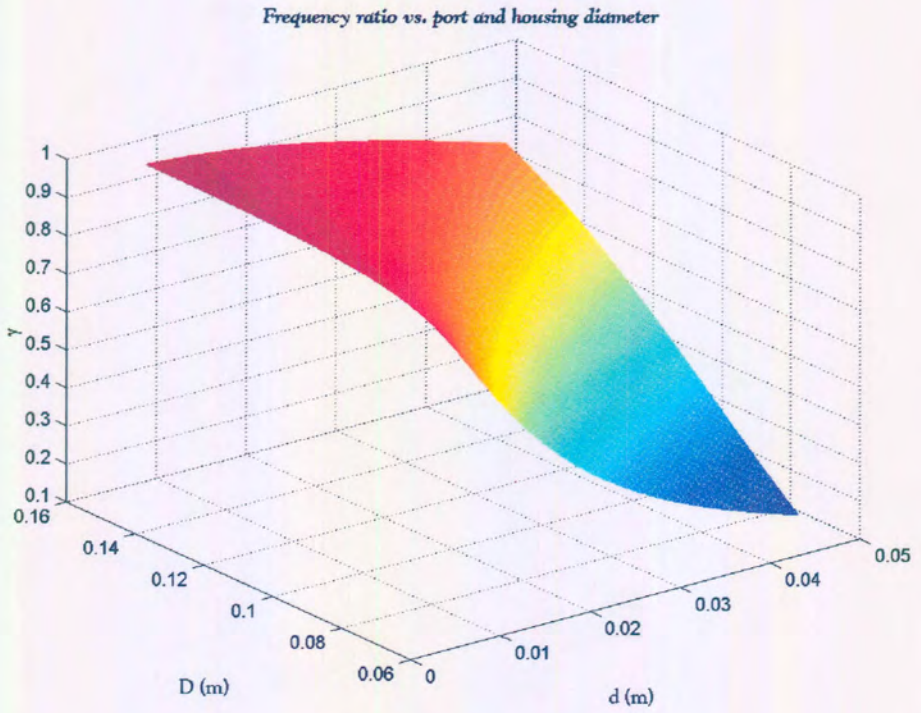

Figure 4.16: Frequency ratio vs. port and housing diameters

These two values would give a rather high isolation frequency, as shown in Fig. 4.17.

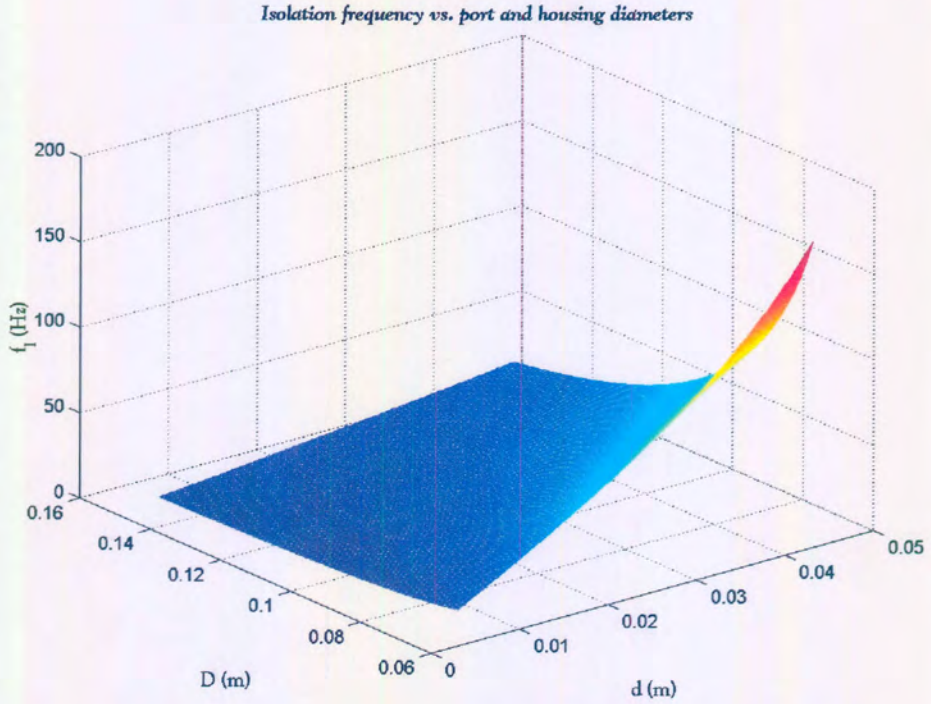

Figure 4.17: Isolation frequency vs. port and housing diameters

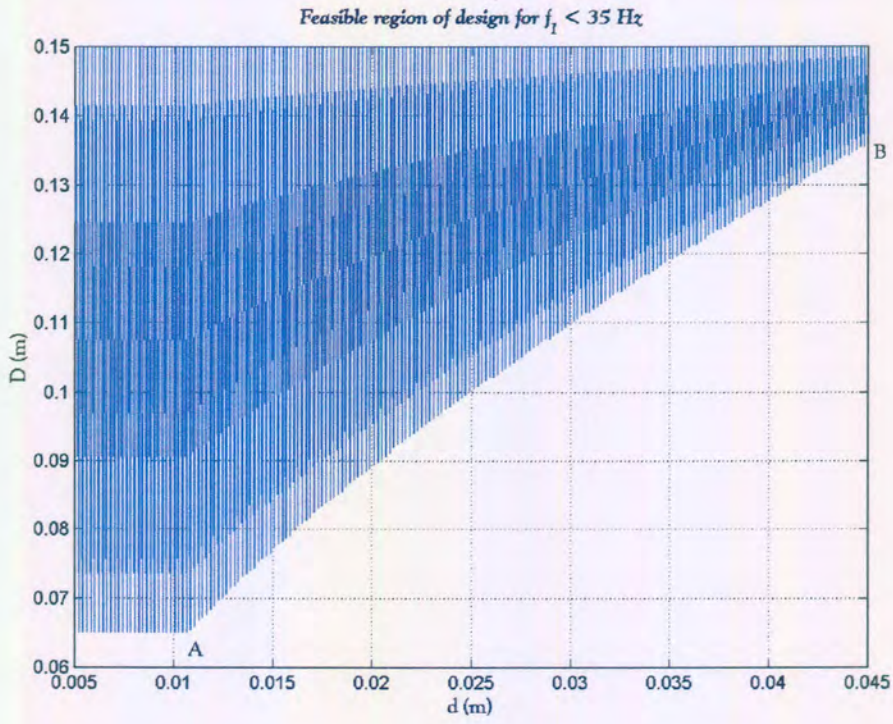

Figure 4.18: Feasible design region for the two diameters

By combining the two graphs in Fig. 4.16 and Fig. 4.17, the optimum area for the two diameters can easily be identified. Fig. 4.18 is the graph in Fig. 4.17 with every value above 35 Hz removed for the domain. In Fig. 4.18 the blue area represents a feasible design region for an isolation frequency smaller than 35 Hz.

The optimum design in terms of γ and thus minimum transmissibility is anywhere on the line AB. If Fig. 4.16 is examined once again, line AB is approximately situated in the yellow region of the surface, which gives a frequency ratio of about 0,7 – 0,8.

In order to minimise damping, the value for the port diameter must be as large as possible. In Fig. 4.18, the housing diameter must then also be as large as possible. The outside diameter of an ordinary drill is not much more than 0,12. Allowing for material and mounting methods, the inside diameter of the housing cannot be more than 0,09 m. The corresponding value for the port diameter is 0,02 m.

4.6 Detail design

The detail design was done mostly according to practical considerations. Because of the fact that this is only a prototype, and will not be implemented on the drill, the design has been done in such a way that the concept can be proven as functional. There has thus been allowed for replacing of parts after manufacturing in order for the concept to be properly tested and tuned.

The fact that the concept will be implemented on a drill in the future was definitely a second consideration, and the design has been done accordingly where possible.

No mechanical strength calculations have been done, because the absorber has been made very rigid to ensure that no higher frequency modes would have an impact on the modes of importance. Metal fatigue was also not considered, because the design is a prototype and operation life is not important at this early stage.

The assembly drawing is shown in Fig. 4.19. An inner pressure ring ensures that the handle port assembly is secured on to the rubber element. An outer pressure ring secures the rubber element onto the fluid housing. A cover plate is mounted with a flange onto the fluid housing and sealed with an O-ring. Two grub screws (in the drawing presented as Allen cap type bolts) are situated on the side of the housing. These screws will ensure that all the air can be bled out of the system. The diaphragm is covered with a diaphragm housing. The port is clamped with a grub screw relative to the port housing, and replaceable to enable area ratio change. The handle bar was designed according to ergonomic standards (Eastman Kodak Company, 1983: 146).

The stiffness for the configuration as shown in Fig. 4.17 is 128 kN/m and has been calculated as discussed in section 4.1. The rubber thickness is 0,01 m. The port has been designed to be slightly shaped like a diffuser to reduce damping, but this has not been implemented in the damping calculations. The calculated damping for the given configuration is C_{eq1} = 195 Ns/m and C_{eq3} = 202 Ns/m.

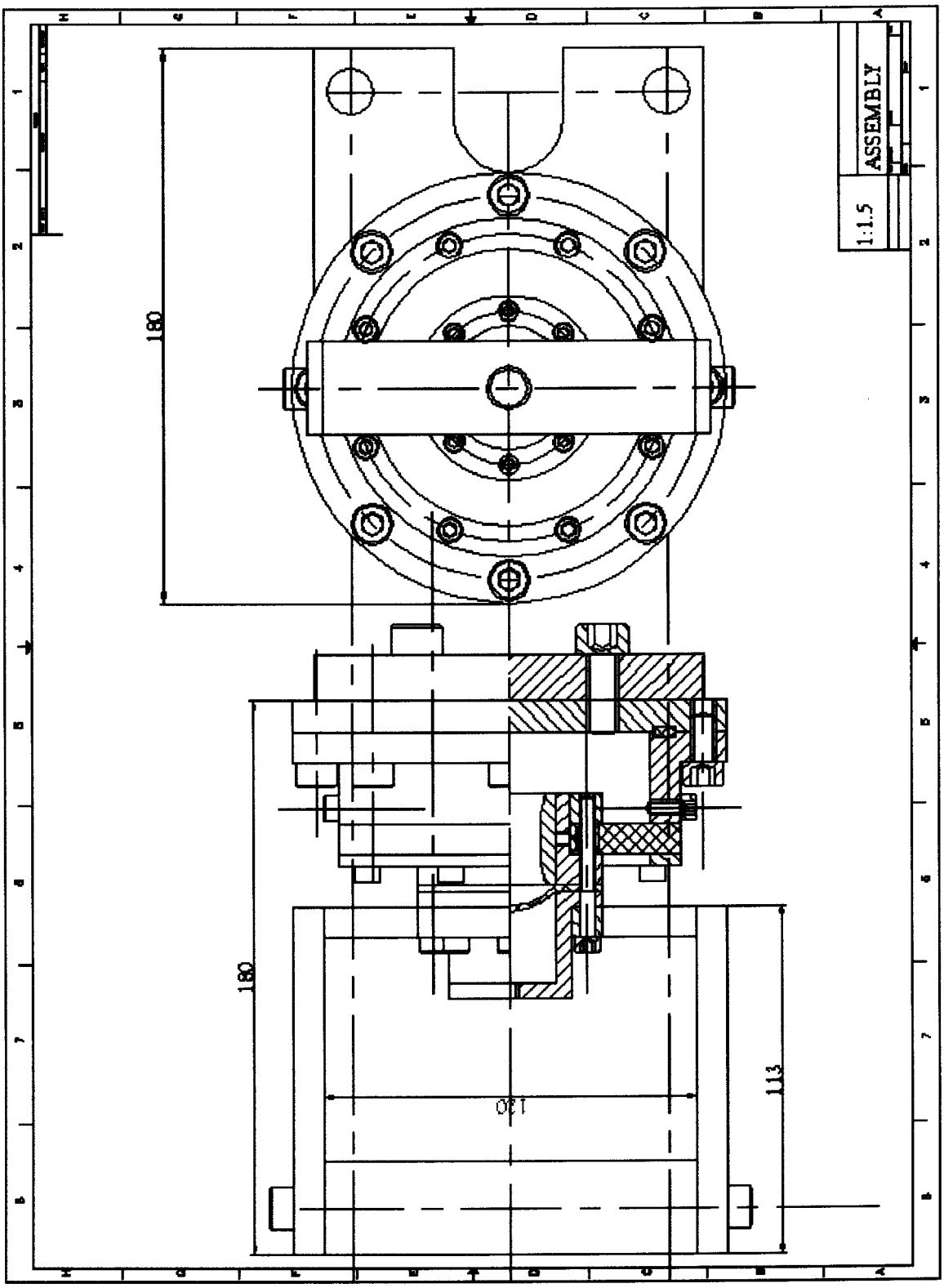

Figure 4.19: Assembly drawing of absorber

The rubber has been cast into a mould that is shown in Fig. 4.20. The mould is made of mild steel and consists of a housing and a cover plate. The two elements are bolted together by a bolt and linked with several pins to create the mounting holes in the rubber casting. The mould has been used to cast a 55-shore and a 35-shore hardness rubber.

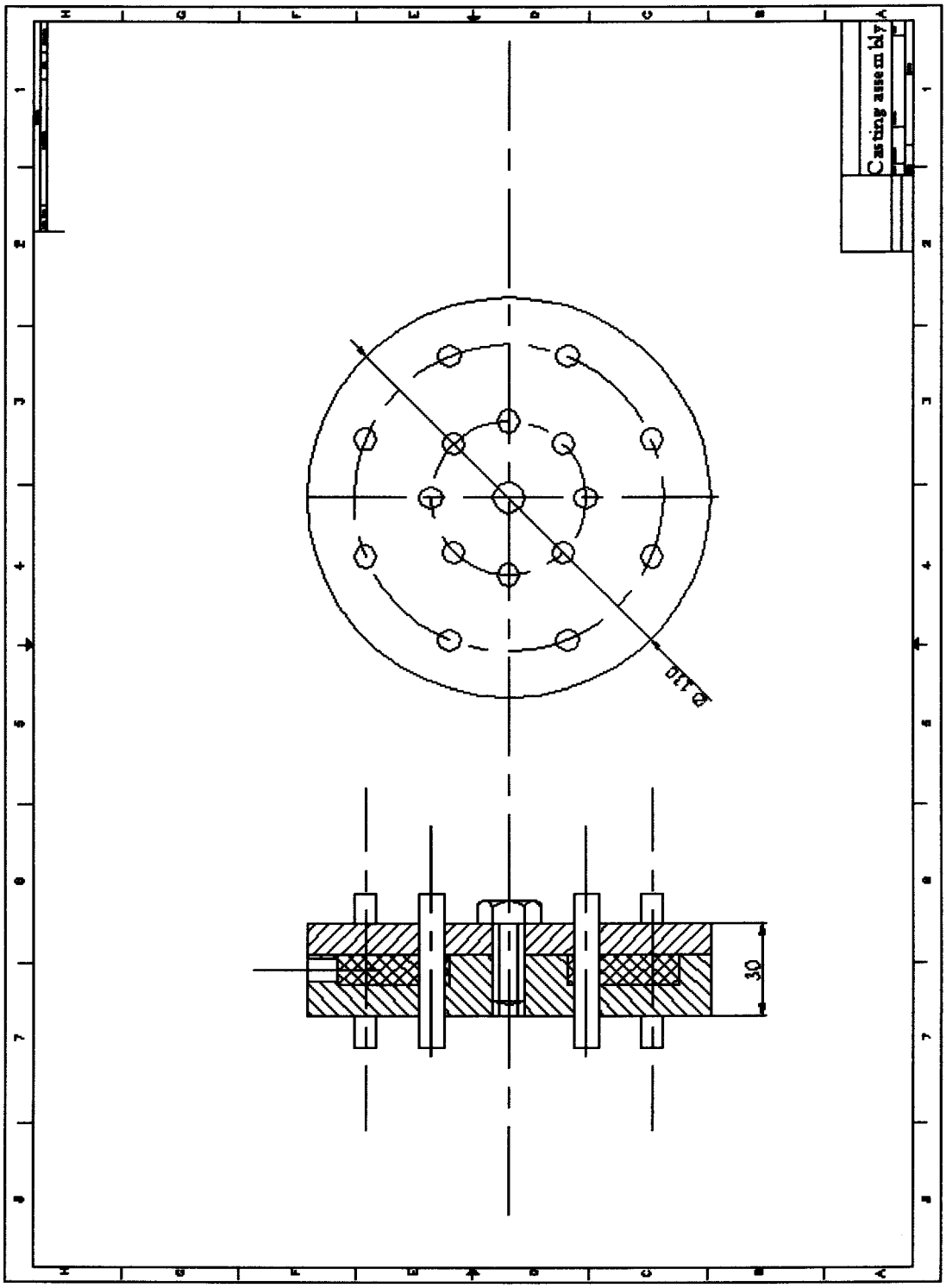

Figure 4.20: Mould assembly

A three-dimensional model of the design has been generated to determine the inertial properties of the system, and to get a better idea of how the design will look after manufacturing. This model can be seen in Fig. 4.21.

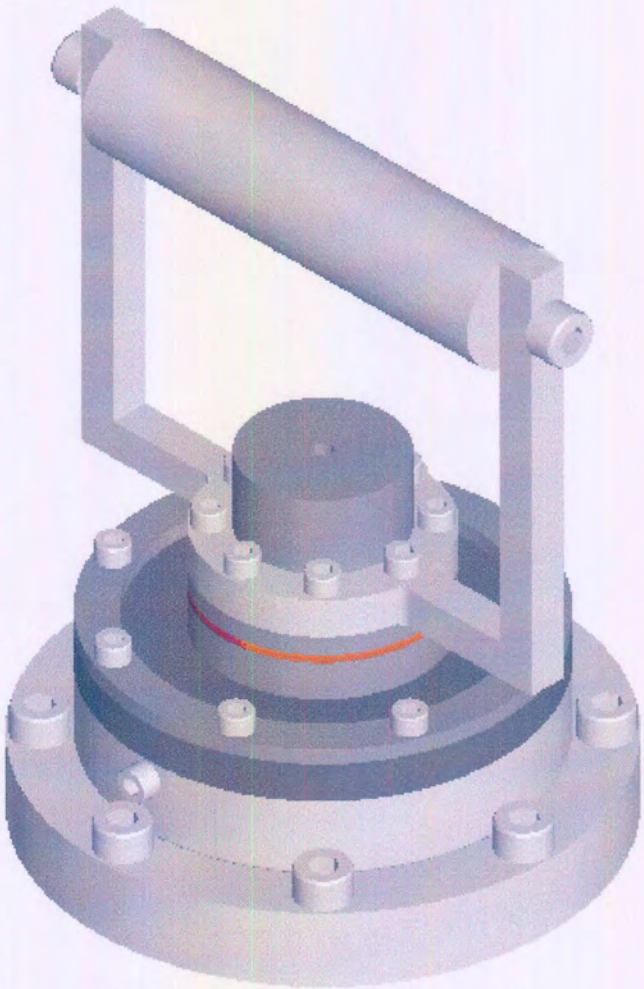

Figure 4.21: 3-Dimensional model of absorber

A mounting plate can be mounted on the cover plate at the bottom for attachment. Two mounting plates have been manufactured, one for mounting on the test rig, and the other for mounting on a rock drill.

The mass properties of the system are the following:

Handle assembly (Everything that moves with the handle)	-	1.689 kg
Housing assembly (Everything that moves with the cover plate)	-	2.43 kg

The rubber element has been discarded in the above calculation. To get a better idea of the configuration and assembly, two section views have been created and can be seen in figure 4.22.

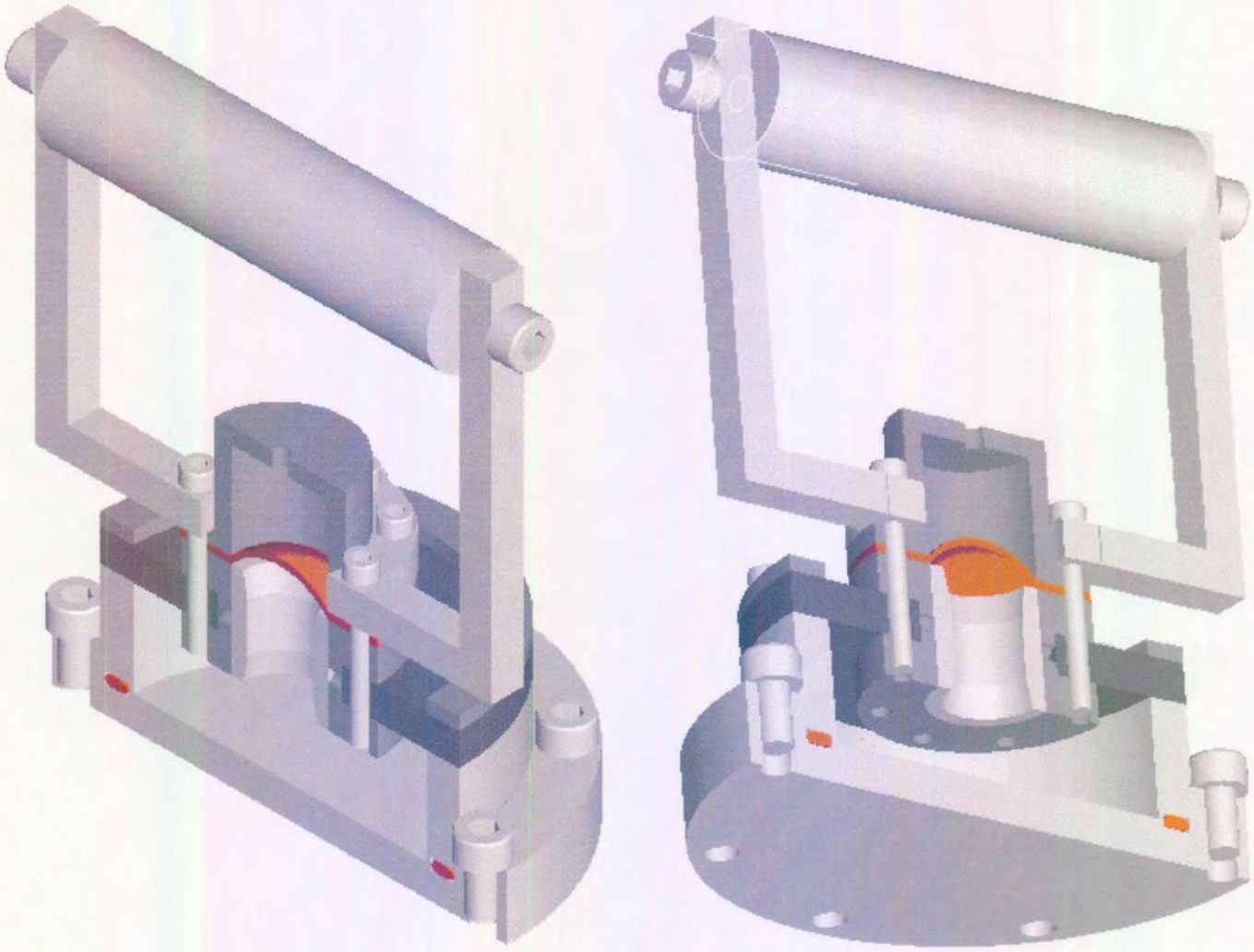

Figure 4.22: Section views of modeled absorber

The assembly and operation of the absorber handle become clear when looking at the section views. The two pressure rings secure the rubber and ensure that no fluid leaks from the fluid chamber. The port housing, rubber, diaphragm, handle and diaphragm housing are all secured with the same bolts in an attempt to make the assembly more compact.

This could cause a sealing problem, because of the fact that two different kinds of rubber is secured with the same bolt. However, this problem was overcome by tightening the bolts with the correct amount of torque. Steel bushings have been placed between the rubber and the bolts. These bushings are shorter than the thickness of the rubber element, to make sure that the rubber is positively secured with tightening.

With compression of the handle relative to the bottom cover plate, the fluid moves up through the port against the diaphragm, which keeps the fluid inside the absorber.

4.7 Simulation of design

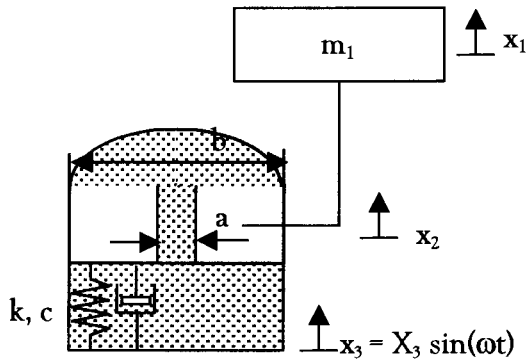

Figure 4.23 Absorber diagram

The design as presented in the previous section can be simulated by using a mathematical program like MATLAB. The equation of motion used is the following:

$$M_{eq1}\ddot{x}_1 + C_{eq1}\dot{x}_1 + kx_1 = M_{eq3}\ddot{x}_3 + C_{eq3}\dot{x}_3 + kx_3 \qquad (4.12)$$

In eq. 4.12 M_{eq1} and M_{eq3} are

$$M_{eq1} = m_1 + \left(\frac{b-a}{a}\right)^2 m_2$$
$$M_{eq3} = \left(\frac{b(b-a)}{a^2}\right) m_2 \qquad (4.13)$$

where m_1 is the apparent mass of the hand-arm system of the operator (section 4.3) plus the mass of the handle-port assembly (section 4.6). The damping coefficient C_{eq1} and C_{eq2}, and the stiffness coefficient are calculated as stated in sections 4.1 and 4.2.

The desired output of such a simulation would be:

- The displacement transmissibility of the system
- The time response of the system for a given input signal
- The typical pressure variations present in the system.

The input variables for the simulation are:

- Fluid density, ρ
- Fluid viscosity, μ_f
- Port length, L
- Port diameter, d_p
- Housing inner diameter, D_1
- Mass of handle, m_h
- Apparent mass of hand-arm system, m_a
- Structural damping coefficient, β

- The dominant excitation frequency, f_{ex}

The variables as given in the concept variable calculation and design chapters are now fed into the simulation. The transmissibility for the system is shown in Fig. 4.24.

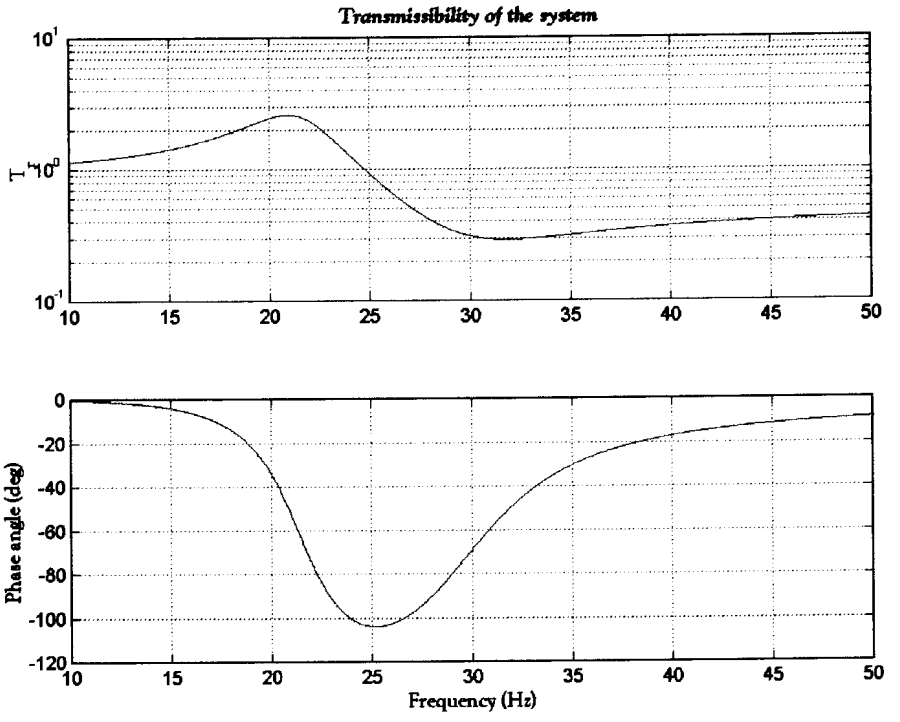

Figure 4.24: Simulation of design model - Transmissibility

The system has an isolation frequency of about 30 Hz, and a MT frequency of 22 Hz. Minimum transmissibility is about 30% at the isolation frequency.

The time response of the system can be calculated by integration of the equation of motion. This can be done with an integration algorithm like `ode45.m` in MATLAB. The time response of the harmonically excited system is shown in Fig. 4.25. The exciting frequency is 34 Hz. The pressure response of the fluid is plotted in fig 4.26.

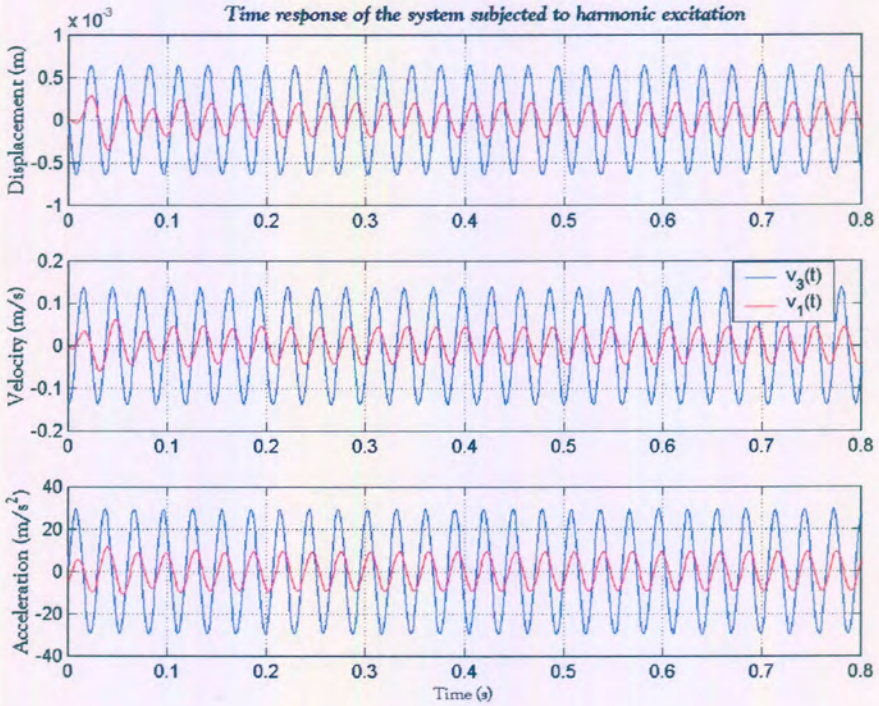

Fig. 4.25: Time response of the system

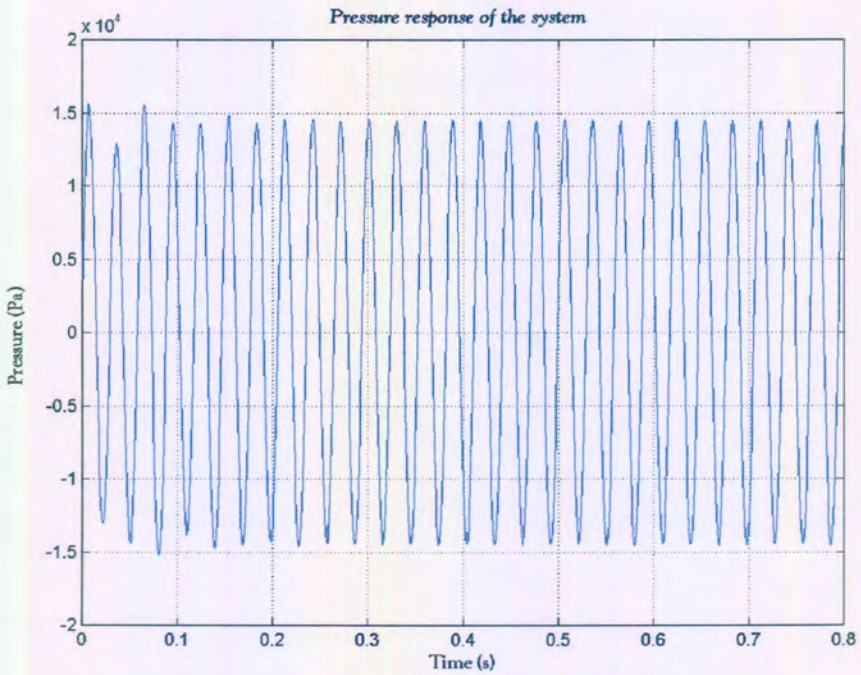

Figure 4.26: Pressure response of working fluid

The above simulation was done for a sinusoidal excitation, and is not truly representative of rock drill. The next simulation is done with a measured rock drill signal. The acceleration of the drill is shown in Fig. 4.27 (Van Niekerk *et al.*, 1998).

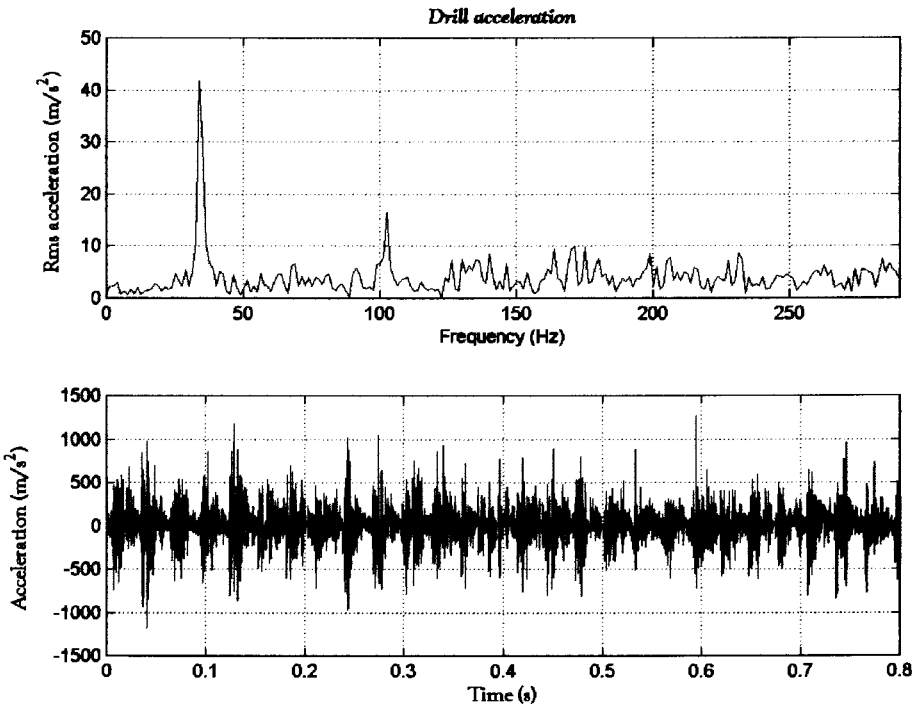

Figure 4.27: Drill acceleration signal

The signal as shown in Fig. 4.27 cannot be used without the necessary filtering procedures, because of the fact that the hydraulic actuator that is used in the experimental verification has a definite frequency response limit of just over 100 Hz. The simulation, however, can be done with such a signal.

Fig. 4.28 and 4.29 show the results of such a simulation in the time and frequency domain. It is clear from the frequency domain results that the absorber attenuates more than 50 % of the drill operating frequency vibration. The absorber also attenuates a significant amount of the vibration over the rest of the frequency spectrum.

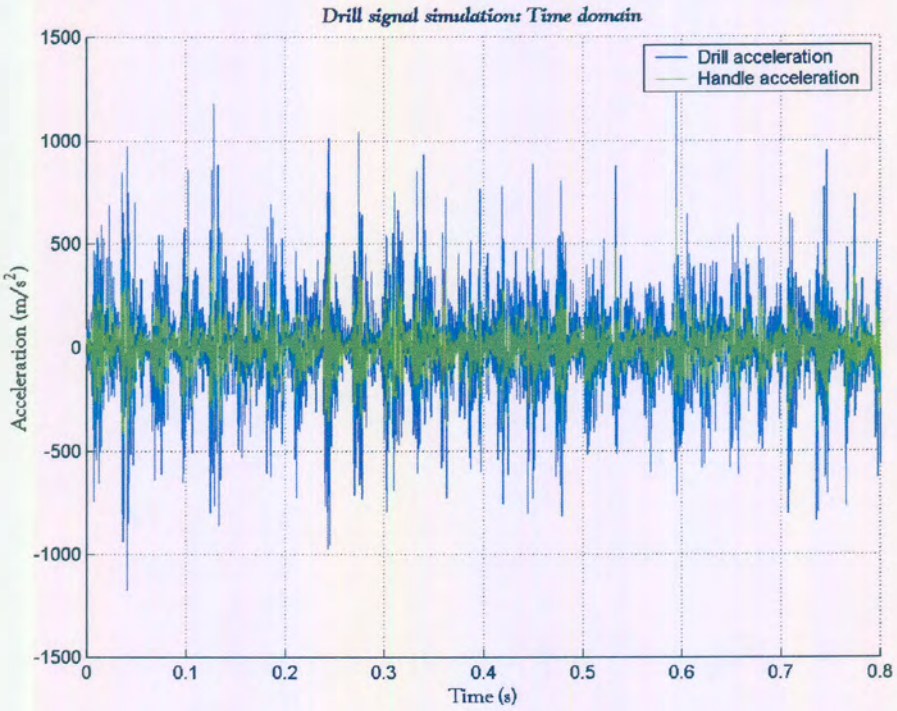

Figure 4.28: Simulation time domain results

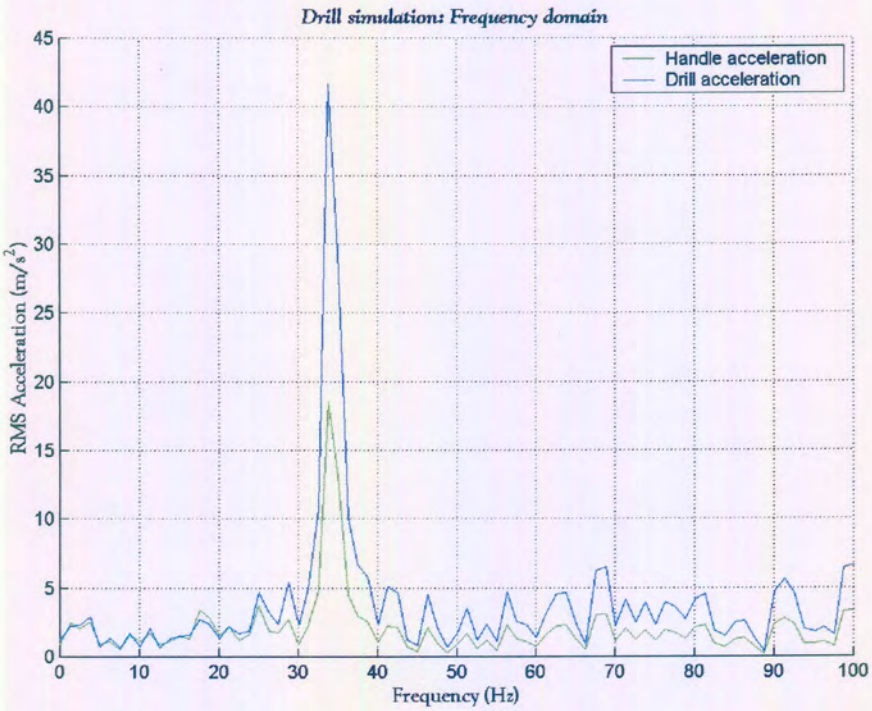

Figure 4.29: Simulation frequency domain results

4.8 Summary

Mathematical models have been created to design the stiffness and damping constants for a given set of variables. An apparent mass model presented by Griffin (1990:543) has been accepted to simulate the effect of the human hand-arm system on the system.

A sensitivity study has been executed to determine the critical variables in the system, and it turns out that the frequency ratio, γ, has a significant impact on the minimum transmissibility of the system at the isolation frequency of the system.

The variables have been optimised to give a minimum transmissibility for a given set of practical constraints. The exact values for each variable have been determined and implemented in a design.

A detail design of an absorber handle for the calculated variables has been done. The basic assembly and functioning of the design have been discussed, and some problems have been pointed out. A three-dimensional model of the design has been generated to determine the mass properties of the system and presented in the chapter.

The design has been implemented in a MATLAB simulation to illustrate the value of such an absorber. Two excitation signals have been used, a sinusoidal and an actual drill signal. It has been shown that the absorber attenuates more than 50% of the vibration energy at the operating frequency of the drill, and also reduces the vibration over the rest of the frequency spectrum.

5 Experimental Verification

5.1. Purpose

The purpose of the experimental verification is to verify the analytical results by experimental procedures and results. The experimental verification is performed to make sure that the concept functions according to design specifications, and to be able to explain any deviations from the theoretical predictions.

The experimental verification is also performed to characterize the design parameters, like mass, stiffness and damping constants. These parameters, especially damping and stiffness, will definitely be frequency dependent, and the results from the experimental procedure will be used to update the design parameters.

The experimental procedure will also be used as an opportunity to review the design in terms of certain practical problems that appear during the course of the tests. These problems will be stated in the evaluation, and also the corrective actions that have been taken to overcome them.

To summarise, the experimental verification will be used to learn more about the concept's abilities and limitations. Also to evaluate which predictions and assumptions made in the mathematical modeling and design were correct, and which would have to be revised. The design has been done in such a way that various parameters and elements can be changed, to ensure that the performance of this concept can be described in terms of most of the critical variables.

5.2. Measurement of inertial properties

The system is characterised by three important parameters: mass, stiffness and damping. The stiffness coefficient will be dealt with in section 5.3, and the damping coefficient is calculated in section 5.5. The mass includes the mass of the handle and port assembly, the mass of the housing and mounting plates, and the mass of the fluid inside the port

The masses of the steel components were measured on an electronic scale, and the results were as follows:
Handle and port assembly: ca. 1.7 kg
Bottom housing and cover plate: ca. 3.4 kg

Two different fluids were used during the tests, a water and anti-freeze mixture, and methylated spirits. The densities of these fluids were measured as:
Water mixture: 1043 kg/m^3
Methylated spirits: 840 kg/m^3
These measurements were done by measuring the mass of a known volume of the substance on an electronic scale.

The mass of the fluid in the port can be calculated by

$$m_2 = \rho \cdot a \cdot L \qquad (5.1)$$

Three different port diameters were used, and for the water mixture the mass of the fluid in the port was:
10 mm port: 2.45 g
12.5 mm port 3.84 g
20 mm port 9.83 g

5.3. Experimental procedure

The tests on the handle were done by exciting the structure at the attachment point by using a hydraulic actuator, and at the same time measuring the response of the handle. At this stage it is important to define the characteristics of the systems that have to be evaluated with the results of the tests. The most important characteristic of the system is the transmissibility function. The transmissibility reveals the isolation frequency, and the frequency of maximum force transfer. Other important characteristics are physical constants like stiffness and damping. These constants are important for the comparison of the analytical predictions with the theoretical results.

5.3.1 Force measurement

Consider the figure in Fig. 5.1. The figure represents the first part of the experimental procedure, where the handle is restrained, and the housing is excited. This part will be referred to as the force measurement. The measured quantities are printed in bold.

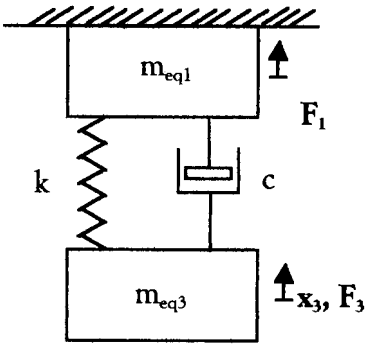

Figure 5.1: Representation of force measurement

The force measurement procedure will be used to calculate the transmissibility and stiffness coefficient of the system. A transmissibility function can be calculated if the measured response is divided by a known or measured input:

$T_r = \frac{F_1}{F_3}$, where F_1 is the force measured on the handle, and F_3 is the force exerted by the actuator.

Stiffness coefficient

The stiffness includes the stiffness of the polyurethane rubber, and that of the diaphragm above the port. The stiffness can be calculated by evaluating the real part of the equation:

$$k = -m_{eq3} \cdot \omega^2 + i \cdot \omega \cdot c - \frac{F_3}{X_3} \qquad (5.2)$$

The force F_3 is the force that the actuator exerts on the system.

Damping coefficient

The damping includes the structural damping of the polyurethane rubber, the fluid losses in the port, the structural damping of the diaphragm above the port, and the damping of the moving air above the diaphragm. The results of the damping coefficient in terms of frequency were not satisfying enough, and the reason for this will be discussed at the end of this chapter. A modal method described by Rao (1995:659) is used to determine the approximate the damping coefficient. The equation

$$\zeta = \frac{\omega_2 - \omega_1}{2\omega_n} \tag{5.4}$$

can be used to calculate the damping ratio. ω_1 and ω_2 are the frequencies corresponding to the half power points of the frequency response function X_3/F_3 (see figure 5.11). The damping coefficient can be calculated with

$$c = 2 \cdot m \cdot \omega_n \cdot \zeta \tag{5.5}$$

5.3.2 Acceleration measurements

The second part of the experimental procedure is schematically shown in Fig. 5.2, and will be referred to as the acceleration measurement.

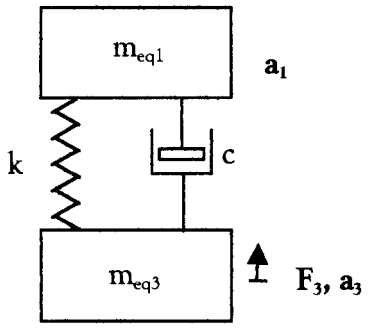

Figure 5.2: Representation of acceleration measurement

During this stage, the handle was free to move during the excitation of the base m_{eq3}. The accelerations of the handle and that of the base were measured. The force exerted on the base by the actuator was also measured. This procedure was performed to confirm the transfer function by using other equipment, and to evaluate the change in attenuation. This will hypothetically also be the operation of such a design on a rock drill, and it would thus be sensible to evaluate the response of the system in such a configuration.

The transmissibility function can be calculated as:

$$T_r = \frac{a_1}{a_3} \tag{5.3}$$

where a_3 is the input acceleration. The damping and stiffness of the system can be calculated by modal analysis methods, but it should be remembered that the these parameters are frequency dependent and it would be a linear estimation of a non-linear system. The non-linearity is primarily due to the rubber elements used in the system.

5.4. Experimental setup

A schematic representation of the force measurement experimental setup is shown in Fig. 5.3, while a photo can be seen in Fig. 5.4. The input signal to the actuator is generated in MATLAB and fed into the controller via the CDAS D/A converter card. The CDAS converter card has 6 input A/D channels and 2 D/A channels. The CDAS has all the appropriate anti-aliasing filters, and can be seen in Fig. 5.5. The controller controls the displacement of the servo valve of the actuator. The controller also controls the minimum and maximum displacement of the actuator. The motion of the actuator is measured by LVDT, and fed into the computer via the CDAS. The top and bottom load cells (F_1 and F_3) are fed via separate amplifiers into the computer for recording. The operating range of the servo valve is 0-100 Hz, and the maximum force on the load cells is 5 tons.

The input signals for this configuration were sine and sine sweep signals of approximately 60 seconds in duration. The first measurements were done by only one sweep, but as the coherence lowered at the later stages of the force measurements, an average over five sweeps was taken. Random signals were also generated, but the resulting measurements were not satisfactory. This could also be due to the phase difference of the amplifiers discussed later in this chapter (see results: Acceleration measurements, pp 83).

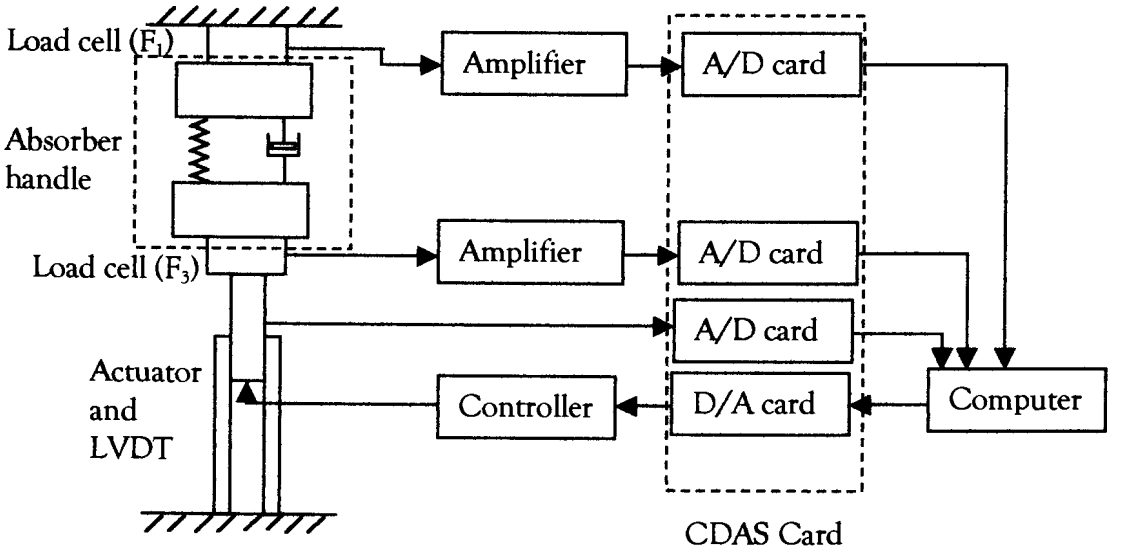

Figure 5.3: Force measurement experimental setup

The measurements were immediately in MATLAB format, and could be processed in the same program. Measurements ranged between 0 and 100 Hz with a sampling

frequency of 1000 Hz. Figures 5.4 to 5.6 show photographs of the force measurement setup.

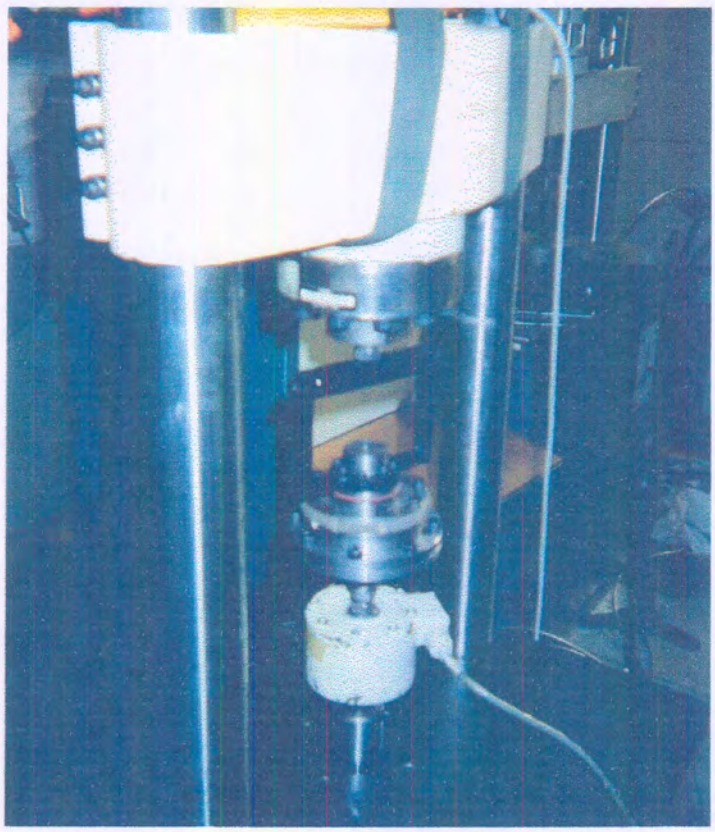

Figure 5.4: Force measurement

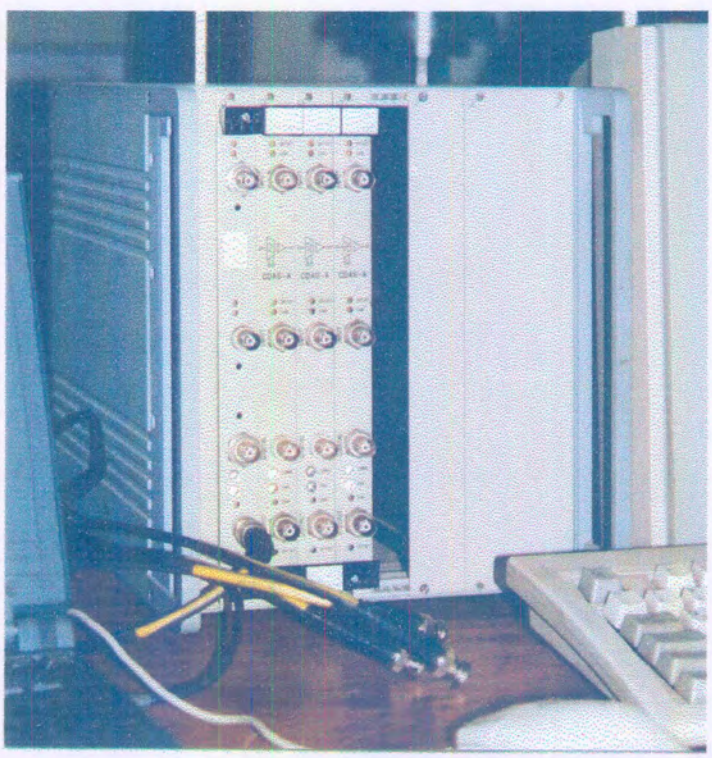

Figure 5.5: CDAS controller

The acceleration measurement setup is shown in fig 5.6 and 5.7.

As previously described, the absorber handle was not constrained in this configuration. The PCB miniature high frequency 10 mV/g accelerometers (Model 353 B17) were mounted at the top and at the bottom. These accelerometers sent an analogue signal via the amplifiers to the Siglab analyser. This analyser converted the signal to digital format and fed it into the computer for recording. The load cell operated through a separate amplifier, but the signal conditioning was also done by the Siglab analyser.

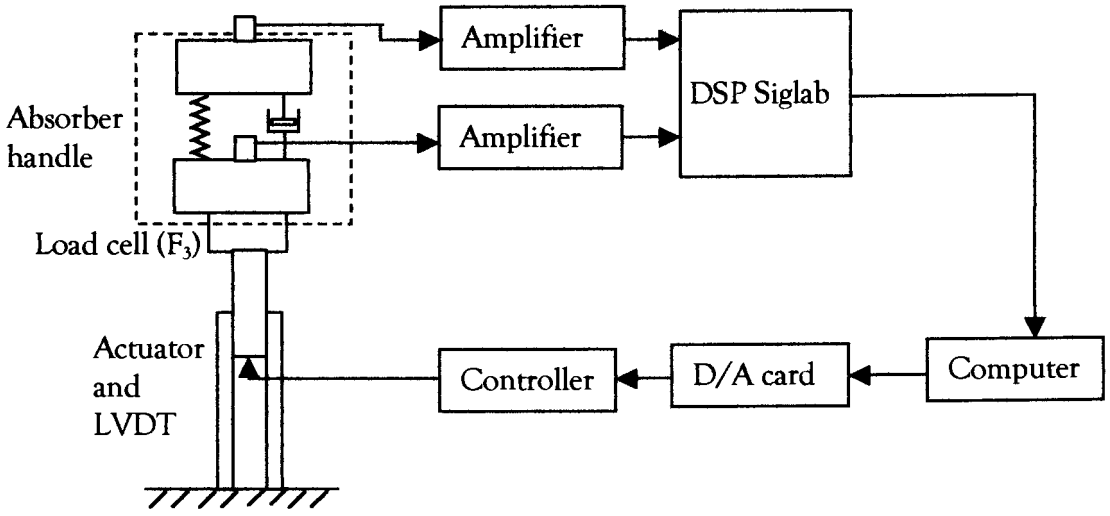

Figure 5.6: Acceleration measurement experimental setup

The input to the actuator was done through the controller via the CDAS converter card, and was band-limited random signals. These signals were generally limited between 5 and 90 Hz with a RMS amplitude varying between 0.5 and 1.5 mm amplitude. The compensation for the apparent mass of the operator's hand-arm system was done by a weight mounted onto the handle of the absorber (Fig. 5.7).

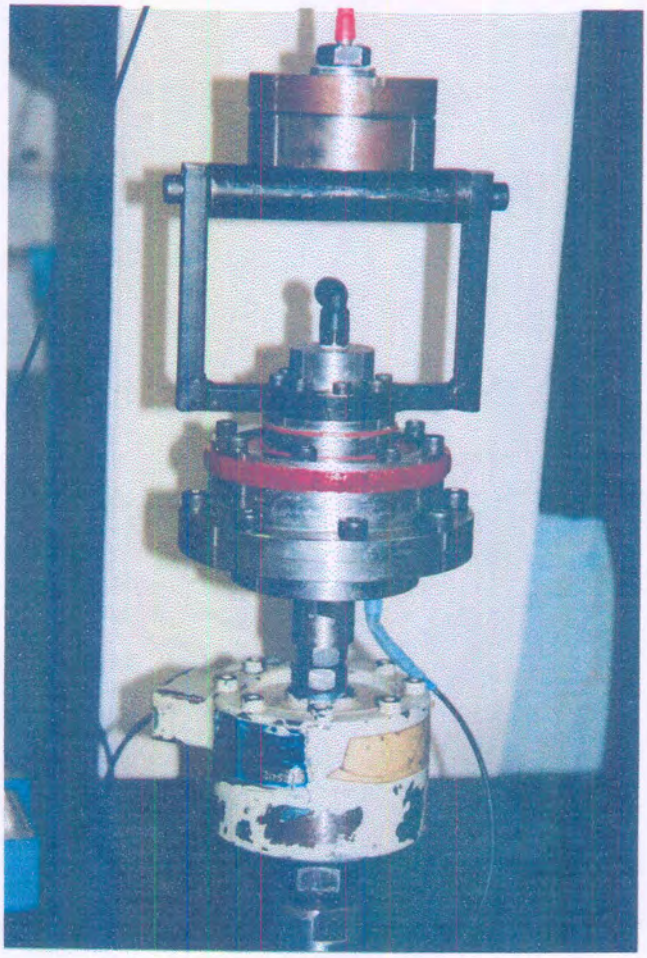

Figure 5.7: Acceleration measurement

5.5. Results

Force measurements

The force measurement was done according to the procedure described in section 5.3.1. This was mainly a characterisation phase during which the system's variables, the stiffness and damping coefficients, were evaluated. These parameters, although estimated during the design phase in chapter 4, were quite different from what had been expected. The theoretical model derived in chapter 4 will thus constantly be updated with the experimentally obtained stiffness and damping coefficients in order to accurately validate the model.

Due to the above-mentioned facts, the isolation frequency has also not been situated at the predicted frequency, and certain parameters like port diameter and diaphragm stiffness have been changed in order to move the isolation frequency to the desired value, which is between 30 and 35 Hz.

System without absorbing fluid

The first results that will be represented, is the response of the system without any fluid inside the absorber. This system can be modelled as a single-degree-of-freedom system,

and the stiffness and damping of the polyurethane rubber can be calculated with these results. An important factor that should be remembered is that the system with fluid inside is much stiffer than the system without fluid inside, due to the added stiffness of the diaphragm. This increase in stiffness due to the diaphragm could not be accurately modelled in the design phase, and the theoretical model will thus be updated after the stiffness of the diaphragm has been calculated.

Transmissibility

The data as received from the CDAS converter card is time domain signals that are filtered with a low-pass filter below 100 Hz. The transmissibility is then calculated by using MATLAB. The transmissibility plot for the system without absorbing fluid is shown is given in Fig. 5.9.

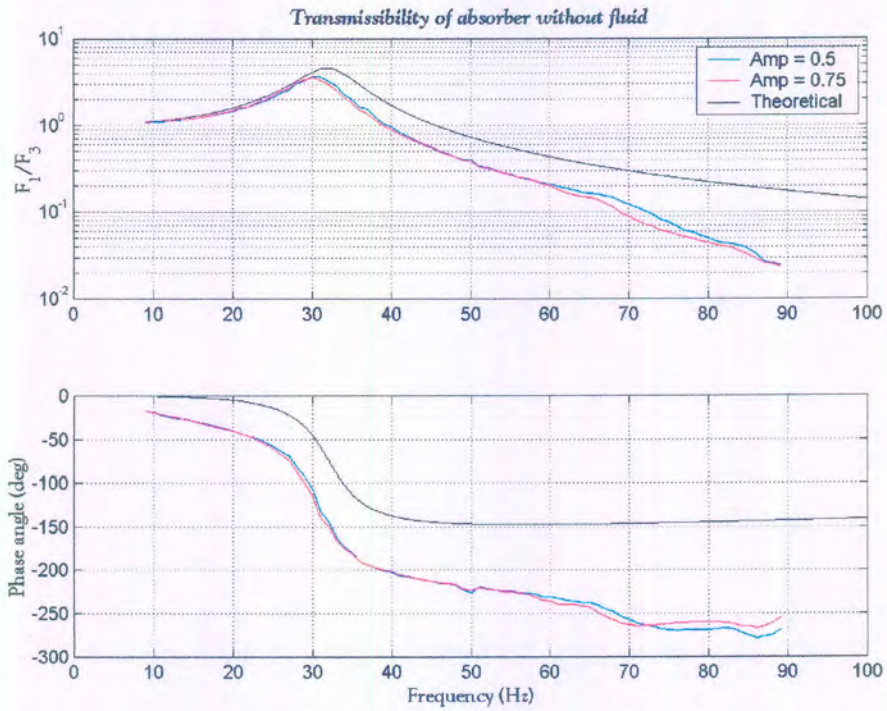

Figure 5.9: System without fluid - Transmissibility

Two amplitudes were used as excitation, nominally 0.5 and 0.75 mm sine sweeps, although the actuator cannot maintain the specified amplitude constant during the entire sweep. The frequency of the sine sweeps was linearly increasing from 0 to 90 Hz.

The system shows, as expected, the characteristics of a single-degree-of-freedom system, with a MT frequency at about 30 Hz. The variation with amplitude of excitation is negligible. The theoretical estimation is also shown in Fig. 5.9. The stiffness coefficient was taken as 100 kN/m, acquired from the graph in Fig. 5.10 at the MT frequency of the system. The damping coefficient was taken as 107 Ns/m as calculated below. The mass used for the theoretical estimation was taken as 2.43, which represents the bottom part of the absorber as calculated in section 4.6.

Stiffness coefficient

The stiffness coefficient was calculated by using eq. 5.2. Fig. 5.10 shows a plot of the stiffness coefficient vs. frequency for the two excitation amplitudes.

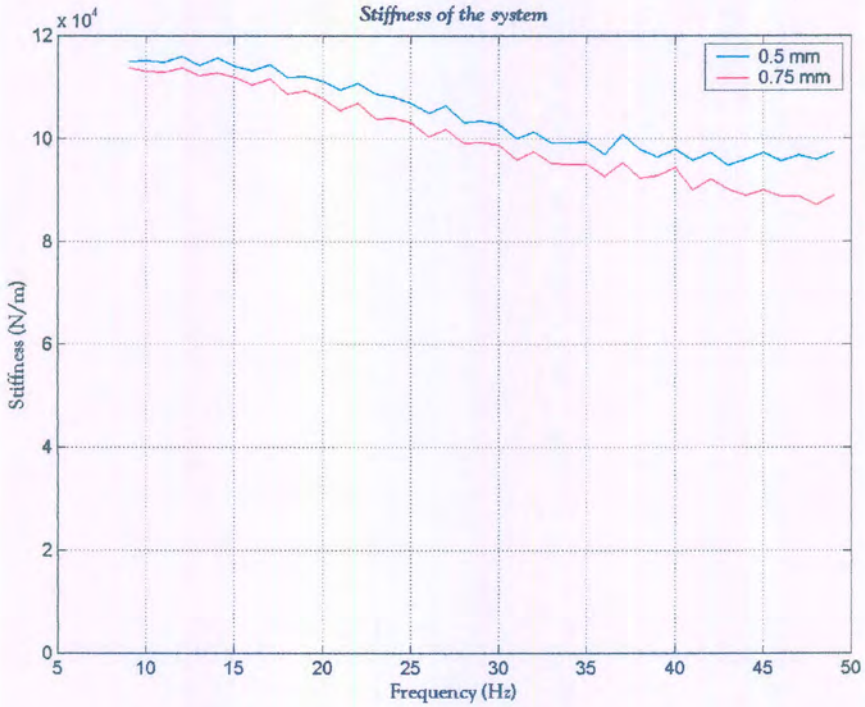

Figure 5.10: System without fluid – Stiffness constant

The figure represents the stiffness of the polyurethane rubber, and shows that the stiffness constant changes with about 30 kN/m over a frequency range of 40 Hz. The static stiffness is between 115 and 120 kN/m.

Damping coefficient

Although the damping coefficient would be frequency dependent, the value near the MT frequency is certainly the most important. Using eqs. 5.4 and 5.5, the damping coefficients for two amplitudes, 0.5 and 0.75 mm, are 128.965 and 107.38 Ns/m respectively. The hysteresis damping coefficient can be evaluated as (Rao, 1995: 224)

$$\beta = \frac{c\omega}{k} \qquad (5.6)$$

The value of this coefficient at the MT frequency for the two amplitudes, 0,5 and 0,75 mm, are 0,2213 and 0,1906 respectively. It is important to remember that eq. 5.4 is only an approximation.

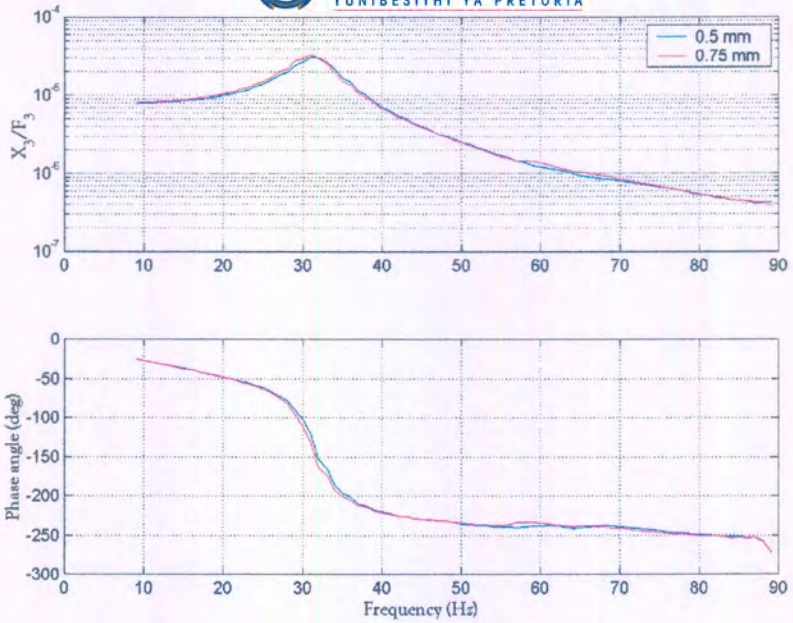

Figure 5.11: System without fluid - Transfer function

An interesting point to notice when looking at Fig. 5.11 is the fact that the resonant frequency is the same as the MT frequency. This is probably due to the simplicity of the system.

Coherence

Coherence is very important to ensure that the data and further processing thereof are reliable and representative. The coherence data for the transmissibility is plotted in Fig. 5.12. The coherence of the transmissibility is good at most frequencies, only falling at the natural frequency, which is normal, and at the Eskom supply frequency of 50 Hz.

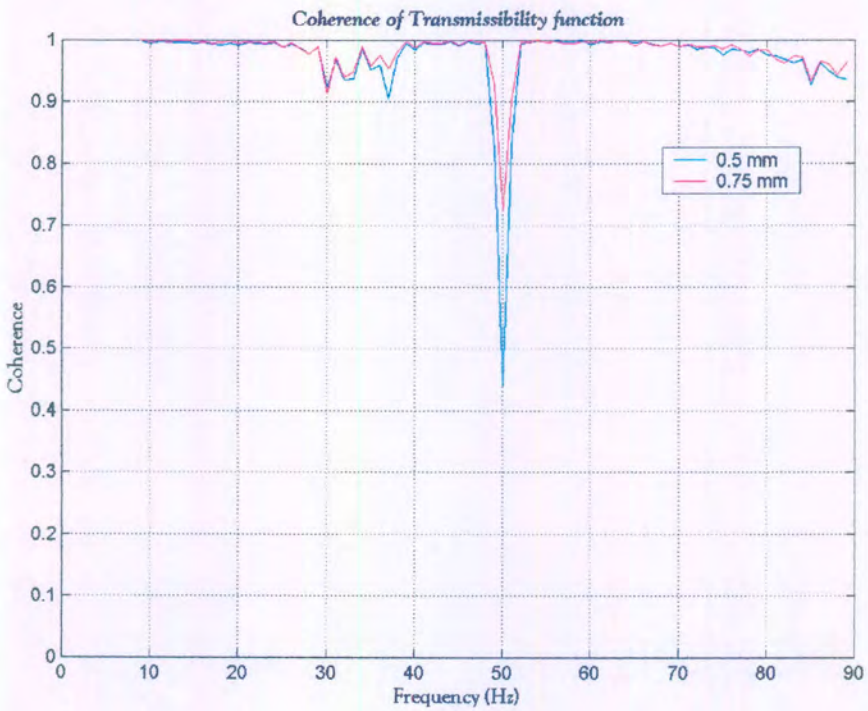

Figure 5.12: System without fluid - Coherence

The coherence also falls a bit at higher frequencies, which is probably due to the fact that the servo valve is not so dependable at frequencies above 80 Hz.

System with water mixture as absorbing fluid and 0.02 mm port

The first absorbing configuration that was tested used the water mixture as the absorbing fluid. The large 0.02 mm port was used, and a stiff 0.002 mm thick rubber as a diaphragm. The results obtained from this test were not very good compared to the rest of the measurements, due to the fact that the isolation frequency is situated at about 80 Hz. As seen in the previous section, the coherence is already lower at higher frequencies, and the isolation frequency lowers the coherence even further. The important aspects to notice at this stage, however, are that there definitely is an isolation frequency, and that the stiffness increased dramatically from the previous tests.

Transmissibility

The transmissibility plot is shown in figure 5.13. It can be seen from the figure that the isolation frequency is situated at about 80 Hz, and the MT frequency at about 47 Hz. The figure also suggests that the stiffness is a little higher with larger amplitudes and much higher than the previous configuration where there was no fluid inside the absorber. The theoretical estimation is also depicted in Fig. 5.13, and will be discussed in section 5.7.

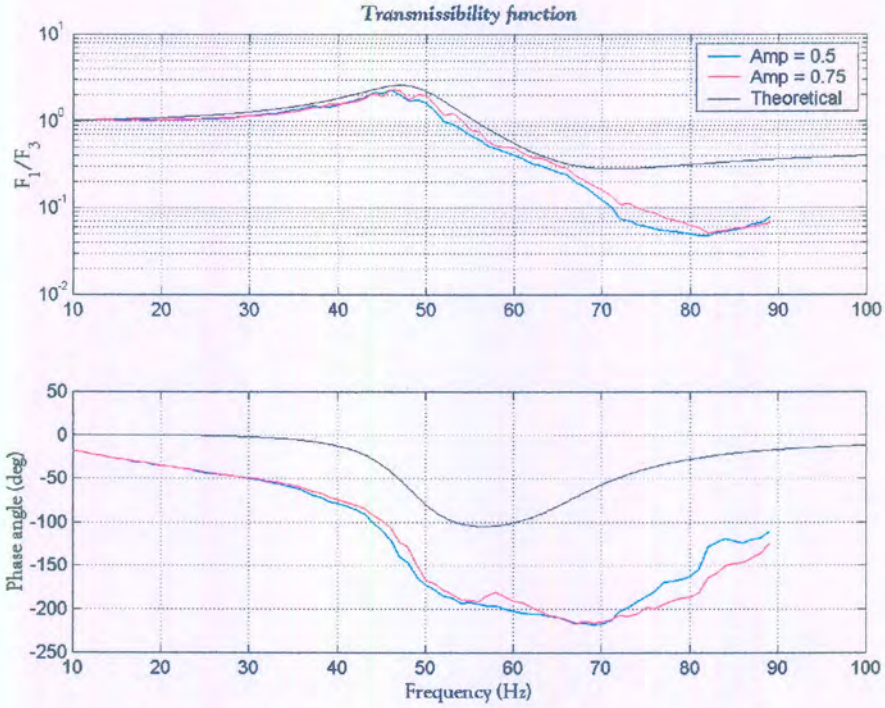

Figure 5.13: Large port with water: Transmissibility

Stiffness constant

The stiffness constant is calculated as described in the previous section. The stiffness constant for the two amplitudes is shown in Fig. 5.14. The stiffness of this configuration is about 300 kN/m static, and increases to about 550 kN/m at 50 Hz.

This is much higher than the system without an absorbing fluid, due to the effect of the diaphragm elongation; the absorber is now functioning. The stiffness also rises with frequency, unlike what was seen with the previous configuration. There is a slight difference in stiffness with different amplitudes.

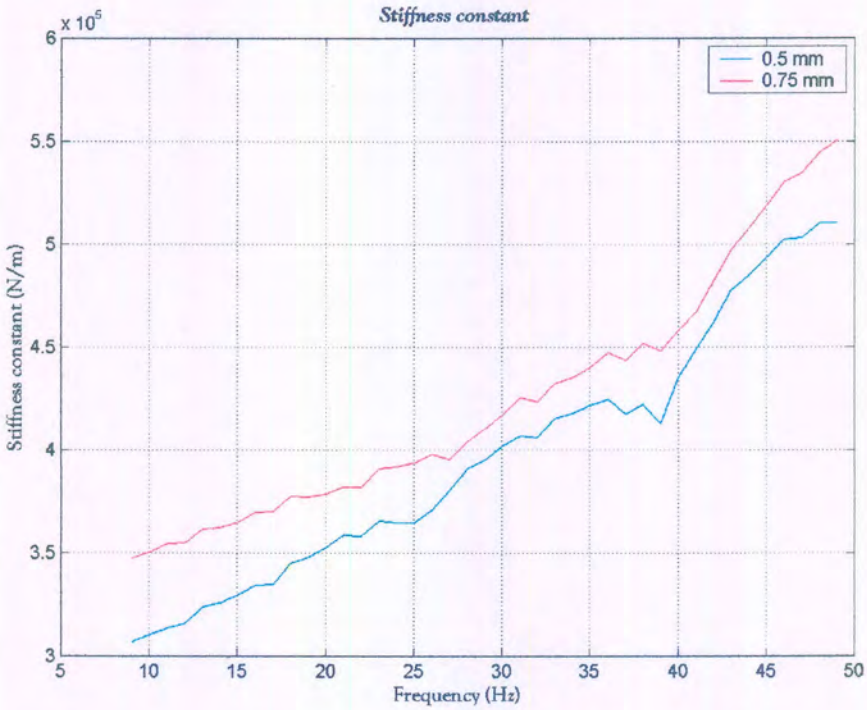

Figure 5.14: Stiffness Coefficient

Damping

The same procedure is used to calculate the damping as in the previous section. The values for the two amplitudes, 0.5 and 0.75 mm, are 366.1714 Ns/m and 457.7142 Ns/m. The variance of c in amplitude is due to the fact that the flow velocities are higher with larger amplitudes, which increase the value of the damping coefficient.

Coherence

The coherence plot for the transmissibility function is shown in Fig. 5.15. The coherence for this data set does not look very satisfactory, probably because the actuator input excitation is lower at high frequencies, and because of the fact that the isolation frequency are situated in the upper region of the frequency band. Both these phenomena causes lower signal to noise ratios.

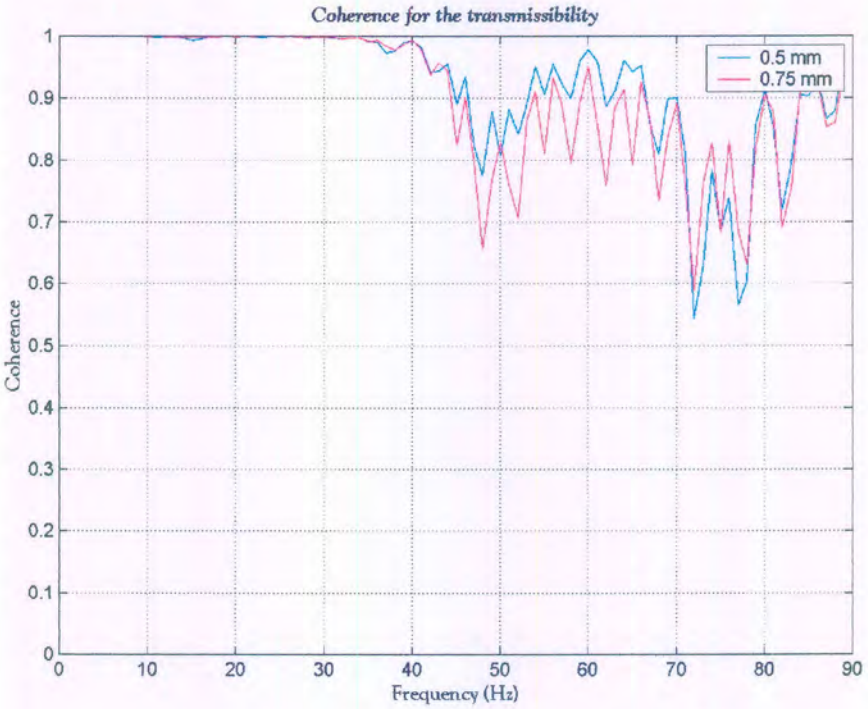

Figure 5.15: Large port with Water - Coherence

Lowering of the isolation frequency by varying certain parameters

As stated in the beginning, the isolation frequency can be lowered by changing certain parameters. The first parameter that has been changed, is the port size. The diameter of the port has been changed from 20 mm to 10 mm. This increases the area ratio of the system from 20.25 to 81. At this stage it was obvious from theoretical predictions that a 10 mm port would imply too much damping (see Fig. 5.16), and that a more flexible diaphragm with a port size between 10 and 20 mm would be the answer. This diameter value will be predicted with the mathematical model. A verification of the 10 mm port has however been considered to be important in terms of the characterisation of the design

A comparison between the transmissibility functions of the new system and the previous configuration is shown in Fig. 5.16. The isolation frequency has shifted with more than 20 Hz, but the damping has increased, and the frequency ratio (isolation frequency/MT frequency) has decreased. This has caused the amount of attenuation to decrease dramatically.

Another interesting aspect about the port change, is the change in stiffness (Fig. 5.17). The smaller port configuration is much stiffer than the large port configuration. One logical explanation for this phenomenon is that the stiff diaphragm cannot be moved away from the port. This causes the effective pressure area against the diaphragm to reduce to just about the port area. This would be especially relevant when the actuator is moving away from the handle, and the diaphragm is forced down the port throat.

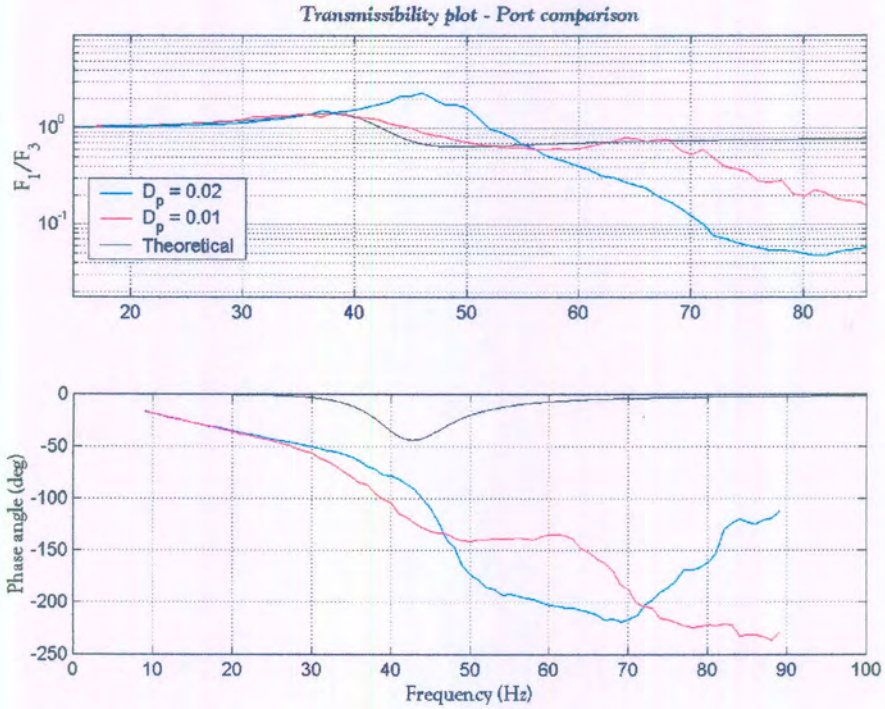

Figure 5.16: Transmissibility comparison – port variation

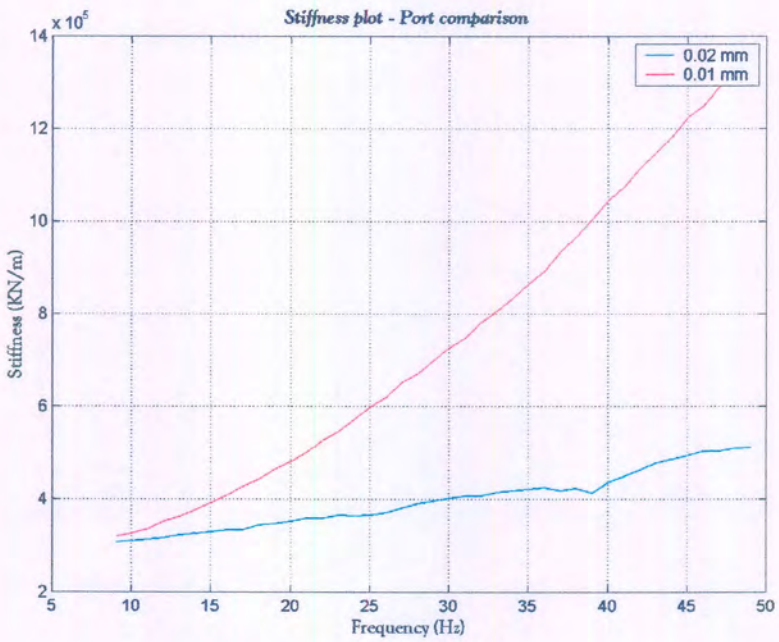

Figure 5.17: Stiffness comparison – Port variation

The next parameter that has been changed, is the diaphragm stiffness. A thinner, more flexible diaphragm has been used. The transmissibility of the new diaphragm is compared to that of the stiff diaphragm in Fig. 5.18. The port diameters are both 0.02-mm.

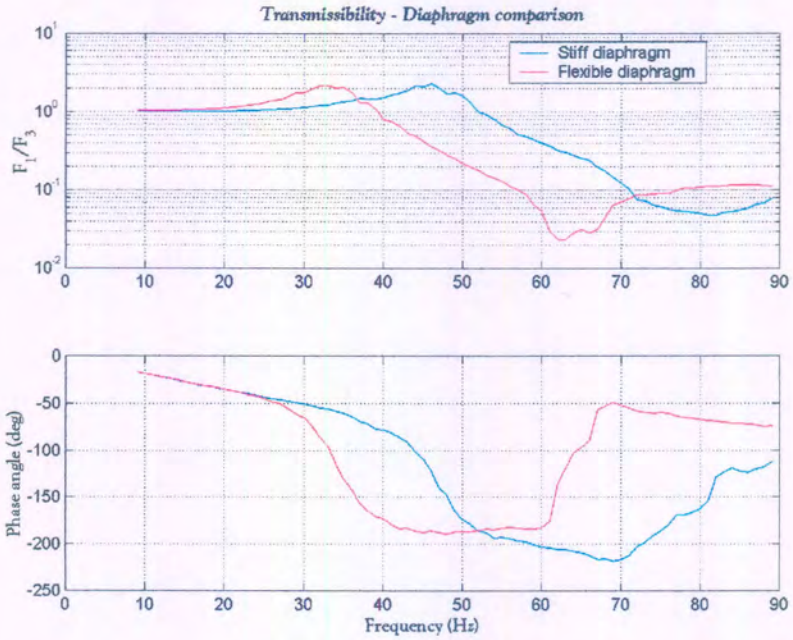

Figure 5.18: Transmissibility comparison – Diaphragm rubber variation

The isolation frequency shifted about 20 Hz with a change in diaphragm rubber. As Fig. 5.18 suggests, and Fig. 5.19 shows, the stiffness has decreased considerably.

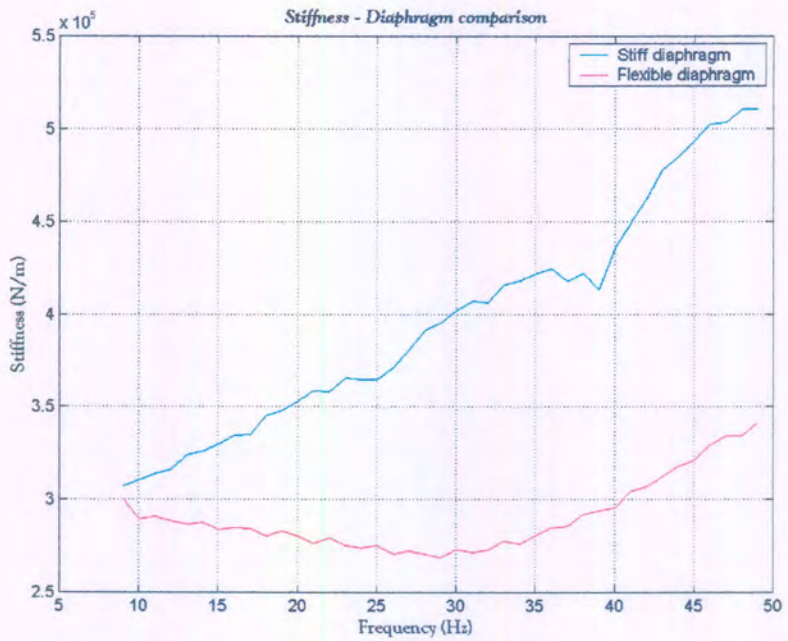

Figure 5.19: Stiffness comparison – Diaphragm variation

The next tests were done with yet a more flexible diaphragm. This diaphragm was a Latex type rubber, and was very flexible. The first test was done with the large 0.02 mm diameter port. An interesting result was obtained when the conventional diaphragm housing was removed to enlarge the pressure area on the diaphragm.

In order to shift the isolation frequency to 30 Hz with a latex rubber diaphragm, the mathematical model was used to calculate the corresponding port diameter. Fig. 5.20 shows the theoretical estimation compared to the measured data for a 12.5 mm port. The theoretical isolation frequency was calculated to be 26 Hz, in order to compensate for the fact that the stiffness will increase with a diameter reduction (Fig. 5.17).

The stiffness of the system was taken from Fig. 5.19 as 270 kN/m. The measured transmissibility is lower than the calculated transmissibility at the isolation frequency due to the fact that the ratio of ω_{MT}/ω_I is lower for the measured transmissibility because of non-linear stiffness effects.

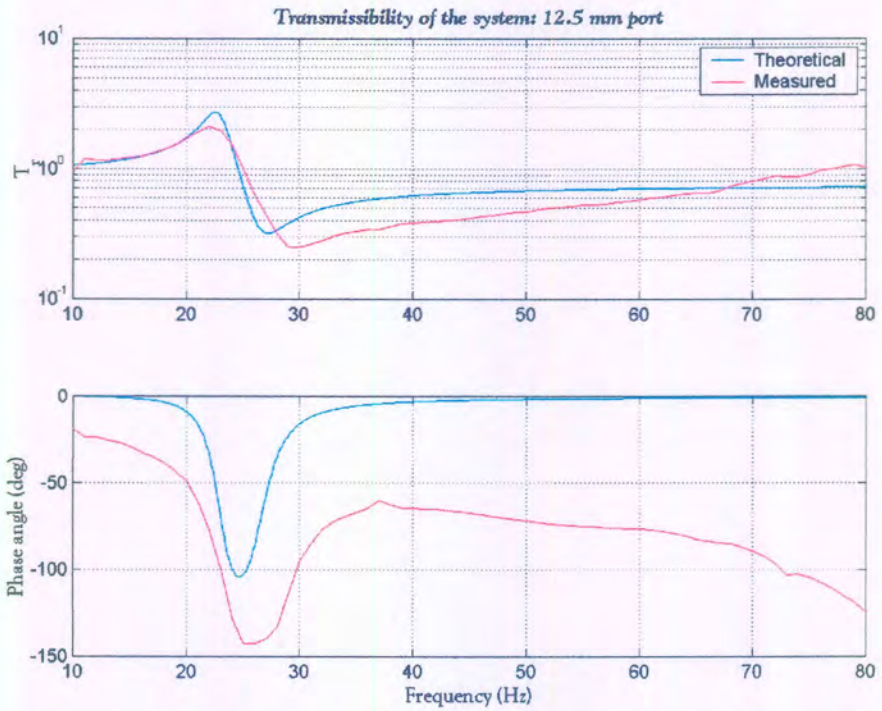

Figure 5.20: Port size verification

The transmissibility functions of three test comparisons are shown in Fig. 5.21. As the figure shows, the isolation frequency reduces when the housing is removed. The enlarged diaphragm pressure area results in a reduction in stiffness. The green line, which shows the transmissibility of the smaller port configuration, has an isolation frequency of 29 Hz. Although the transmissibility of this configuration is higher than the other two configurations, it is still only about 25 %.

The stiffness comparison is shown in Fig. 5.22. The plot shows that the stiffness of the configuration without the diaphragm is indeed lower. The stiffness of the 0.0125 mm port configuration is higher, due to the phenomenon described earlier in this chapter.

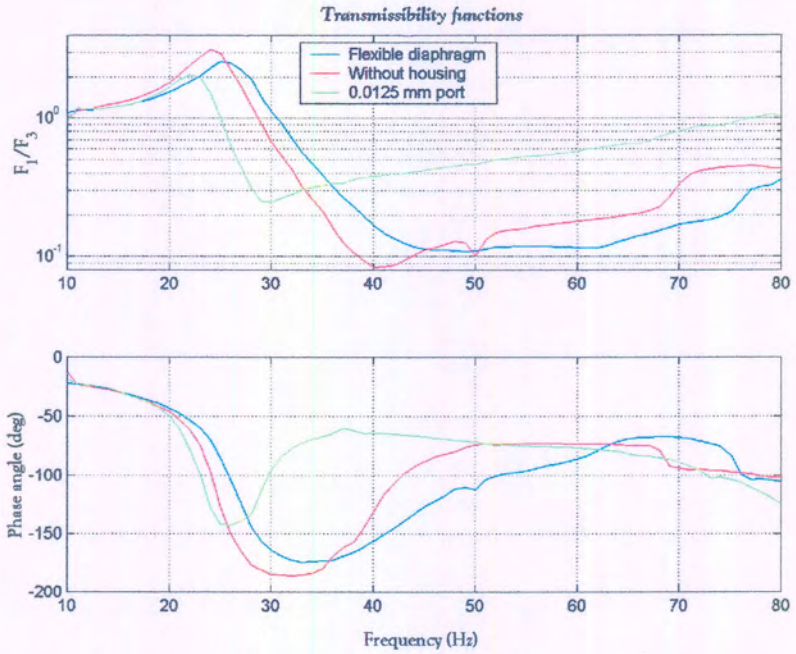

figure 5.21: Transmissibility functions of three different configurations

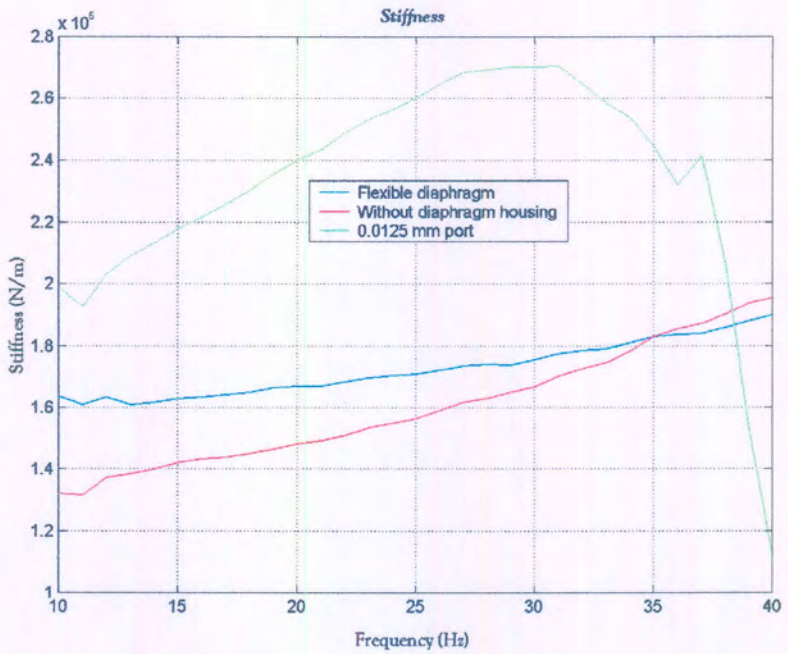

Figure 5.22: Stiffness of three different configurations

Acceleration measurements

The acceleration measurements produced much better results. As stated before, the duration of the input signal of the force measurements was 60 seconds, which was repeated five times. The five results were then averaged to produce one result that is in the time domain. The results were processed in MATLAB to produce frequency domain data. In the case of the acceleration measurements, the Siglab analyser was used. The input signal was a much longer band-limited random function, and the results were frequency domain data, already averaged 20 times. As a result, much better data was obtained.

The first configuration that was subjected to the acceleration measurements was a configuration that included a latex type diaphragm, a large port (0.02 mm diameter) and water as the absorbing fluid. The transmissibility functions for four different amplitudes (Peak – Peak values used as legend) are shown in Fig. 5.23.

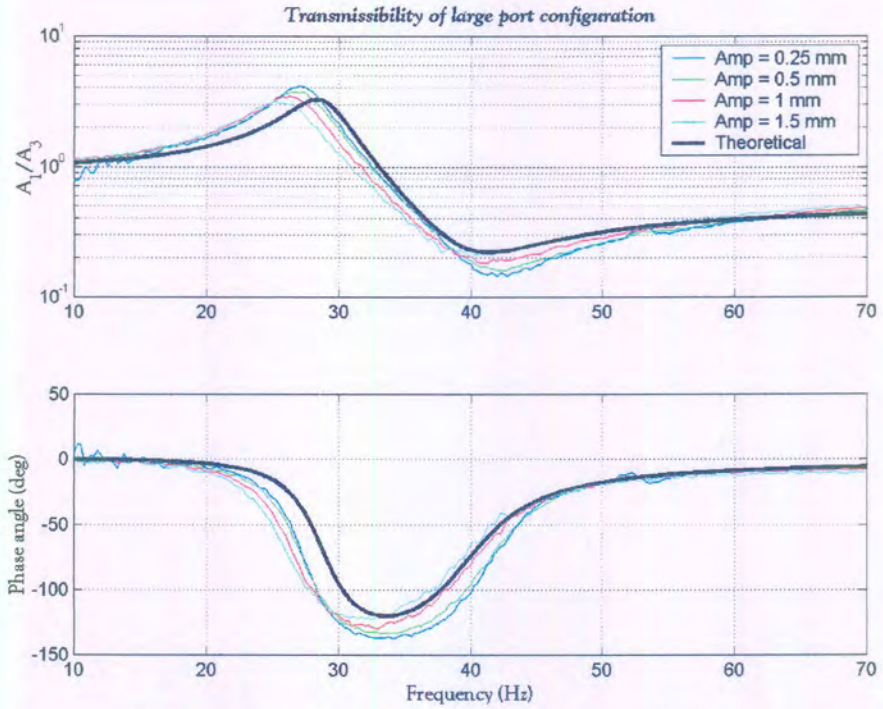

Figure 5.23: Transmissibility of large port & latex type diaphragm configuration

The isolation frequency, is just over 40 Hz, and the MT frequency is about 28 Hz. Important to notice from Fig. 5.23 is that the amplitude variation is relatively small, possibly due to small variations in stiffness and damping. The transmissibility increased slightly, due to the fact that the handle was free to translate.

The quality improvement of this measurement relative to the force measurements is clearly visible, especially when the phase angle functions are compared. The non-linear diagonal movement that was visible when the force measurements were taken, is largely eliminated. This phenomenon in the force measurements was probably due to a small phase difference between the load cell and LVDT amplifiers.

The configuration was kept the same, but the port size was changed to a 0.0125 mm diameter. The transmissibility functions of four different amplitudes (Peak – Peak values used as legend) are shown in Fig. 5.24.

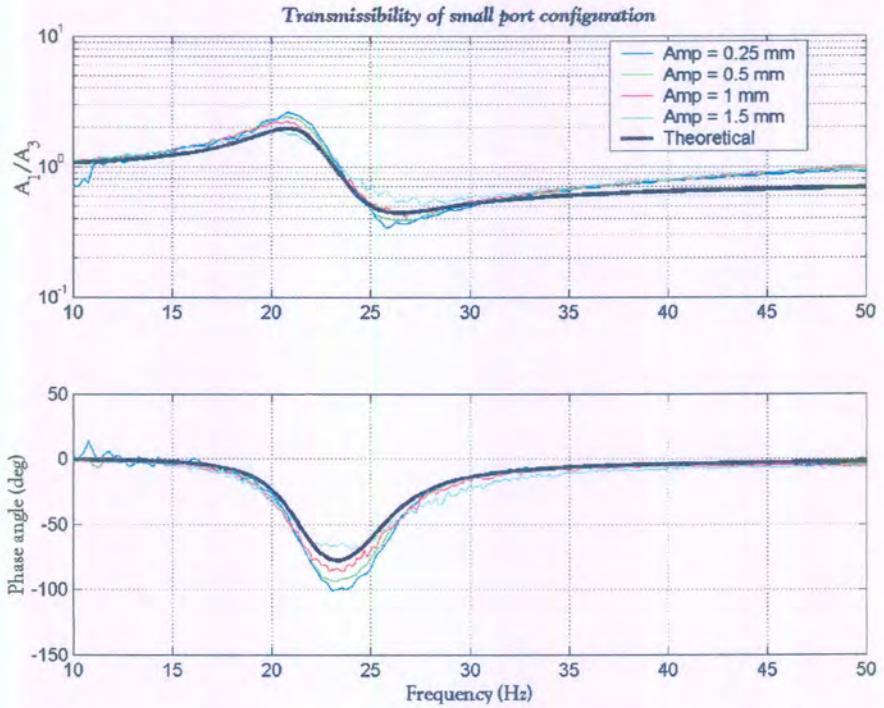

Figure 5.24: Transmissibility of small port & latex type diaphragm configuration

The isolation frequency for this configuration is about 26 Hz, and the MT frequency about 21 Hz. The minimum transmissibility for this configuration is about 40-50%.

5.6 Control system design and experimental results

The experimental results clearly show that an isolation frequency has been obtained, and also that the system responds to changes in fluid density, port diameter and stiffness. As stated in the problem specification, the system must be able to compensate for variations in the operating frequency of the rock drill due to variations in operational conditions such as pneumatic air pressure or rock hardness.

Another issue that will be addressed in this section is the problem stated in chapter 3 (Modeling of vibration absorbers) which is the problem of the MT frequency that is situated in front of the isolation frequency on the frequency spectrum. This will result in unstable or uncomfortable operating conditions during startup and hole collaring. The control system must be able to compensate for this phenomenon in a practical, suitable way.

To be able to vary the isolation frequency of the absorber, a parameter that has a noticeable effect on the isolation frequency has to be changed. The most obvious, and probably most sensitive parameter (Refer to section 4.4) is the port diameter. The port

diameter as a control variable has two important setbacks. When the port diameter is changed, the frequency ratio, γ, will change. This will cause variations in the transmissibility. The second problem is that it will be quite difficult to vary the port diameter effectively without sacrificing any sealing efficiency.

Another parameter that can cause a change in the isolation frequency is the port length. The isolation frequency will change linearly with respect to a change in port length. Although the system is not so sensitive to changes in the port length, varying the port length would probably be the easiest geometrical variable to control.

Another variable that influences both the isolation and the MT frequency, is the stiffness coefficient. The sensitivity of the isolation frequency to changes in the stiffness coefficient is not as evident as diameter variation, but on the design it would perhaps be the simplest to implement.

Compensating for unsuitable MT frequency placement

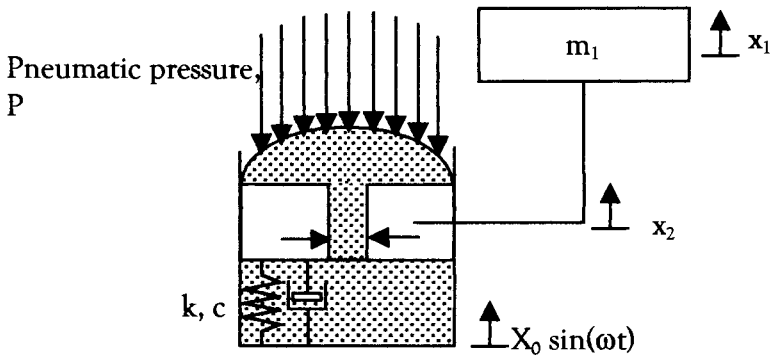

Figure 5.25: Schematic representation of absorber

To compensate for the fact that the MT frequency is below the isolation frequency on the frequency spectrum, the stiffness of the absorber has to be changed in order to move the MT frequency away from the drill operating frequency.

The stiffness change has been achieved by applying sufficient pneumatic air pressure above the diaphragm, as shown in Fig. 5.25. When applying the pressure, the system goes through a non-linear stage where the stiffness actually drops with an increase in air pressure. Thereafter, the stiffness of the system rises dramatically with further increase in air pressure. The transmissibility of the system measured at an air pressure of about 40 kPa is shown in Fig. 5.26.

As the figure shows, the stiffness has been increased from about 340 kN/m to 1.18 GN/m with an increase of 40 kPa in air pressure upon the diaphragm. This caused a 40 Hz jump in MT frequency. The figure also shows that the transmissibility will be much lower in the 0 to 28 Hz region with the air pressure applied. This will enable much more control of the drill during startup or hole collaring.

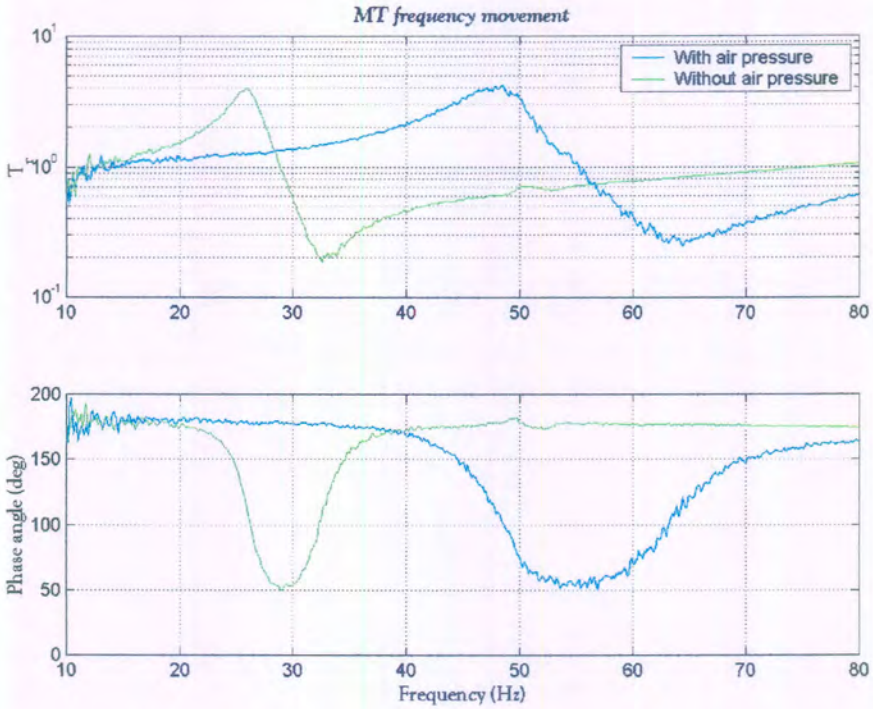

Figure 5.26: MT frequency movement due to air pressure increase

Compensating for minor changes in drill operating frequency.

The compensation for minor changes in the operating frequency was made by varying the air pressure behind the rubber diaphragm. The pressure differences were much smaller, and as a result, the control of the system was done in the highly non-linear region of the system. The reason for the non-linearity is mainly geometrical and is explained in Fig. 5.27.

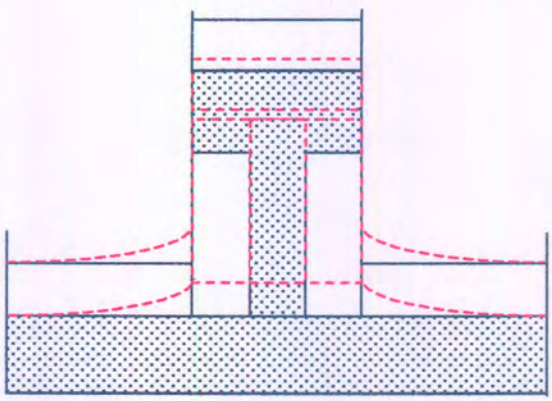

Figure 5.27: Geometrical non-linearity

The diaphragm has been modeled as a piston-cylinder configuration. The dotted lines represent the movement of the absorber port relative to the base. The handle is attached to the port, and will thus move with the port. When air pressure is applied upon the diaphragm, the port will move away from the base of the absorber. This forces the rubber into a non-linear position where the stiffness of the rubber is related to the position of the port.

This phenomenon makes the control system very difficult to analyse analytically. The governing equation for the pneumatic force due to air pressure is:

$$F_c(x) = \frac{P_o V_o^{\frac{1}{3}}}{(V_o - A_d x_d)^{\frac{1}{3}}} \qquad (5.6)$$

The variables P_o, V_o, A_d and x_d are the initial pressure, the initial volume above the diaphragm, the diaphragm area, and the movement of the diaphragm respectively. The equation shows that the system is non-linear in that the pneumatic force is a function of the movement of the diaphragm. It would not be a valid assumption to keep the value of x_d constant as a function of time or frequency. The diaphragm area, A_d, will also be a function of the diaphragm movement, because of the fact that the diaphragm moves down the throat of the port at the end of the downward stroke. The two variables, V_0, and P_0 have been varied by changing the volume above the diaphragm with a bellow type controller.

The pressure has been measured with a manometer, and measurements have been taken at 100 Pa intervals from 0 to 680 Pa. The isolation frequency has been moved down with about 8 Hz, and back up to ensure repeatability. Fig. 5.28 shows the control measurements. The excitation signal in this instance was a random signal with a peak to peak value of 1 mm and a frequency range between 10 and 90 Hz. The measurement quality is a bit lower than that plotted in Fig. 5.23, because of the non-linearity effects of increasing the air pressure behind the diaphragm.

Fig. 5.29 shows a plot of isolation frequency vs. air pressure. The isolation frequency actually drops with increasing pressure, which is somewhat different from what is expected, and from what eq. 5.6 suggests. The reason for this decrease in stiffness with increasing pressure cannot be explained mathematically at this stage and can only assumed to be related to the non-linear effects described in the previous paragraphs and the dynamics of the polyurethane as described in Fig. 5.27.

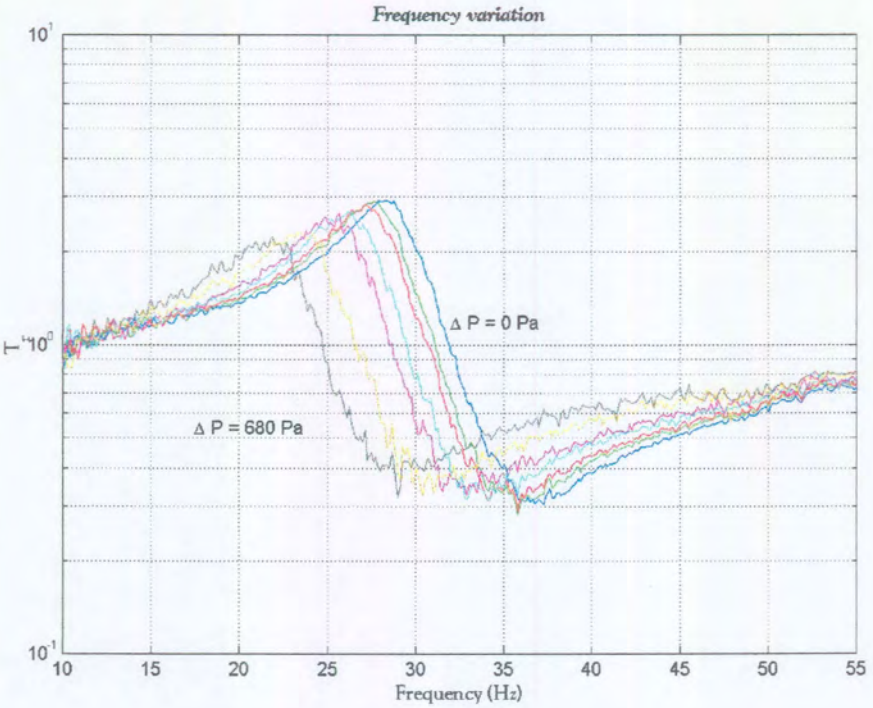

Figure 5.28: Control measurements

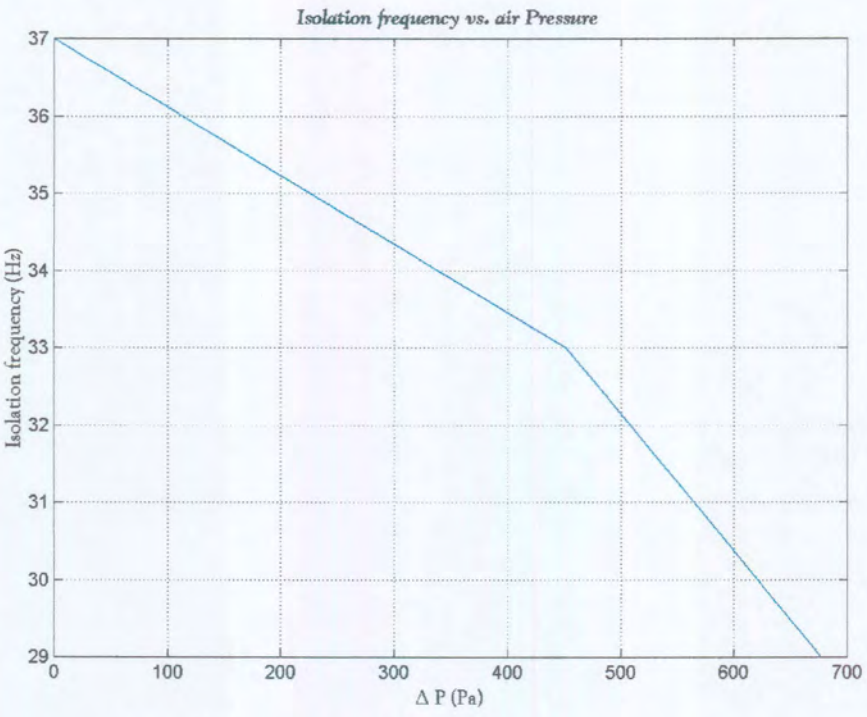

Figure 5.29: Isolation frequency change vs. air pressure

The stiffness thus reduces for pressure increases between 0 and 680 Pa. After 680 Pa the geometry of the polyurethane changes as described in Fig. 5.27, and the system becomes very stiff. Nevertheless, the result was evaluated with different diaphragms

and successfully tested for repeatability. Fig 5.30 shows a diagram of the control system. An important aspect to notice about Fig. 5.28 is that although the isolation frequency has only been moved by about 8 Hz, the frequency band between 26 and 44 Hz has a transmissibility lower than 60 %.

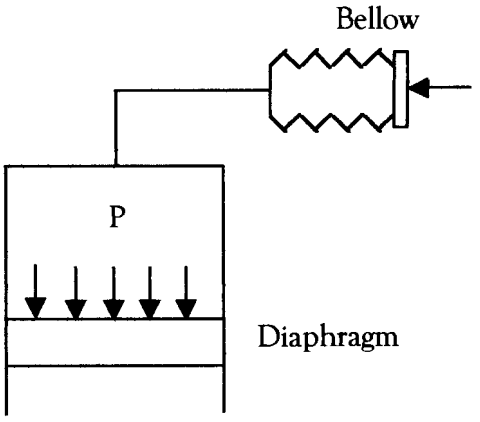

Figure 5.30: Diagram of control system

5.7 Comparison between experimental and theoretical results

Stiffness:
The stiffness of the polyurethane rubber has been analytically calculated in section 4.1 by using elementary plate theory. The calculated stiffness for the design as discussed in section 4 is 128 kN/m. This result can be verified by looking at the measurements where the absorber was tested without a working fluid. Fig. 5.10 shows the stiffness constant as a function of frequency for the system without fluid. At 10 Hz, the stiffness was calculated to be 115 kN/m. A static test was not done because of the fact that the rubber stiffness changes by a considerable amount as a function of frequency.

The theoretical estimation was thus quite adequate for a design that nearly has the same critical frequencies in theory and in practice.

The stiffness contribution of the diaphragm was considered to be much less than the stiffness of the polyurethane rubber. This, however, has proved not to be a very good assumption, even with latex rubber acting as a diaphragm. A reduction in port diameter has been used to compensate for this assumption, but this caused the transmissibility to increase slightly due to frequency ratio reduction and increased fluid damping. This effect can be witnessed in Fig. 5.22.

Damping:

Although damping is relatively difficult to quantify, an attempt has been made in section 4.2 to estimate the damping coefficient. The damping coefficient for the 20 mm port has been calculated to be 200 Ns/m for an amplitude of 0.5 mm and 245 Ns/m for an amplitude of 0.75 mm.

The damping coefficient measured for this configuration has been 366 Ns/m for an amplitude of 0.5 mm and 457 Ns/m for an amplitude of 0.75mm (See Fig. 5.17). The theoretical calculations must be corrected for the incorrect stiffness value of 128 kN/m that has been used for the structural damping coefficient calculation. The theoretical estimation for the damping coefficient after a corrected stiffness constant of 500 kN/m (see Fig. 5.17) has been used for the system, which has a MT frequency of 45 Hz, the theoretical estimation for the damping coefficient is 397 Ns/m.

Transmissibility

Various configurations have been tested, and the most critical parameters have been varied in the experimental procedure. It is important to verify that the measured transmissibility can be correlated with the theoretical prediction. It is also important to verify that the changes in parameters produced the same trends as had been predicted in the theoretical derivation.

The first verification is that of a theoretical transmissibility plot with a measured plot that has basically the same critical parameter values. Fig. 5.31 shows a comparison between theoretical results and experimental measurements for the large port, stiff configuration (see Fig. 5.13).

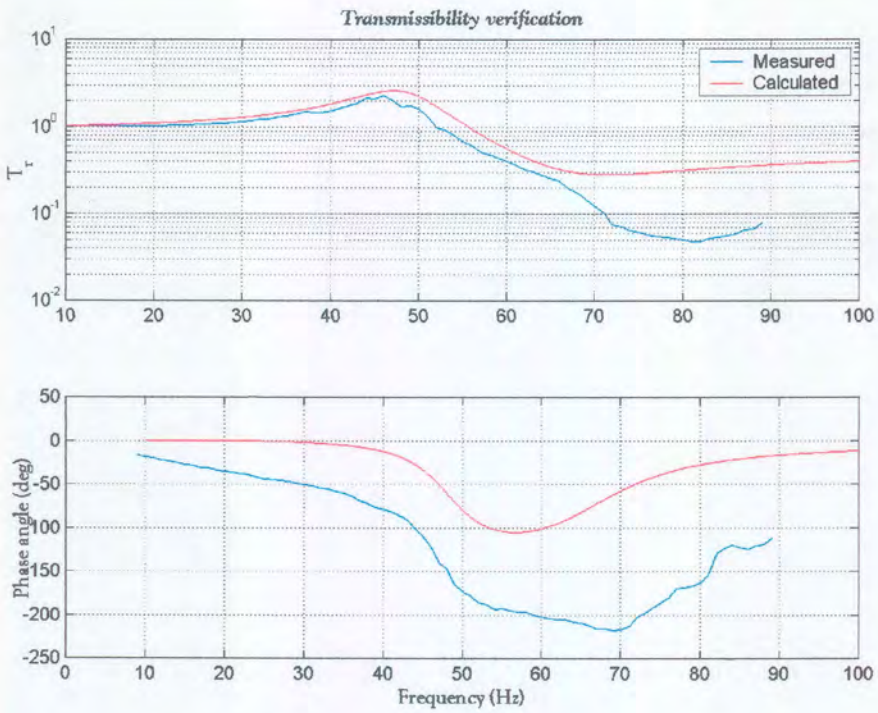

Figure 5.31: Theoretical vs. measured transmissibility

The theoretical calculation has been done with a revised stiffness constant of 650 kN/m extrapolated between the MT and isolation frequencies (See Fig. 5.18). The natural frequency of the theoretical result is thus a bit higher than the measured value. The isolation frequency of the theoretical result is lower than the isolation frequency of

the measured result because of a stiffness constant that increases with increasing frequency (Fig. 5.14).

The system response to a smaller port has also been verified theoretically and is shown in Fig. 5.32 together with the experimental analogue. The stiffness constant has been taken from Fig. 5.17 at 45 Hz as 1.2 GN/m.

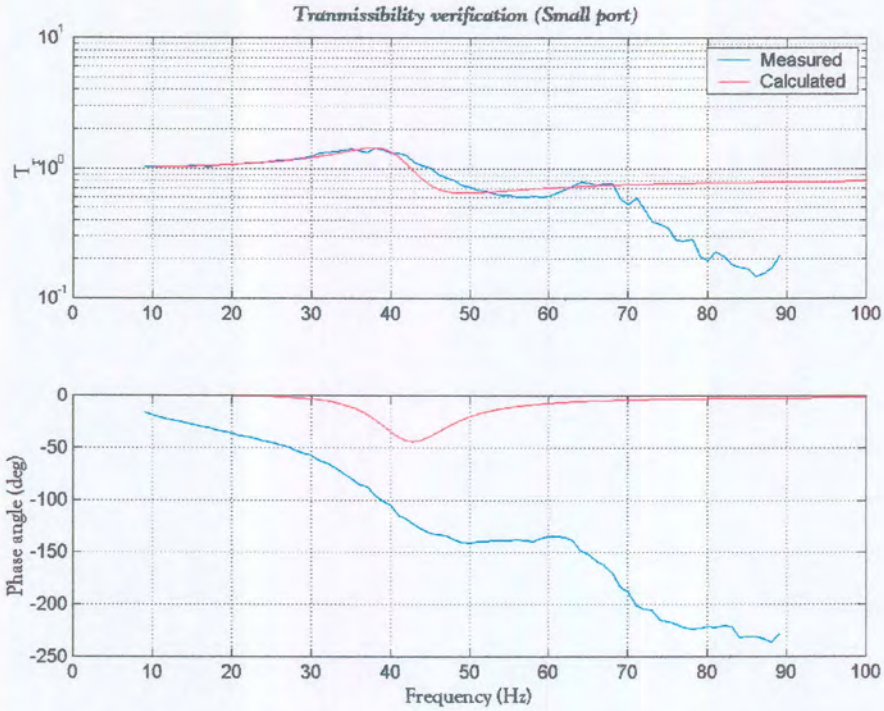

Figure 5.32: Small port verification

The transmissibility corresponds relatively well, except for the isolation frequency that deviates by 7 Hz because of a non-linear stiffness constant (Fig. 5.17). The phase angle differs quite noticeably, which is probably due to the phase difference between the two amplifiers mentioned previously in this chapter (see 5.5 Results: Acceleration measurements: P 83).

The system's response to density variation has also been investigated. The system has been tested and theoretically simulated with both water and methylated spirits. The density of methylated spirits has been measured as 840 kg/m^3. Fig. 5.33 and 5.34 show a comparative plot of the theoretical results vs. the measured responses. The stiffness constant for the system with the diaphragm used in instance, latex, has been measured and calculated as shown in section 5.5 as 260 kN/m.

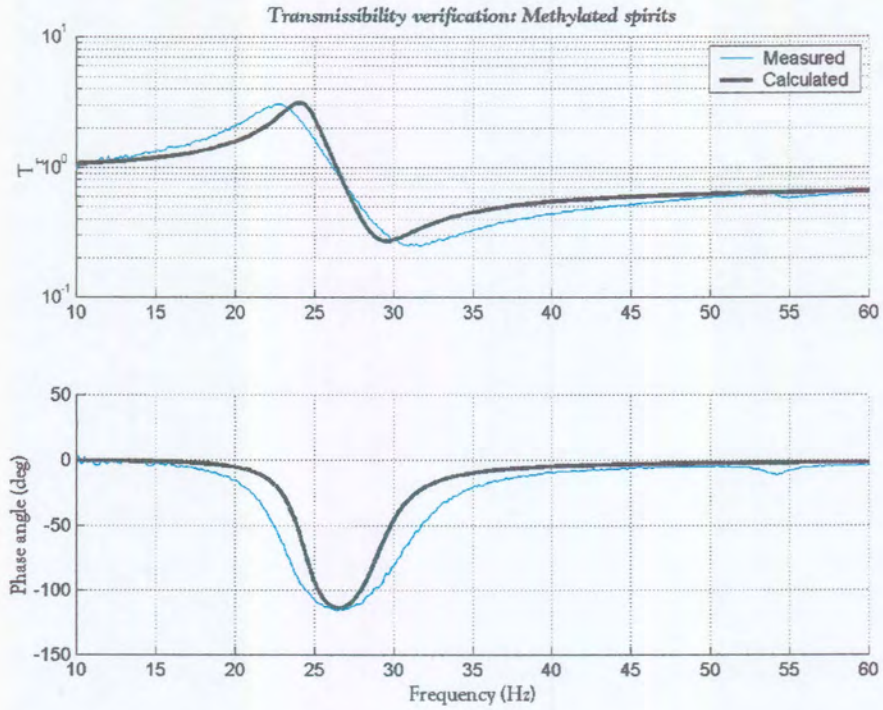

Figure 5.33: Transmissibility of system with spirits

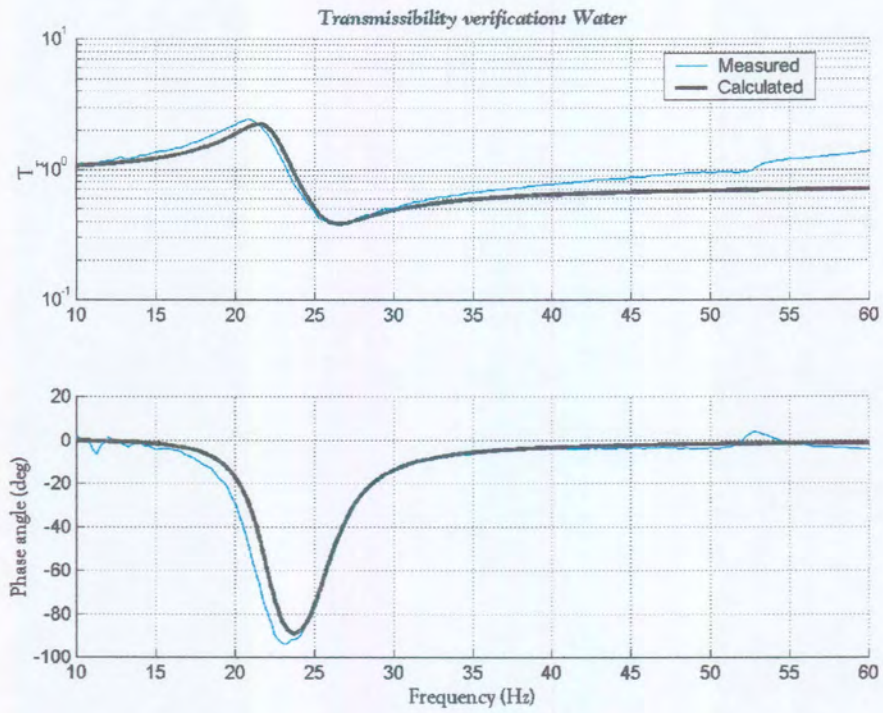

Figure 5.34: Transmissibility of system with water

The theoretical results is, as discussed in this section, are very accurate when the stiffness constant of the system is known. Damping constant will have to be determined experimentally, because a theoretical estimation is not satisfactory. The stiffness constant of the polyurethane rubber can, with the current geometery, accurately predicted by analytical formulas.

6. Conclusion

6.1 Accomplishments

The results have identified a definite isolation frequency, and the experimental verification has verified the analytical design and optimisation procedure. The analytical procedures can now be used with confidence to design this type of absorber in the future. The stiffness coefficient of the system must be known or accurately predicted.

The results have shown that the transmissibility can be reduced to between 20-40 % of the unattenuated rock drill handle transmissibility. The analytical procedures that have been presented can be used to design an absorber for a specific type of drill with a specific operating frequency. It has been proven that the stiffness of the system can be relatively high, even with a tool operating frequency below 50 Hz. This means that the operator will still have adequate control of the drill, whilst subjected to less vibration.

The MT frequency might be a problem during collaring and startup. As the MT frequency placement is somewhat troublesome, and difficult to position above the isolation frequency, it has been proposed that the concept must be able to compensate for this problem by moving the MT frequency higher up the frequency spectrum during collaring and startup. The results have shown that the MT frequency can be shifted with about 30-40 Hz upwards on the frequency spectrum by increasing the air pressure behind the diaphragm with about 40 kPa. This resulted in a very near unity transmissibility in the zero to operating frequency region. The absorber may thus be 'switched off' during the collaring or startup procedure.

In the problem statement it has been noted that the concept must be able to compensate for minor changes in the operating frequency of the drill. This is due to variations in pneumatic pressure, rock hardness etc. The experimental procedure has proven that it is possible to shift the isolation frequency with about 7 Hz by applying minor pressure changes to the diaphragm. The results have verified that this procedure is repeatable regardless of the port configuration or diaphragm type. Although the change is already a ±10 % shift in isolation frequency to both sides, the absorber functions over a relatively broad frequency band of attenuation. If Fig. 5.28 is studied, it will be noted that the absorber is able to reduce the transmissibility by more than 50% from 26 Hz to 45 Hz.

A serious disadvantage of the suggested control system however, is the fact that it could not be verified analytically due to the non-linear variables that play a role in the dynamics of the system. This makes the control system a bit unpredictable in the sense that the frequency band cannot be predicted in the design phase.

The major contributions of this thesis is the fact that the concept has been designed, manufactured, tested and proven for a given configuration. Adjustment of the isolation frequency is made possible by means of a pneumatic control system. The practical implications and problems of this type of attenuation has been defined and solved.

6.2 Aspects that require more research

A number of issues have been identified that warrants further research. An aspect that definitely requires more research is the characteristics of the polyurethane rubber. Aspects like the stiffness and damping dependency on frequency have to receive enough attention in order to make the design process more accurate and reliable. The analytical result for the static stiffness constant of the rubber is acceptable, but not sufficient. A stiffness – frequency dependency must be defined in order to predict the isolation frequency in the design phase.

More experimental work is required to confirm the structural damping constant of polyurethane to ensure that it is indeed the optimum material for the application. The structural damping constants for other elastomers must also be evaluated and compared, for this kind of information is limited in the literature today.

Another aspect that should receive more research is the optimum design of the diaphragm. The diaphragms used in this thesis have a flat, plate like geometry. It will be better to use a concave or even a bellow type geometry for the diaphragm. The reason for this is to ensure that the diaphragm only bends with the flow. With the current geometry the diaphragm actually has to 'blow up' and deform. This causes the stiffness of the system to be affected noticeably.

Although adequate isolation frequency shift has been achieved, more research should be concentrated on the control issue. The control system should be designed in such a way that the transmissibility, and the isolation and MT frequency ratio, is not affected noticeably. This fact makes a stiffness change very attractive, although a considerable change in stiffness is necessary to make an impact on the isolation frequency.

The stiffness of the designed absorber in the directions other than the drill operating frequency is not enough. The type and geometry of the structural rubber should be experimented with in an attempt to stiffen the absorber in these directions. A two- or three-dimensional absorber would also be a solution to this problem.

References

Andersson, L. R., 1990, Design and testing of a vibration attenuating handle: *International Journal of Industrial Ergonomics*, 6, pp. 119-125

Bovenzi, M., 1994, Hand-arm vibration syndrome and dose-response relation for vibration induced white finger among quarry drillers and stone carvers: *Occupational & Environmental Medicine*. 51(9), pp. 603-11

Bovenzi, M., Franzinelli, A., Strambi, F., 1988, Prevalence of Vibration-induced white finger and assessment of vibration exposure among travertine workers in Italy: *International Archieves of Occupational and Environmental Health*, 61, pp. 25-34

Brammer, A.J., 1986, Dose-response relationships for hand transmitted vibration: *Scandinavian Journal of Work, Environment and Health*, 12(4), pp. 284-288

Brammer, A. J., Taylor, W., Lundborg, G., 1987, Sensorineural stages of the hand-arm vibration syndrome: *Scandinavian Journal of Work, Environment and Health*, 13(4), pp. 279-283

Brubaker, R. L., Hutton, S. G., Mckenzie, C. J. G., 1986, Vibration induced white finger among selected underground rock drillers in British Columbia: *Scandinavian Journal of Work, Environment and Health*, 12(4), pp. 296-300

Bursal, F. H., 1995, On vibration absorbers for periodic excitation: *Proceedings of the 1995 ASME International Mechanical Engineering Congress and Exposition*; 57(1), published by: ASME Dynamic Systems and Control Division Vibration Control American society of Mechanical Engineers, N-Y USA, pp. 1-7

De Souza, E. M., Moore, T. N., 1993, Field performance evaluation of a rock drill handle design: *Mining Engineering*, 45(11), November 1993

Du Toit, J. J., 1998, Attenuasie van die effek van rotsboorvibrasie op die menslike liggaam, University of Pretoria, February, 1998

Eastman Kodac Company, 1983, *Ergonomic design for people at work*, vol I

Flannelly, W. G., 1963, Dynamic anti-resonant vibration absorber (DAVI), Kaman Aircraft report, 63-1, Kaman Aircraft Corporation, Bloomfield, Connecticut, November 1963

Gabel, R., Teare, P., Desjardins, R. A., 1981, Flight demonstration of an integrated floor/fuel isolation system: *American society Northeast region national specialists' meeting on helicopter vibration*, Hartford, Connecticut, Nov 1981

Gemne, G., Saraste, H., 1987, Bone and joint pathology in workers using hand-held vibrating tools, *Scandinavian Journal of Work, environment and Health*, 13(4), 1987, pp. 290-300

Griffin, M. J., 1997, Measurement, evaluation and assessment of occupational exposures to hand-transmitted vibration: *Occupational and Environmental Medicine*, 54, pp. 73-89

Griffin, M.J., 1990, *Handbook of human vibration*: Academic Press: London.

Griffin, M.J., 1982, Transmission of vibration to the hands and the influence of gloves. *Vibration Effects on the Hand and Arm in Industry*: Edited by A.J. Brammer and W Taylor. Wiley: New York, pp.102-116.

Halwes, D. R., 1981, Total main rotor system analysis: Bell Helicopter Textron, *NASA, Contractor Report* No. 165667, Langley Research centre, Hampton, Virginia, June 1981

Halwes, D. R., 1981, Total main rotor isolation system: *American Helicopter Society*, Hartford, Connecticut, November 1981, Reprint 15, pp. 1-7

Heyns, P. S., Benadé, W. N. v. d. S., 1996, Optimisation of vibration absorbers for aircraft cannon: *Aeronautical journal of the Royal Aeronautical Society*, March 1996

Inman, D. J.,1998, Smart structure solutions to vibration problems: ISMA23, *International Conference on Noise and Vibration Engineering*, September 16-18, *Katholieke Universiteit Leuven*, Belgium

Lundström, R., Burström, L., 1988, Mechanical impedance of the human hand-arm system: *Industrial Ergonomics* (Accepted for publication, August 1988)

Midé Technology Corporation, Material comparison: http://www.mide.com

Miwa, T., 1982, Vibration isolation systems for hand-held vibrating tools. *Vibration Effects on the Hand and Arm in Industry*. Edited by A.J. Brammer and W Taylor. Wiley: New York, pp.303-310.

Moon, Y. H., Roh, J. H., Cheon, Y. H., 1982, Vibration hazards in rock-drill operators of the anthracite mine, *Proceedings of the 10th Asian Conference on Occupational Health* (1), pp. 402-407

Narini, P. P., Novak, C. B., 1993, Occupational exposure to hand vibration in nothern Ontario gold miners: *The Journal of Hand Surgery*, 18A, pp. 1051-1058

Prajapati, K., Hes, P, 1999, Reduction of hand-arm transmitted vibration on jackleg rock drills. *CIM Conference Paper No. 4MPM2-47*, 2-5 May 1999, Calgary, Canada

Pelmear, P. L., Leong, D., Taylor, W., Nagalingam, M., Fung, D., 1989, Measurement of Vibration of Hand-Held Tools: Weighted or Unweighted?: *Journal of Occupational Medicine*, 31, pp. 902-908

Peters, J. H. W., 1993, Hand-arm vibration and railway maintenance work a case study: *Proceedings of the 6th International Conference on Hand-arm Vibration*, published by HVBG, pp. 347-355, Bonn

Rao, S. S., 1995, *Mechanical vibrations*, Third edition, Addison Wesley Publishing Company

Rodgers, L. A., Eglin, D., Hart, W. F. D., 1982, Rock-drill vibration and white fingers in miners, *Vibration Effects on the Hand and Arm in Industry*: Edited by A.J. Brammer and W Taylor. Wiley: New York, pp.321-323

Suggs, C. W., Hanks, J. M., 1982, Resilient handgrips, *Vibration Effects on the Hand and arm in Industry*. Edited by A.J. Brammer and W Taylor. Wiley: New York, pp.333-337

Taylor, W, 1987, Biological effects of the hand-arm vibration syndrome: Historical perspective and current research: *Journal of the Acoustical Society of America*, 83(2), February 1988, pp. 415-422

Taylor, W., Wasserman, D., Behrens, V., Samuelhof, S., Reynolds, D., 1984, Effect of the Air hammer on the hands of stone cutters. The limestone quarries of Bedford, Indiana, revisited: *British Journal of Industrial Medicine*, 41(3), pp. 289-295

Thomas, C., Rakheja, S., Bhat, R. B., Stiharu, I., 1996, A study of the modal behaviour of the human hand-arm system: *Journal of Sound and Vibration,* 191(1), 1996, pp. 171-176

Tsai, H. C., 1995, Envelope of Green's function for structural response with slightly detuned vibration absorbers: *Earthquake engineering & structural dynamics*, 25(1), January 1996, pp. 1-13

Ugural, A. C., 1981, *Stresses in plates and shells*: McGraw-Hill Inc

Van Niekerk, J. L., Heyns, P. S., Heyns, M. Hassall, J. R., 1998, The measurement of vibration characteristics of mining equipment and impact percussive machines and tools: Laboratory for Advanced Engineering, SIMRAC Interim Report, University of Pretoria, May 1998

Van Wylen, G., Sonntag, R., Borgnakke, C., 1994, *Fundamentals of classical thermodynamics*: 4th edition, John Wiley and Sons, Inc

Wasserman, D. E., 1991, Human vibration standards: *Sound and Vibration*, 25, July 1991, pp. 30-32

White, F. M., 1994, *Fluid mechanics*: 3rd edition, McGraw-Hill, Inc

Appendix A: Transmissibility for SDOF system

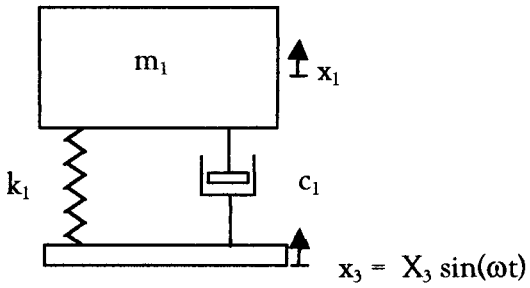

The equation of motion for the system is

$$m_1\ddot{x}_1 + c\dot{x}_1 + kx_1 = k_1x_3 + c_1\dot{x}_3 \tag{10.1}$$

The Laplace transformation for eq. 10.1 is

$$m_1X_1s^2 + c_1X_1s + k_1X_1 = k_1X_3 + c_1X_3s \tag{10.2}$$

After simplification and substituting $s = i\omega$

$$T_r = \frac{X_1}{X_3} = \frac{k_1 + ic_1\omega}{k_1 + ic_1\omega - m_1\omega^2} \tag{10.3}$$

or in non-dimensional form

$$T_r = \frac{1 + i(2\zeta r)}{1 - r^2 + i(2\zeta r)} \tag{10.4}$$

where $r = \frac{\omega}{\omega_n}$ and $\zeta = \frac{c_1}{2m_1\omega_n}$.

The magnitude for the above function can be plotted as the absolute value of the function, and the phase angle is $P = \frac{180}{\pi}\tan^{-1}\left(\frac{\text{imag}(T_r)}{\text{real}(T_r)}\right)$.

Appendix B: Transmissibility for SDOF system with absorber

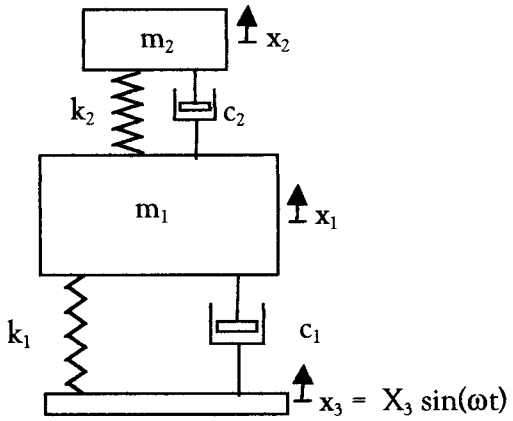

The system with the absorber mass m_2 can now be modeled as a multi-degree-of-freedom (MDOF) system. The equations of motion of the system can be written as:

$$\begin{aligned} m_1\ddot{x}_1 + (k_1+k_2)x_1 + (c_1+c_2)\dot{x}_1 - k_2x_2 - c_2\dot{x}_2 &= k_1x_3 + c_1\dot{x}_3 \\ m_2\ddot{x}_2 + k_2x_2 + c_2\dot{x}_2 - k_2x_1 - c_2\dot{x}_1 &= 0 \end{aligned} \tag{10.5}$$

Eq. 1.4 can be written in matrix form

$$\begin{bmatrix} m_1 & 0 \\ 0 & m_2 \end{bmatrix}\begin{bmatrix} \ddot{x}_1 \\ \ddot{x}_2 \end{bmatrix} + \begin{bmatrix} c_1+c_2 & -c_2 \\ -c_2 & c_2 \end{bmatrix}\begin{bmatrix} \dot{x}_1 \\ \dot{x}_2 \end{bmatrix} + \begin{bmatrix} k_1+k_2 & -k_2 \\ -k_2 & k_2 \end{bmatrix}\begin{bmatrix} x_1 \\ x_2 \end{bmatrix} = \begin{bmatrix} c_1 \\ 0 \end{bmatrix}[x_3] + \begin{bmatrix} c_1 \\ 0 \end{bmatrix}[\dot{x}_3] \tag{10.6}$$

The three system variables M, K and C can be extracted from eq. 10.5

$$[M] = \begin{bmatrix} m_1 & 0 \\ 0 & m_2 \end{bmatrix} \quad [K] = \begin{bmatrix} k_1+k_2 & -k_2 \\ -k_2 & k_2 \end{bmatrix} \quad [C] = \begin{bmatrix} c_1+c_2 & -c_2 \\ -c_2 & c_2 \end{bmatrix} \tag{10.7}$$

The frequency response function can be evaluated as:

$$[X] = \left[[K] + i\omega[C] - [M]\omega^2\right]^{-1}[F] \tag{10.8}$$

The above equation results in the form

$$\begin{bmatrix} X_1 \\ X_2 \end{bmatrix} = \begin{bmatrix} H_{11} & H_{12} \\ H_{21} & H_{22} \end{bmatrix}\begin{bmatrix} F_1 \\ F_2 \end{bmatrix} \tag{10.9}$$

H_{11} is the frequency response function for X_1/F_1, in other words, the response of m_1 relative to a force applied at m_1. The same argument applies for the other elements of the [H] matrix. For this derivation however, the system is excited through base

excitation. The force F_2 will thus be 0, and the Force $F_1 = k_1X_3 + ic_1\omega X_3$. By substituting this into eq. (10.9), the transmissibility function is obtained.

$$T_{11} = H_{11}(k_1 + ic_1\omega) \tag{10.10}$$

The absorber can be optimally tuned by minimizing the numerator of the transmissibility function of $T_{11}=X_1/X_3$. T_{11} looks like this:

$$T_{11} = \frac{(k_2 - m_2\omega^2 + ic_2\omega)(k_1 + ic_1\omega)}{[k_1 + k_2 - m_1\omega + i\omega(c_1 + c_2)][k_2 - m_2\omega^2 + i\omega c_2] - (k_2 + i\omega c_2)^2} \tag{10.11}$$

Eq. (10.11) can also written in dimensionless form:

$$T_{11} = \frac{(1 + i(2\zeta_1 r))(1 - \gamma^2 r^2 + i(2\gamma\zeta_2 r))}{\left[1 + \left(\frac{1}{\gamma^2}\right)\mu - r^2 + i(2\zeta_1 r) + i\left(\frac{2\mu\zeta_2 r}{\gamma}\right)\right][1 + i(2\gamma\zeta_2 r) - \gamma^2 r^2] - [1 + i(2\gamma\zeta_2 r)]\left[\left(\frac{1}{\gamma^2}\right)\mu + i\left(\frac{2\mu\zeta_2 r}{\gamma}\right)\right]} \tag{10.12}$$

where

$$\gamma = \frac{\omega_1}{\omega_2},\ r = \frac{\omega}{\omega_1},\ \zeta_1 = \frac{c_1}{2m_1\omega_1},\ \zeta_2 = \frac{c_2}{2m_2\omega_2} \text{ and } \mu = \frac{m_2}{m_1}$$

if (10.13)

$$\omega_1 = \sqrt{\frac{k_1}{m_1}} \text{ and } \omega_2 = \sqrt{\frac{k_2}{m_2}}.$$

The transmissibility is a minimum at the frequency where the denominator of eq. (10.10) is zero. The term $(k_2 - m_2\omega^2 + ic_2\omega)$ must thus be equal to zero, which will be true at the damped natural frequency of the second mass. The absorber should thus be designed in such a way that $\omega_d = \omega_2\sqrt{1-\zeta_2^2}$ is equal to the exciting frequency of the system. For a given mass m_2, and damping constant c_2, the stiffness k_2 can be calculated. Substituting the relations given in eq. (10.12) and rearranging gives

$$k_2^2 - m_2\omega_{ex}^2 k_2 - \frac{c_2^2}{4} = 0 \tag{10.14}$$

where ω_{ex} is the exciting frequency.
Solving the quadratic equation (10.11):

$$k_2 = \frac{\omega_{ex}^2 m_2}{2} + \frac{\sqrt{\omega_{ex}^4 m_2^2 + c_2^2}}{2} \text{ or } k_2 = \frac{\omega_{ex}^2 m_2}{2} - \frac{\sqrt{\omega_{ex}^4 m_2^2 + c_2^2}}{2} \tag{10.15}$$

The second solution of k_2 yields a negative value and will thus be ignored. The isolation frequency will be equal to the original system's resonant frequency when the natural frequency ratio, γ, is equal to 1.

The natural frequencies and mode shapes can be calculated by solving the eigenvalue problem:

$$\left|[K]-\omega^2[M]\right| = 0$$

Appendix C: Transmissibility for theoretical lever absorber (DAVI)

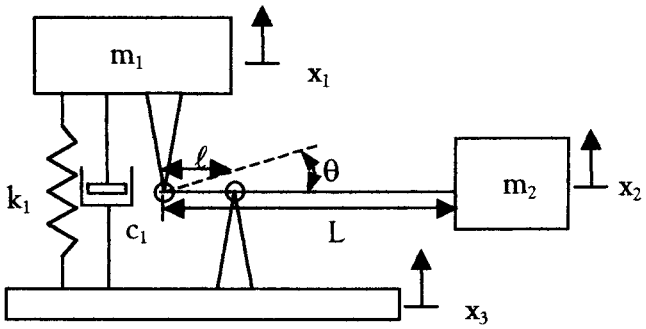

Various methods can be used to derive the equation of motion for the system, but an energy principle method would probably be the less cumbersome way to do it. The Lagrange method will be used to derive the equations of motion for most of the concepts. The first step is to express the motion of the absorber mass, x_2, in terms of the motion of the isolation mass, x_1, and the base motion, x_3.

$$x_2 = \frac{L}{\ell}x_3 - \left(\frac{L-\ell}{\ell}\right)x_1 \tag{10.16}$$

The kinetic energy of the system is:

$$E_k = \frac{1}{2}m_1\dot{x}_1^{\,2} + \frac{1}{2}m_2\dot{x}_2^{\,2} + \frac{1}{2}I\dot{\theta}^2 \tag{10.17}$$

where

$$\theta = \left(\frac{x_1 - x_3}{\ell}\right) \tag{10.18}$$

Substituting eq. (10.16) and (10.18) into eq. 10.17:

$$E_k = \frac{1}{2}m_1\dot{x}_1^{\,2} + \frac{1}{2}m_2\left(\frac{L}{\ell}\dot{x}_3 - \left(\frac{L-l}{\ell}\right)\dot{x}_1\right)^2 + \frac{1}{2}I\left(\frac{\dot{x}_1 - \dot{x}_3}{\ell}\right)^2 \tag{10.19}$$

The potential energy can be defined as:

$$E_p = \frac{1}{2}k_1(x_1 - x_3)^2 \tag{10.20}$$

Rayleigh's dissipation function is:

$$R = \frac{1}{2}c_1(\dot{x}_1 - \dot{x}_3)^2 \tag{10.21}$$

The Lagrangian formulation states:

$$\frac{d}{dt}\left(\frac{\partial E_k}{\partial \dot{x}_i}\right)-\frac{\partial E_k}{\partial x_i}+\frac{\partial R}{\partial \dot{x}_i}+\frac{\partial E_p}{\partial x_i}=F_i \tag{10.22}$$

The external force vector F_i is zero in this application, and after substitution the equation of motion looks like this:

$$\begin{aligned}&\left[m_1+\left(\frac{L}{\ell}-1\right)^2 m_2+\frac{I}{\ell^2}\right]\ddot{x}_1+c_1\dot{x}_1+k_1x_1=\\&\left[\left(\frac{L}{\ell}-1\right)\left(\frac{L}{\ell}\right)m_2+\frac{I}{\ell^2}\right]\ddot{x}_3+c_1\dot{x}_3+k_1x_3\end{aligned} \tag{10.23}$$

For simplicity two alternative variables are defined as:

$$\begin{aligned}M_{eq1}&=m_1+\left(\frac{L}{\ell}-1\right)^2 m_2+\frac{I}{\ell^2}\\M_{eq3}&=\left(\frac{L}{\ell}-1\right)\left(\frac{L}{\ell}\right)m_2+\frac{I}{\ell^2}\end{aligned} \tag{10.24}$$

After substitution, following the procedure described in B.1, the transmissibility of the system can be computed with the following equation:

$$T_r=\frac{X_1}{X_3}=\frac{k_1+ic_1\omega-M_{eq3}\omega^2}{k_1+ic_1\omega-M_{eq1}\omega^2} \tag{10.25}$$

Eq. (10.25) can also be written in dimensionless form

$$T_r=\frac{1+i(2\zeta r)-\gamma_d{}^2 r^2}{1+i(2\zeta r)-r^2} \tag{10.26}$$

where

$$\zeta=\frac{c_1}{2M_{eq1}\omega_{MT}},\ r=\frac{\omega}{\omega_{MT}}\ \text{and}\ \gamma=\frac{\omega_{MT}}{\omega_I}.$$

The frequencies ω_{MT} and ω_I are the frequency of maximum transmissibility and isolation frequency respectively.

$$\begin{aligned}\omega_{MT}&=\sqrt{\frac{k_1}{M_{eq1}}}\\\omega_I&=\sqrt{\frac{k_1}{M_{eq3}}}\end{aligned} \tag{10.27}$$

The phase angle can be computed with

$$P = \frac{180}{\pi} \tan^{-1}\left(\frac{\text{imag}(T_r)}{\text{real}(T_r)}\right) \tag{10.28}$$

The transmissibility function $\frac{X_2}{X_3}$ can be calculated by substituting eq. (10.25) into eq. (10.16).

Appendix D: Mode shapes of nodal beams

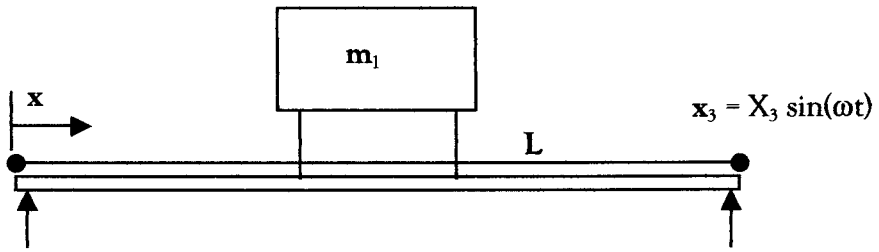

For a uniform beam, using elementary theory of bending of beams and vibration principles, the differential equation of motion can be written down (Rao, 1995: 524):

$$v^2 \cdot \frac{\partial^4 w}{\partial x^4}(x,t) + \frac{\partial^2 w}{\partial t^2}(x,t) = 0 \qquad (10.29)$$

Where

$$v = \sqrt{\frac{EI}{\rho A}} \qquad (10.30)$$

The variables w, E, I, ρ and A are vertical displacement, Young's modulus, moment of inertia, density and area respectively. Note that there is no external force in eq. (10.29). That is because only the mode shapes are important for the purpose of this thesis, and not the exact response of the beam.
The solution of eq. (10.29) can be found by using the method of separation of variables. The vertical displacement in terms of x is:

$$W(x) = C_1 \cos(\beta x) + C_2 \sin(\beta x) + C_3 \cosh(\beta x) + C_4 \sinh(\beta x) \qquad (10.31)$$

Where

$$\beta^4 = \frac{\rho A \omega^2}{EI} \qquad (10.32)$$

Applying the boundary condition for the specific application can solve the constants $C_{1\text{-}4}$ in eq. (10.31). The boundary condition for a pinned beam is:

$$W(0,L) = 0$$
$$EI\frac{\partial^2 W(0,L)}{\partial x^2} = 0 \qquad (10.33)$$

The solution for a beam pinned on both ends thus yields:

$$W_n(x) = C_n \sin(\beta_n x) \qquad (10.34)$$

Appendix E: Transmissibility for LIVE system

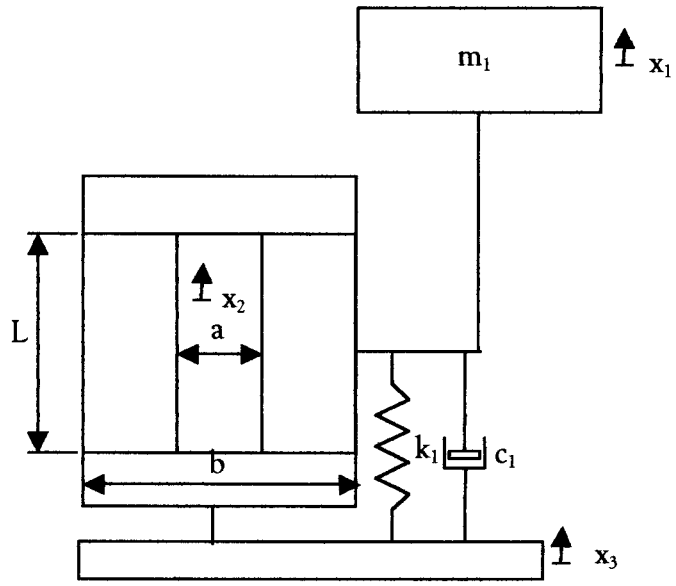

The equations of motion for the LIVE system will once again be derived with the Lagrange method. The first step is to write the displacement x_2 in terms of the displacements x_1 and x_3. By applying flow continuity:

$$x_2 = \frac{b}{a}x_3 - \frac{b-a}{a}x_1 \tag{10.35}$$

The kinetic energy of the system is described by:

$$E_k = \frac{1}{2}m_1\dot{x}_1^{\,2} + \frac{1}{2}m_2\dot{x}_2^{\,2} \tag{10.36}$$

where m_2 is the mass of the fluid in the port.
After substitution,

$$E_k = \frac{1}{2}m_1\dot{x}_1^{\,2} + \frac{1}{2}m_2\left(\frac{b}{a}\dot{x}_3 - \frac{b-a}{a}\dot{x}_1\right) \tag{10.37}$$

The potential energy of the system can be written as:

$$E_p = \frac{1}{2}k_1(x_1 - x_3)^2 \tag{10.38}$$

Rayleigh's dissipation function:

$$R = \frac{1}{2}c_1(\dot{x}_1 - \dot{x}_3)^2 \tag{10.39}$$

After substitution in eq. 10.17, the equation of motion is:

$$\left(m_1+\left(\frac{b-a}{a}\right)^2 m_2\right)\ddot{x}_1+c_1\dot{x}_1+k_1x_1=\left(\frac{b(b-a)}{a^2}\right)m_2\ddot{x}_3+c_1\dot{x}_3+k_1x_3 \tag{10.40}$$

For simplicity define

$$M_{eq1}=m_1+\left(\frac{b-a}{a}\right)^2 m_2$$
$$M_{eq3}=\left(\frac{b(b-a)}{a^2}\right)m_2 \tag{10.41}$$

After substitution, following the procedure described in B.1, the transmissibility of the system can be computed with the following equation:

$$T_r=\frac{X_1}{X_3}=\frac{k_1+ic_1\omega-M_{eq3}\omega^2}{k_1+ic_1\omega-M_{eq1}\omega^2} \tag{10.42}$$

The phase angle can be computed with

$$P=\frac{180}{\pi}\tan^{-1}\left(\frac{\text{imag}(T_r)}{\text{real}(T_r)}\right) \tag{10.43}$$

The transmissibility function $\frac{X_2}{X_3}$ can be calculated by substituting eq. (10.42) into eq. (10.35).

The isolation and MT frequencies can be evaluated eq. (10.27):

Appendix F: Transmissibility for alternative liquid absorber

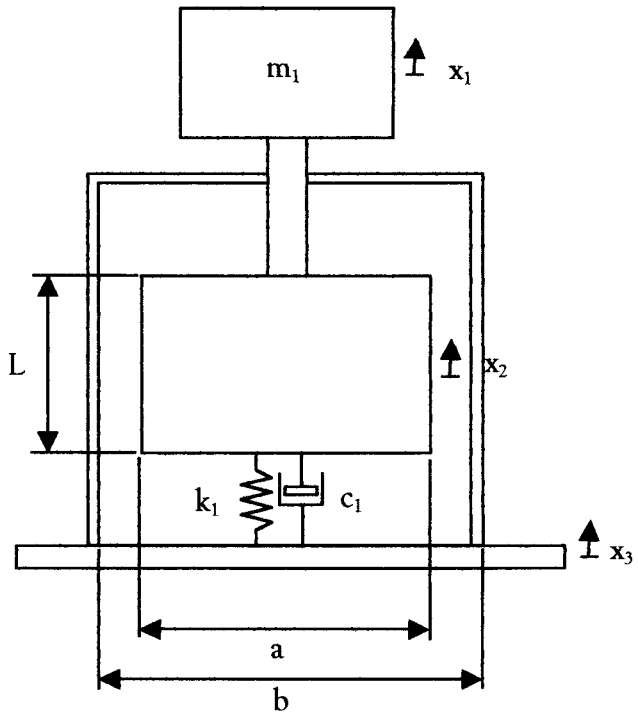

The first step in the Langrange formulation is:

$$x_2 = \frac{bx_3 - ax_1}{b-a} \tag{10.44}$$

By following the same steps used in the previous derivations, the equivalent masses can be calculated as:

$$M_{eq1} = m_1 + m_2\left(\frac{a}{b-a}\right)^2$$
$$M_{eq3} = m_2\frac{b\cdot a}{(b-a)^2} \tag{10.45}$$

The transmissibility function can be calculated using eq. (10.42) and (10.43), while the MT and isolation frequencies can be calculated using eq. (10.27).

Appendix G: Transmissibility for hand arm vibration absorber

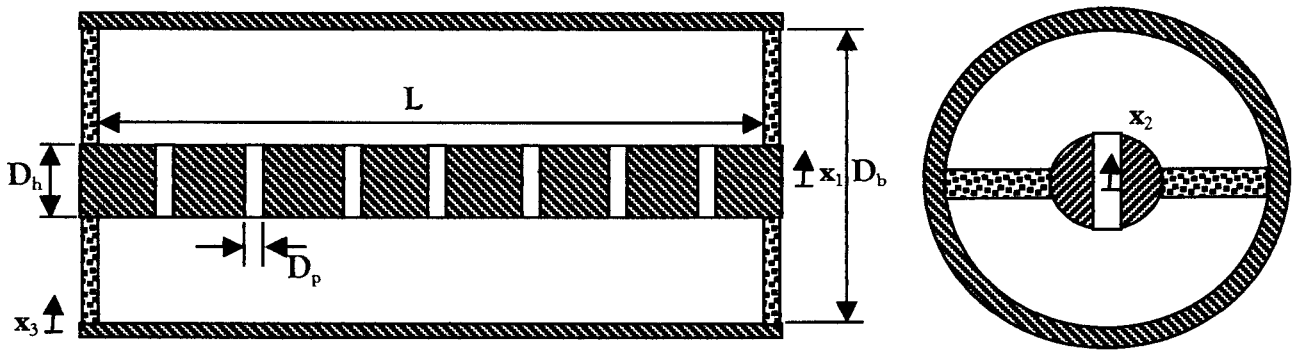

Definition of geometrical variables:

$$b = D_b L$$
$$a = n_p \frac{\pi}{4} D_p^{\,2} \qquad (10.46)$$

Following the first step in the Lagrange formulation:

$$x_2 = \frac{b}{a} x_3 - \frac{b-a}{a} x_1 \qquad (10.47)$$

Eq. (10.47) is the same as eq. (10.35). The rest of the derivation will thus be the same as that of the LIVE system.

Appendix H: Transmissibility for diaphragm type absorber

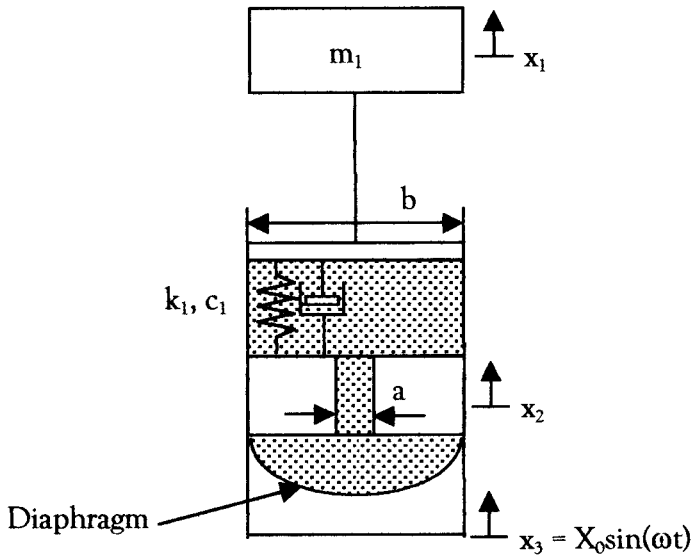

The declaration of geometrical variables:

$$a = \frac{\pi}{4} D_p^{\,2}$$
$$b = \frac{\pi}{4} D_1^{\,2} \qquad (10.48)$$

The displacement of the fluid in the port in terms of the base and handle displacements is:

$$x_2 = \frac{b-a}{a} x_3 - \frac{b}{a} x_1 \qquad (10.49)$$

The transmissibility can now be calculated as done in the previous derivations.

Appendix I: Rubber stiffness calculation

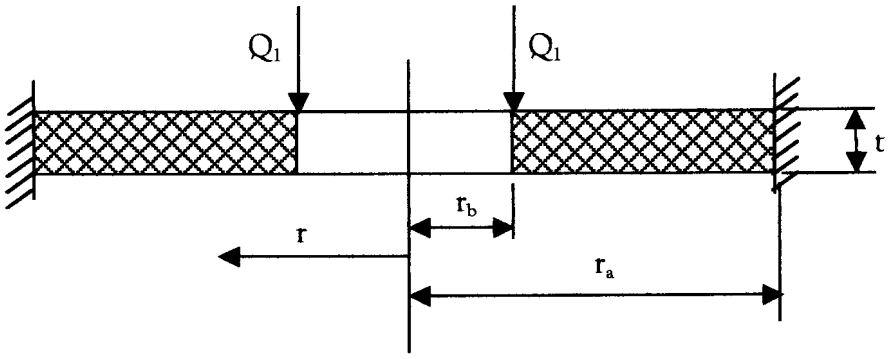

The total load $F_t=2\pi r_b Q_1$ must be equal to the total shear force at a distance r from the center, $2\pi r Q_r$. Thus

$$Q_r = -\frac{Q_1 r_b}{r} \tag{10.50}$$

Ugural (1981,31) gives the governing shear force differential equation for axisymmetrical as

$$Q_r = -D\frac{d}{dr}\left[\frac{1}{r}\frac{d}{dr}\left(r\frac{dw}{dr}\right)\right] \tag{10.51}$$

where $D=\frac{Et^3}{12(1-\nu^2)}$ (E is Young's modulus, and ν is Poisson's ratio.

After substitution of eq. (10.50), and integration of eq. (10.51), the displacement is

$$w=\frac{Q_1 r_b r^2}{4D}(\ln(r)-1)+\frac{c_1 r^2}{4}+c_2\ln(r)+c_3 \tag{10.52}$$

The integration constants can be found by applying the boundary conditions

$$\begin{aligned} w(r_a)&=0 \\ \frac{dw}{dr}(r_a)&=0 \\ \frac{dw}{dr}(r_b)&=0 \end{aligned} \tag{10.53}$$

The last boundary condition in eq. (10.53) implies that although the rubber is free to translate at $r = r_b$, it cannot rotate.

The stiffness of the rubber is thus:

$$k_r = \frac{2\pi r_b}{\frac{r_b^3}{4D}\left(\ln(r_b) - 1\right) + \frac{c_1 r_b^2}{4} + c_2 \ln(r_b) + c_3} \tag{10.54}$$

Appendix J: Flow damping calculation

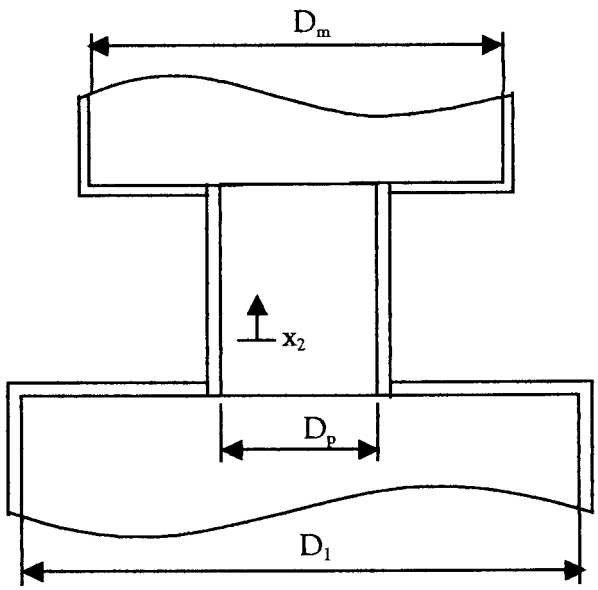

The flow losses in the port for laminar flow is (White, 1994)

$$h_{fL} = \frac{32\mu_f L\dot{x}_2}{\rho g D_p^{\ 2}} \tag{10.55}$$

Eq. (10.55) will only be valid for a Reynolds number $R_{ed} < 2100$, where

$$R_{ed} = \frac{\rho\dot{x}_2 D_p}{\mu_f} \tag{10.56}$$

The pressure loss due to fluid damping is thus

$$\Delta P_L = \frac{32\mu_f L\dot{x}_2}{D_p^{\ 2}} \tag{10.57}$$

The damping force can now be calculated as

$$F_L = \frac{32\mu_f L\dot{x}_2}{D_p^{\ 2}} \cdot A \tag{10.58}$$

where $A = \pi D_p L$.

If the Reynolds number is higher than 2300, turbulent flow is assumed. The flow losses for this case is

$$h_{fT} = 0{,}316 \cdot R_{ed}^{\frac{1}{4}} \cdot \frac{L\dot{x}_2^{\,2}}{2D_p g} \tag{10.59}$$

The pressure loss is then

$$\Delta P_L = 0{,}158 \cdot R_{ed}^{\frac{1}{4}} \cdot \frac{L\rho\dot{x}_2^{\,2}}{D_p} \tag{10.60}$$

The damping force is

$$F_L = 0{,}158 \cdot R_{ed}^{-\frac{1}{4}} \cdot \pi L^2 \rho \dot{x}_2^{\,2} \tag{10.61}$$

The flow losses due to sudden contraction and expansion are also calculated. Although the port has been slightly angled to reduce flow losses, the damping calculation will make the conservative assumption that there is no diffuser action. The loss coefficient for sudden expansion is

$$K_{SE} = \frac{2h_m g}{\dot{x}_2^{\,2}} = \left(1 - \frac{D_p^{\,2}}{D_1^{\,2}}\right)^2 \tag{10.62}$$

The loss coefficient for sudden contraction is:

$$K_{SC} = \frac{2h_m g}{\dot{x}_2^{\,2}} = 0.42\left(1 - \frac{D_p^{\,2}}{D_1^{\,2}}\right) \tag{10.63}$$

The flow losses due to sudden expansion and contraction is:

$$h_{SE/C} = K_{SE/C}\frac{\dot{x}_2^{\,2}}{2g} \tag{10.64}$$

The pressure drop can be calculated as:

$$\Delta P_L = K_{SE/C}\frac{\rho\dot{x}_2^{\,2}}{2} \tag{10.65}$$

The resulting damping force is then:

$$F_L = K_{SE/C}\frac{\pi d^2 \rho \dot{x}_2^{\,2}}{8} \tag{10.66}$$

In both the turbulent flow and entrance-exit compensation, the damping force is a function of $\dot{x}_2^{\,2}$. This implies that the equivalent damping coefficient is a function of

the port velocity. Rao (1995, 227) presents an energy method to approximate this quadratic damping effect. The equivalent damping coefficient is

$$c_{eq} = \frac{8}{3\pi} a\omega X \text{, if } F_L \text{ is in the form } F_L = a\dot{x}^2 \qquad (10.67)$$

The solution method is thus the following procedure:

- Determine the Reynolds number by using eq. 10.56 and decide turbulent or laminar flow.
- Guess a mean value for X_2 and V_2.
- Calculate the damping coefficient by adding all the above damping forces.
- Verify the values of X_2 and V_2 according to dynamic principles and correct if necessary.
- Verify the Reynolds number and iterate again if necessary